NASA
Technical
Paper
2497

December 1985

# Aerodynamic Characteristics of a High-Wing Transport Configuration With an Over-the-Wing Nacelle-Pylon Arrangement

William P. Henderson
and William K. Abeyounis



NASA

NASA
Technical
Paper
2497

1985

# Aerodynamic Characteristics of a High-Wing Transport Configuration With an Over-the-Wing Nacelle-Pylon Arrangement

William P. Henderson
and William K. Abeyounis

*Langley Research Center*
*Hampton, Virginia*

National Aeronautics
and Space Administration

**Scientific and Technical
Information Branch**

## SUMMARY

An investigation has been conducted in the Langley 16-Foot Transonic Tunnel to determine the effects on the aerodynamic characteristics of a high-wing transport configuration of installing an over-the-wing nacelle-pylon arrangement. The tests were conducted at Mach numbers from 0.70 to 0.82 and at angles of attack from $-2^{\circ}$ to $4^{\circ}$. The configurational variables under study included symmetrical and contoured nacelles and pylons, pylon size, and wing leading-edge extensions. Adding the symmetrical nacelles and pylons to the configuration resulted in a reduction in lift coefficient, a significant increase in drag coefficient, and a nose-up pitching-moment-coefficient increment. Contouring the nacelles and pylons significantly reduced the interference drag for the configuration. Even with this reduction, the interference drag for the over-the-wing nacelle was excessive. Increasing the size of the pylons decreased the local velocities around the pylons and the lower part of the nacelle, and thus resulted in a reduction in the drag coefficient of about 0.0011 at a Mach number of 0.80. Adding the wing leading-edge extension inboard of the nacelle-pylon arrangement did not significantly alter the interference characteristics for the configuration.

## INTRODUCTION

Transport aircraft must offer substantially improved performance if the competitive position of the United States aircraft industry is to be maintained. Accomplishing this very demanding task will require the development and application of many new and innovative technologies. Among these will be the integration of the engine with the airframe, for which advanced engine and nacelle concepts will be integrated with advanced high-aspect-ratio (>10) wing designs. As these advanced engines become larger (with higher bypass ratios for increased efficiency), the integration problems will become considerably more difficult. The data presented in reference 1 illustrate the sensitivity of several configuration geometric parameters (e.g., changes to the nacelle shape and location) to the nacelle-pylon-wing interference drag. Studies are currently being conducted to determine alternate nacelle arrangements which offer the potential for eliminating this unfavorable interference drag. (See refs. 2 and 3.) One of the studies described in reference 2 involved the integration effects of an over-the-wing nacelle arrangement. In the study of reference 2, nonmetric over-the-wing nacelles were used to determine the interference effects of the nacelle on the aerodynamic characteristics of a wing-body configuration. The results of that study indicate that nacelle position has a significant effect on the wing-body drag. In fact, a location above the wing was found which resulted in a reduction in the drag of the wing-body configuration, indicating favorable interference effects. Since no direct effects (i.e., nacelle drag) of the nacelle-pylon arrangement were measured during this test, it was difficult to fully assess the integration characteristics of this configuration. As a result, an ongoing program on nacelle-pylon-wing integration was expanded to include an over-the-wing nacelle arrangement.

Another reason that novel nacelle arrangements may become of interest is that as the engine and nacelle become larger, the distance between the engine and the

ground for conventional arrangements decreases, naturally increasing the possibility of engine damage because of foreign particle ingestion. One possible method of reducing this problem would be to relocate the engine in an over-the-wing position.

Because of these two reasons, an investigation was conducted to study the effects of an over-the-wing nacelle arrangement on the aerodynamic characteristics of a high-wing transport configuration. This investigation was conducted in the Langley 16-Foot Transonic Tunnel at Mach numbers from 0.70 to 0.82 and at angles of attack from $-2^{\circ}$ to $4^{\circ}$. The results of this investigation are discussed in this paper.

## SYMBOLS AND ABBREVIATIONS

All the longitudinal forces and moments are referred to the wind axis system. The data are presented with respect to 25 percent of the wing mean geometric chord. (See fig. 1.) Dimensional quantities are presented in the International System of Units (SI).

$b$ wing span, cm

$C_D$ total drag coefficient, $\frac{\text{Drag}}{qS}$

$C_L$ lift coefficient, $\frac{\text{Lift}}{qS}$

$C_m$ tail-on pitching-moment coefficient, $\frac{\text{Pitching moment}}{qSc}$

$C_p$ pressure coefficient, $\frac{p_\ell - p_\infty}{q}$

$C_{p,s}$ pressure coefficient for local sonic flow

$c$ local wing chord, cm

FS fuselage station, cm

$M$ free-stream Mach number

$p_\ell$ local static pressure on the surface of wing, nacelle, or pylon

$p_\infty$ free-stream static pressure

$q$ free-stream dynamic pressure

$r_e$ nacelle external radius, cm

$r_i$ nacelle internal radius, cm

$S$ wing reference area, for leading and trailing edge extended to fuselage centerline

$x$ axial distance along wing, nacelle, or pylon, cm

$y$ spanwise distance, cm

$\alpha$ angle of attack, deg

$\phi$ radial position around nacelle measured in a clockwise direction, $\phi = 0^{\circ}$ at top of nacelle, deg

Configuration designations:

OWC-A contoured over-the-wing nacelle with small pylon

OWC-B contoured over-the-wing nacelle with large pylon

OWS-A symmetrical over-the-wing nacelle with small pylon

## WIND TUNNEL AND MODEL SUPPORT

This investigation was conducted in the Langley 16-Foot Transonic Tunnel. This facility is a single-return, continuous-flow, atmospheric wind tunnel with a slotted octagonal test section. The slots, located at the corners of the octagon, vent the test section to a surrounding plenum to provide transonic capability. Test-section airspeed is continuously variable between Mach numbers of 0.20 and 1.30. The model was sting mounted and held near the test-section centerline at all angles of attack by the support system. Further information on the wind tunnel and model support equipment can be found in references 4 and 5.

## MODEL

This investigation was conducted on a model representative of advanced STOL transport having over-the-wing twin engines. A sketch showing the configuration with symmetrical over-the-wing nacelles is presented in figure 1(a) and with contoured over-the-wing nacelles is presented in figure 1(b). Photographs of the model sting mounted in the Langley 16-Foot Transonic Tunnel are shown in figure 2. As illustrated in figure 1, the transport configuration had a high wing, a wide body, and a T-tail. The wing had an aspect ratio of 7.52, a quarter-chord sweep of $30^{\circ}$, and a supercritical airfoil section. Details of the model, including ordinates of the airfoils for the wing and empennage surfaces, are given in reference 6.

### Nacelle-Pylon Definition

The geometric details of the three-piece, axisymmetric, flow-through nacelle are shown in figure 3. The inlet section, designated NACA 1-83-75, was designed through the use of the data of reference 7. The ratios of highlight diameter and external length (length of inlet section) to maximum nacelle diameter were 0.83 and 0.75, respectively, and the ratio of highlight area to throat area (contraction ratio) was 1.09. The center section of the nacelle provided for smooth internal lines between the inlet and the afterbody.

The nacelle afterbody had a shallow, circular-arc profile with a fineness ratio of approximately 1.87. The closure, or ratio of exit diameter to maximum diameter, was 0.70, which is representative of medium-bypass-ratio turbofan installations. The interior of the afterbody was shaped to provide a shallow, conically convergent nozzle for the internal flow. A drawing of the symmetrical pylon that was used with the axisymmetric nacelle is shown in figure 3(b).

A second nacelle-pylon arrangement was studied on this transport configuration. This nacelle-pylon arrangement (see fig. 1(b)) was contoured such that the inboard surface followed the local flow streamlines. A more detailed discussion of the methods used in contouring this nacelle is presented in the next section of this paper. A sketch of the contoured nacelle is shown in figure 4, and a cross-sectional drawing at various stations is shown in figure 5. The inlet and cylindrical sections of the contoured nacelle were identical to those of the axisymmetric nacelle. The afterbody section, the last 49 percent of the nacelle, was the only part of the nacelle that was contoured. This local shaping was accomplished by contouring the inboard surface of the nacelle while keeping the cross-sectional area of the nacelle the same as that for the axisymmetric nacelle. Two different pylons (shown in fig. 6) were studied with this contoured nacelle. Pylon A is considered to be the minimum size required to provide the necessary structure to attach a nacelle of this type to a full-scale airplane. Pylon B was tested primarily to ascertain if a larger pylon (size required if turbopower simulators were used to simulate the propulsion system) would have any significant effect on the airframe and propulsion-system integration characteristics of the configuration.

This model was heavily instrumented with 525 pressure orifices over the wings, nacelles, and pylons. (See ref. 6.) Figure 7 presents a sketch of the wings with the spanwise location of rows of pressure orifices shown, and table I presents the locations of the orifices on the nacelles.

## Nacelle Design Consideration

The Boeing Co., under contract to NASA, conducted a study which provided the local contouring for the nacelles used in this study. A detailed explanation of this design philosophy is presented in reference 8. The Boeing Co. used a generalized potential-flow program which uses panel distributions to represent the surface geometry and lifting elements. The computational design Mach number for this case was 0.70 since the extensive transonic flow at $M = 0.80$ could not be adequately simulated at the time these calculations were made. According to reference 8, as the Mach number is increased from $M = 0.70$ (the analysis condition) to $M = 0.80$ (the design condition), the wing streamlines remain essentially unchanged in the plan view. They change shape in the side view as expansion to transonic flow occurs, but the critical contours of over-the-wing nacelles are in the plan view, not the side view. Therefore, the plan-view wing streamlines generated analytically at $M = 0.70$ were used for the design of the nacelle contours at $M = 0.80$. In the actual design process the real airplane nacelle lines had to be considered. As a result, the primary design contoured the inboard surface of the nacelle to align the surface with the wing-body streamlines and let the outboard contours develop as required to provide the necessary nacelle internal volume.

## Wing Leading-Edge Extension

During the course of this study, a wing leading-edge extension was tested on the configuration. This extension, shown in figure 8, was designed in an attempt to reduce the adverse interference effects on the inboard side of the nacelle. The design philosophy for this extension is discussed in reference 9.

## TEST AND CORRECTIONS

This investigation was conducted in the Langley 16-Foot Transonic Tunnel at Mach numbers from 0.70 to 0.82 and at nominal angles of attack from $-2^{\circ}$ to $4^{\circ}$. The average Reynolds number over all test conditions was $11.88 \times 10^6$ per meter.

Boundary-layer transition was fixed on the model by 0.25-cm-wide strips of silicon carbide grit sized and positioned based on the recommendations of references 10 and 11. Number 100 grit was applied 2.54 cm behind the fuselage nose, 2.54 cm behind the leading edge of the pylon, and along a line at $x/c = 0.10$ on both the horizontal and vertical tails. Number 120 grit was applied 2.54 cm behind the nose of the tail bullet fairing, and at 0.95 cm behind the nacelle highlight on both the internal and external surfaces. Transition was fixed on the upper surface of the wing by placing a strip of no. 90 grit along a line that extended from a point at $x/c = 0.15$ at a semispan station of 0.154, through a point at $x/c = 0.25$ at the wing-break station, to a point at $x/c = 0.25$ at the wing tip. On the lower surface of the wing, a strip of no. 80 grit was placed along a line at $x/c = 0.40$.

Aerodynamic forces and moments were measured with an internal six-component strain-gage balance. Model angle of attack was obtained by correcting the angle of the model support system for deflections of the sting and balance under aerodynamic loads and for test-section flow angularity. The force data were adjusted to the conditions of free-stream static pressure at the fuselage base. Model force data with flow-through nacelles installed were corrected for the axial force produced by the internal flow in the nacelles. A value of axial-force coefficient of approximately 0.0010 (total for both nacelles), determined by measurement of the static pressure in the duct and use of these data to compute the mass flow, the duct Mach number, and finally the internal drag, was subtracted from the data.

## PRESENTATION OF RESULTS

All the aerodynamic force and moment data taken during this study are presented graphically in the figures. During this study a massive amount of pressure data was obtained, significantly more than could be presented in this paper. Therefore, only a portion of these data (those pressures at a Mach number of 0.70 and 0.80) is presented.

The major results of this investigation are presented in the following figures.


| | Figure |
|---|---|
| Aerodynamic force and moment data . . . . . | 9 |

Wing pressure distributions for the configurations with:
Symmetrical nacelles (OWS-A) at $M = 0.70$ . . . . . 10
Symmetrical nacelles (OWS-A) at $M = 0.80$ . . . . . 11
Contoured nacelles (OWC-A) at $M = 0.70$ . . . . . 12
Contoured nacelles (OWC-A) at $M = 0.80$ . . . . . 13
Contoured nacelles (OWC-B) at $M = 0.70$ . . . . . 14
Contoured nacelles (OWC-B) at $M = 0.80$ . . . . . 15

Pressure distributions for clean wing:
At $M = 0.70$, $\alpha = 1.71^{\circ}$, and $C_L = 0.48$ . . . . . 16
At $M = 0.80$, $\alpha = 1.24^{\circ}$, and $C_L = 0.49$ . . . . . 17

Pressure distributions plotted on wing planform for configuration with:
Symmetrical nacelles (OWS-A) at $M = 0.70$, $\alpha = 1.63^{\circ}$, and $C_L = 0.47$ . . . . . 18
Symmetrical nacelles (OWS-A) at $M = 0.80$, $\alpha = 1.14^{\circ}$, and $C_L = 0.45$ . . . . . 19
Contoured nacelles (OWC-A) at $M = 0.70$, $\alpha = 1.57^{\circ}$, and $C_L = 0.46$ . . . . . 20
Contoured nacelles (OWC-A) at $M = 0.80$, $\alpha = 1.12^{\circ}$, and $C_L = 0.45$ . . . . . 21
Contoured nacelles (OWC-B) at $M = 0.70$, $\alpha = 1.62^{\circ}$, and $C_L = 0.47$ . . . . . 22
Contoured nacelles (OWC-B) at $M = 0.80$, $\alpha = 1.08^{\circ}$, and $C_L = 0.45$ . . . . . 23

Effect of nacelle-pylon contouring on nacelle, pylon, and wing pressures at:
$M = 0.70$, $\alpha = 1.60^{\circ}$, and $C_L = 0.47$ . . . . . 24
$M = 0.80$, $\alpha = 1.13^{\circ}$, and $C_L = 0.45$ . . . . . 25
$M = 0.80$, $\alpha = 4.11^{\circ}$, and $C_L = 0.82$ . . . . . 26

Effect of pylon size on nacelle, pylon, and wing pressures at:
$M = 0.70$, $\alpha = 1.60^{\circ}$, and $C_L = 0.46$ . . . . . 27
$M = 0.80$, $\alpha = 1.10^{\circ}$, and $C_L = 0.45$ . . . . . 28
$M = 0.80$, $\alpha = 4.14^{\circ}$, and $C_L = 0.83$ . . . . . 29

Effect of wing leading-edge extension on nacelle, pylon, and wing pressures at $M = 0.80$, $\alpha = 0.90^{\circ}$, and $C_L = 0.44$ . . . . . 30

Drag coefficient and variation with Mach number at $C_L = 0.45$ . . . . . 31

## RESULTS AND DISCUSSIONS

The major emphasis in this investigation was to determine the effects on the aerodynamic characteristics of installing over-the-wing nacelles on a high wing transport configuration. The longitudinal force and tail-on moment characteristics

are presented in figure 9, wing pressure distributions are presented in figures 10 to 23, and nacelle, pylon, and wing pressure distributions in figures 24 to 30.

## Symmetrical Nacelles

Adding the symmetrical nacelles and pylons to the wing-body configuration significantly affects the aerodynamic characteristics of the clean-wing configuration. A reduction in lift coefficient, particularly at angles of attack from $-1^{\circ}$ to $2^{\circ}$, is evident from the data presented in figure 9. At the lowest Mach number tested ($M = 0.70$), this reduction is very small but tends to increase significantly as the Mach number increases (compare fig. 9(a) with 9(g)). These results illustrate the sensitivity of this type of nacelle-pylon arrangement to the high-speed flows which are present on the wing upper surface. The wing pressure distributions for a Mach number of 0.70 presented in figure 18 show very little response to nacelle installation except at wing semispan stations 0 and 0.154 on the wing upper surface. At these two stations, the pressure distributions indicate some increase in velocity (a decrease in pressure), probably resulting from a channeling of the flow between the nacelles and pylons. At the higher Mach numbers ($M = 0.80$ in fig. 19), adding the nacelles and pylons results in a significant increase in the local velocities on the forward portion of the wing in the area between the nacelle-pylon arrangement and the fuselage (nacelles located at $y/(b/2) = 0.250$); the data terminate in a fairly strong normal shock wave. On the outboard side of the nacelles ($y/(b/2) = 0.328$, 0.440, and 0.550), the nacelle-pylon arrangement causes a forward movement and a strengthening of the shock wave on the wing upper surface, resulting in the loss of lift shown in figure 9(e). Even though the shapes of the pressure distribution curves change significantly for the stations inboard of the nacelles, the level of lift remains essentially unchanged. The pressure distributions on the lower surface of the wing and on the outboard 25 percent of the wing upper surface show only small effects of adding the nacelles and pylons, indicating that the primary effects are confined to the wing upper surface in the area around the nacelle-pylon arrangement. As a result, no further discussion of the wing lower surface or the wing-tip region is included in this paper. The force and moment data presented in figures 9 and 31 illustrate a very large increase in drag coefficient attributable to adding the nacelles and pylons to the configuration. At a Mach number of 0.70 and a lift coefficient of 0.45, the drag increment due to the nacelles and pylons is over three times that attributed to the skin-fraction drag. The estimated skin-friction drag for the nacelle-pylon arrangement is 0.0027 (estimated with the method of ref. 12) and the experimental drag increment determined from the data of figure 9(a) is 0.0087. At a Mach number of 0.80 and a lift coefficient of 0.45, the experimental drag increment is over four times the estimated skin-friction drag. The estimated skin-friction drag for the nacelles and pylons is 0.00267 and the experimental drag increment is 0.0113. These data, of course, indicate a very large unfavorable interference drag for this type of nacelle installation. At a Mach number of 0.70, the majority of the interference drag is probably on the nacelles and pylons since there is very little difference in the pressure distributions between the clean wing and the wing with the symmetrical nacelles. (See fig. 18.) As indicated earlier, the pressure distributions on the wing show some increase in velocity over the forward portion of the wing, particularly inboard of the nacelle. Even though this flow is supersonic ($C_{p,s} = -0.78$ for $M = 0.70$), there do not appear to be large effects due to the nacelles.

The pressure distributions on the symmetrical nacelles and pylons for $M = 0.70$ are presented in figures 24(a) and 24(b). At nacelle radial stations of $150^{\circ}$ and $210^{\circ}$ and on the pylon there is a significant velocity increase (supersonic flow) in the area just behind the wing leading edge. This result indicates that this velocity increase is due to a local channeling of the flow in this area. These high negative pressures acting on the nacelle boattails and pylons (aft-facing area), along with what appears to be flow separation primarily on the outboard side of the pylon, appear to be the major contributors to the high level of interference drag. At a Mach number of 0.80 (see figs. 25(a) and 25(b)), the flow characteristics are very similar to those illustrated by the data at a Mach number of 0.70 except that the negative pressures are greater, the areas of flow separation are more extensive, and the shock-induced effects are stronger.

Adding the symmetrical nacelles and pylons resulted in a significant nose-up increment in the pitching-moment coefficient at a constant lift coefficient, with a small decrease in the stability level. (See fig. 9.) This effect is expected since the lift and drag of the nacelle-pylon arrangement are acting above and ahead of the aircraft moment center.

## Contoured Nacelles

Contouring the nacelles and pylons had very little effect on the lift characteristics of the configuration, particularly at the lower Mach numbers and the lower angles of attack. (Compare configuration OWS-A with OWC-A in fig. 9(a).) At $M = 0.78$ to 0.80 (see figs. 9(c) to 9(e)), some effect on lift is indicated at angles of attack above approximately $2^{\circ}$. The most dramatic effect of nacelle-pylon contouring is shown in the drag-coefficient characteristics. (See fig. 31.) Contouring the nacelles and pylons significantly reduces the drag penalty associated with the nacelle installation. For example, at a Mach number of 0.70, the drag-coefficient reduction because of contouring for a lift coefficient of 0.45 is about 0.0018, whereas for a Mach number of 0.80 the reduction is about 0.0034.

As indicated in the model section, the local contouring of the nacelles was accomplished primarily to align the inboard surfaces of the nacelles and pylons with the local flow angle, thereby reducing the local disturbances in the region between the nacelles. The data of figure 20 for $M = 0.70$ do illustrate the reduction in velocity on the inboard sides of the nacelles ($y/(b/2) = 0$ and 0.154); however, the general characteristics of the flow are essentially the same for both nacelle-pylon arrangements. On the outboard side of the nacelle there is an increase in the local velocities (higher negative pressure coefficients) around the wing leading edge but very little difference in the characteristics of the flow except at a wing semispan station of 0.328, where this velocity increase terminates in a strong shock wave and possibly some flow separation. Although this increased suction pressure around the wing leading edge probably reduces the wing drag due to lift, the stronger shock waves and flow separation probably have a detrimental effect on the drag-coefficient characteristics.

At a Mach number of 0.80, the effects of nacelle-pylon contouring are quite similar to the results that occurred at the lower Mach number but of larger magnitudes. (Compare fig. 21(a) with 20(a).) At the sections inboard of the nacelles, the pressure data show a fairly significant loss in lift (i.e., a reduction in negative pressure coefficients). This loss of lift naturally causes an increase in

drag since the angle of attack would have to be increased to achieve the same lift coefficient as with the symmetrical nacelle. On the outboard side of the nacelles, the shock wave present at the wing leading edge has increased in strength and moved forward on the wing. It is not fully known whether the combined effect of increased leading-edge pressures, formation of a stronger shock wave, and more forward location of the shock wave is beneficial.

The effect of nacelle-pylon contouring on the nacelle-pylon pressures at the cruise lift coefficient of about 0.45 is presented for a Mach number of 0.70 in figure 24 and for a Mach number of 0.80 in figure 25. At both Mach numbers, contouring reduces the pressure coefficients on the inboard side of the nacelle. The velocities, however, are still supersonic, particularly at the stations around the lower part of the nacelles, where significant channeling of the flow would be expected. On the outboard side of the nacelle only small effects are noted. Again, the local velocities on the nacelle are supersonic, particularly at nacelle radial stations of $210^{\circ}$ and $270^{\circ}$. The method of contouring reduced the nacelle-pylon local slopes on the inboard side and increased them on the outboard side. In fact, the inboard contouring resulted in forward-facing surfaces on portions of the nacelle afterbody. This reduction in local slopes coupled with the decrease in local velocities on the inboard side of the nacelle results in the drag reduction indicated in figure 9. On the outboard side, the high negative pressure acting on the increased aft-facing areas of the nacelle indicates a high level of pressure drag, which may be reduced with a redesign of the nacelle. Contouring the pylon appears to have an adverse effect on the local flow characteristics around the pylon. As shown in figures 24(a) and 25, contouring the pylon does not reduce the local velocities; in fact, there appears to be an increase in the local velocities for a Mach number of 0.70 shown in figure 24(a). In addition, there appears to be a large area of flow separation on the pylon occurring at a fuselage station of approximately 72.5 cm. Although these flow characteristics result in a reduction in the drag coefficient, it is still evident that by careful design a further reduction of considerable magnitude is possible.

## Nacelle Pylon

In this study, two pylon sizes were tested. (See fig. 6.) The smaller pylon (pylon A) was envisioned to be the minimum size required to provide the structural support necessary for a full-scale engine nacelle. The larger pylon (pylon B) was designed to provide a housing for instrumentation and air lines necessary to incorporate a turbopower simulator in this nacelle. The data of figure 9 (compare OWC-A with OWC-B) show that increasing the size of the pylon had only a small effect on the lift coefficient and the pitching-moment coefficient for the configuration. The drag-coefficient data show that at a lift coefficient of 0.45, increasing the pylon size reduces the drag coefficient by about 0.0008 for a Mach number of 0.70 and by about 0.0011 for a Mach number of 0.80. The exact mechanism responsible for this drag reduction is not known. However, the pressure data for Mach numbers of 0.70 (figs. 20 for OWC-A and 22 for OWC-B) and 0.80 (figs. 21 for OWC-A and 23 for OWC-B) indicate that the larger pylon causes a reduction in the velocity of the local flow on the pylon and on the lower part of the nacelle. This reduction in velocity (reduction of the high negative pressure coefficients) must cause a reduction in the pressure drag of this nacelle-pylon arrangement.

## Wing Leading-Edge Extension

In an attempt to reduce the interference drag for this over-the-wing nacelle installation, a theoretical study was conducted in which a small-disturbance approximation with the Bailey-Balhaus finite-difference relaxation algorithm was used. (Results are reported in ref. 9.) This study was primarily aimed at reducing the supersonic flow on the inboard side of the nacelle, which could be accomplished by thinning the wing section or changing the local wing contours. Since the model was constructed of steel, it would have been very difficult to modify the wing sections; therefore, it was decided to thin the wing and alter the velocity distribution by adding an extension to the wing leading edge. As shown in reference 9 and in figure 8 of this report, the extension was added to the wing leading edge on the inboard side of the nacelle. This extension should result in a decrease in local wing-flow-field velocities not only by decreasing the wing thickness ratio but also by reducing the local wing leading-edge radius. In addition, the extension was also drooped slightly in an attempt to take advantage of the large negative pressures around the leading edge, thus providing thrust and reducing the drag coefficients.

Selected results of this study are presented in figure 30 as the pressure distributions over the wing, nacelles, and pylons near the cruise conditions ($M = 0.80$ at $C_L \approx 0.45$). The results indicate that adding the extension reduces the drag coefficient by about 0.0003 (unpublished data) at these conditions. The pressure distributions presented in figure 30(b) show that adding the leading-edge extension on the inboard side of the nacelle does not alter the pressure distributions on the outboard side of the nacelle as you would expect. On the inboard side of the nacelle, adding the leading-edge extension slightly reduces the local velocities and slightly decreases the strength of the local shock waves. These effects are evidently very small because the drag reduction is also small. These results may not be unexpected because the local slopes of the wing, pylons, and nacelles in this area are very small. These results also indicate that the primary source of the interference effects of the over-the-wing nacelle-pylon arrangement is attributable to the loss in lift on the wing and to a high-pressure drag on the outboard side of the nacelle.

## CONCLUDING REMARKS

A study has been conducted to determine the effects on the aerodynamic characteristics of a high-wing transport configuration of installing an over-the-wing nacelle-pylon arrangement. As a result of this study, the following conclusions can be drawn:

1. Adding symmetrical nacelles and pylons to the configuration caused a reduction in the lift coefficient, a significant increase in the drag coefficient, and a nose-up pitching-moment-coefficient increment.

2. Contouring the nacelles and pylons significantly reduced the interference drag for the configuration. Even with this reduction, the interference drag for the over-the-wing nacelle was excessive.

3. Increasing the size of the pylons decreased the local velocities around the pylon and the lower part of the nacelle and thus resulted in a reduction in the drag coefficient of about 0.0011 at a Mach number of 0.80.

4. Adding the wing leading-edge extension did not significantly alter the aerodynamic characteristics for the over-the-wing nacelle-pylon arrangement.

NASA Langley Research Center
Hampton, VA 23665-5225
July 10, 1985

## REFERENCES


1. Henderson, William P.; and Patterson, James C., Jr.: Propulsion Installation Characteristics for Turbofan Transports. AIAA-83-0087, Jan. 1983.

2. Reubush, David E.: Effect of Over-the-Wing Nacelles on Wing-Body Aerodynamics. J. Aircr., vol. 16, no. 6, June 1979, pp. 359-365.

3. Bangert, L. H.; Krivec, D. K.; and Segall, R. N.: Effects of Nacelle Configuration/Position on Performance of Subsonic Transport. NASA CR-3743, 1983.

4. Corson, Blake W., Jr.; Runckel, Jack F.; and Igoe, William B.: Calibration of the Langley 16-Foot Transonic Tunnel With Test Section Air Removal. NASA TR R-423, 1974.

5. Peddrew, Kathryn H., compiler: A User's Guide to the Langley 16-Foot Transonic Tunnel. NASA TM-83186, 1981.

6. Lee, Edwin E., Jr.; and Pendergraft, Odis C., Jr.: Installation Effects of Long-Duct, Pylon-Mounted Nacelles on a Twin-Jet Transport Model With Swept, Supercritical Wing. NASA TP-2457, 1985.

7. Re, Richard J.: An Investigation of Several NACA 1-Series Axisymmetric Inlets at Mach Numbers From 0.4 to 1.29. NASA TM X-2917, 1974.

8. Gillette, W. B.: Nacelle Installation Analysis for Subsonic Transport Aircraft. AIAA Paper 77-102, Jan. 1977.

9. Wai, J. C.; Sun, C. C.; and Yoshihara, H.: Transonic Perturbation Analysis of Wing-Fuselage-Nacelle-Pylon Configurations With Powered Jet Exhausts. NASA CR-165852, 1982.

10. Braslow, Albert L.; Hicks, Raymond M.; and Harris, Roy V., Jr.: Use of Grit-Type Boundary-Layer-Transition Trips on Wind-Tunnel Models. NASA TN D-3579, 1966.

11. Blackwell, James A., Jr.: Preliminary Study of Effects of Reynolds Number and Boundary-Layer Transition Location on Shock-Induced Separation. NASA TN D-5003, 1969.

12. Shapiro, Ascher H.: The Dynamics and Thermodynamics of Compressible Fluid Flow. Volume II. Ronald Press Co., c.1954.

TABLE I.- LOCATION OF PRESSURE ORIFICES ON NACELLES

| x, cm | Orifices present for $\phi$, deg, of - | | | | | | | |
|---|---|---|---|---|---|---|---|---|
| | 0 | 30 | 90 | 150 | 180 | 210 | 270 | 330 |
| 0.51 | × | | × | | × | | × | |
| 1.78 | × | | × | | × | | × | |
| 3.05 | × | | | | | | | |
| 3.81 | | × | × | | × | | × | × |
| 5.84 | | × | × | | × | | × | × |
| 7.87 | | × | × | | × | | × | × |
| 11.43 | × | | | | | | | |
| 11.68 | | | × | × | | × | × | |
| 13.72 | | | × | × | | × | × | |
| 14.99 | × | | | | | | | |
| 15.75 | | | × | × | | × | × | |
| 18.03 | × | | × | × | | × | × | |
| 20.60 | × | | × | × | | × | × | |
| 23.14 | × | | × | × | | × | × | |
| 25.68 | × | | × | × | | × | × | |
| 27.20 | × | | × | × | | × | × | |
| 28.98 | × | | × | × | | × | × | |
| 30.76 | × | | × | × | | × | × | |
| 32.54 | × | | × | × | | × | × | |
| 34.32 | × | | × | × | | × | × | |
| 36.09 | × | | × | × | | × | × | |
| 37.87 | × | | × | × | | × | × | |
| 39.40 | × | | × | × | | × | × | |

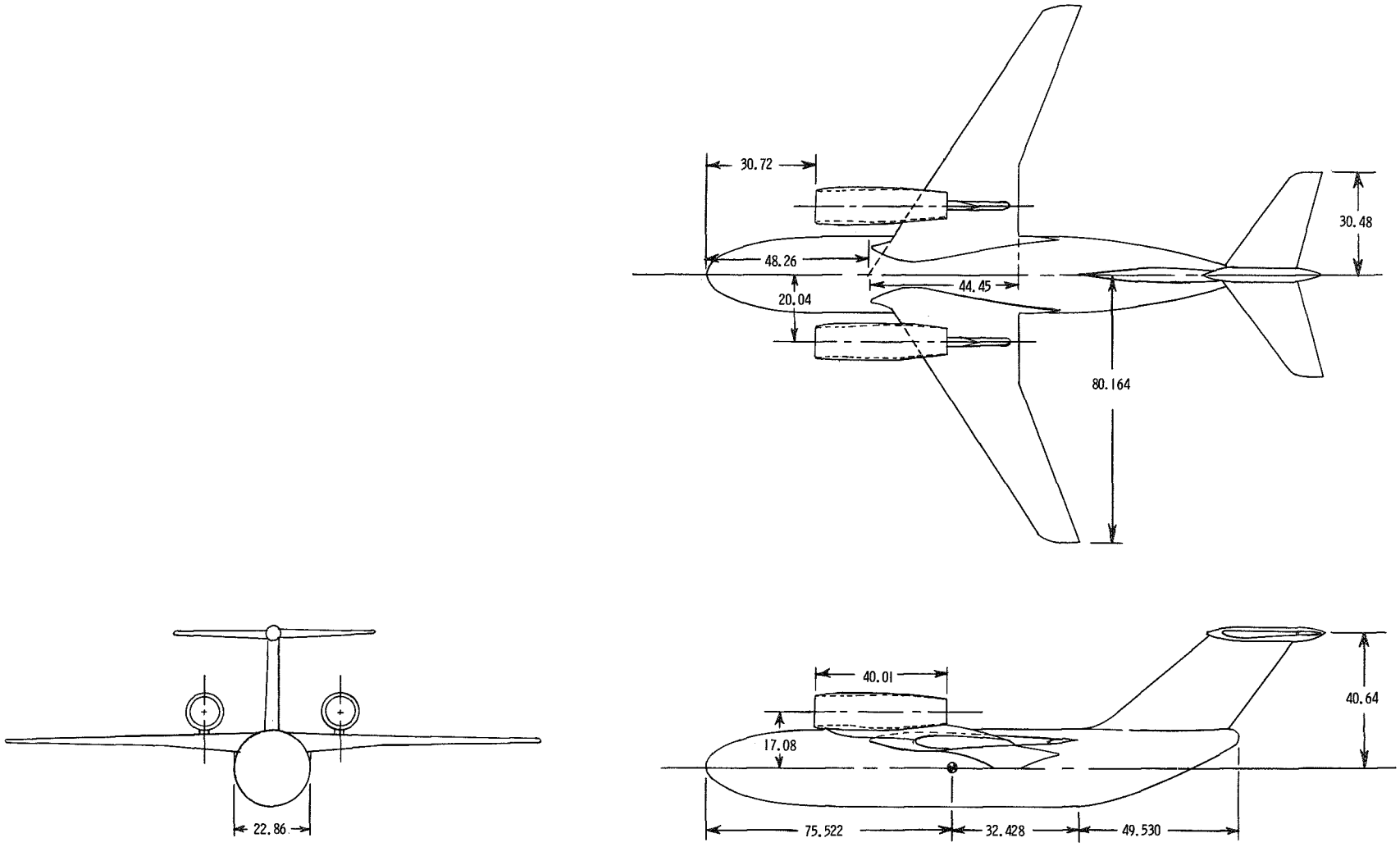


(a) Symmetrical over-the-wing nacelle-pylon arrangement.

Figure 1.- Three-view drawing of configuration tested. Linear dimensions are in centimeters.

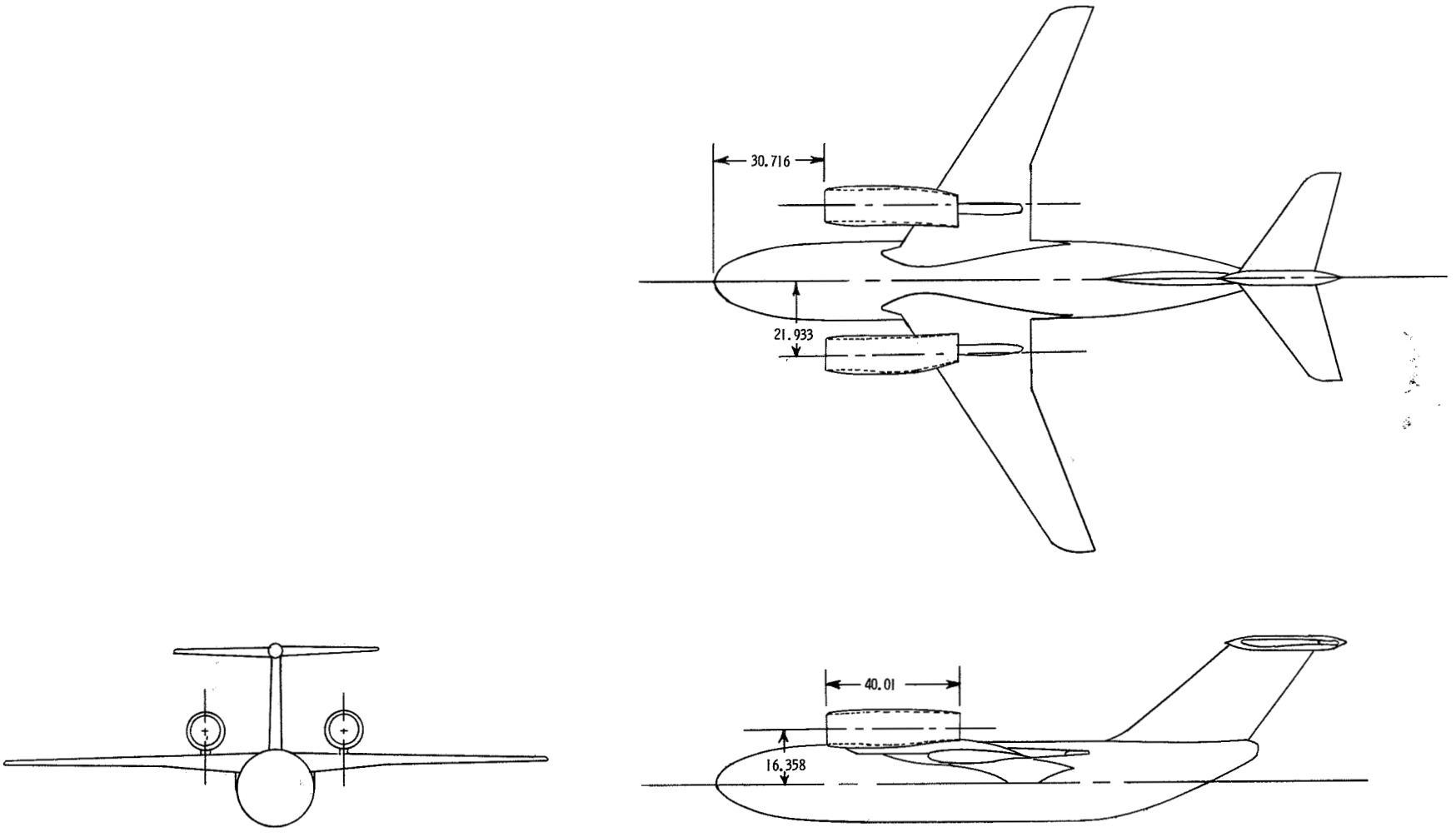


(b) Contoured over-the-wing nacelle-pylon arrangement.

Figure 1.- Concluded.

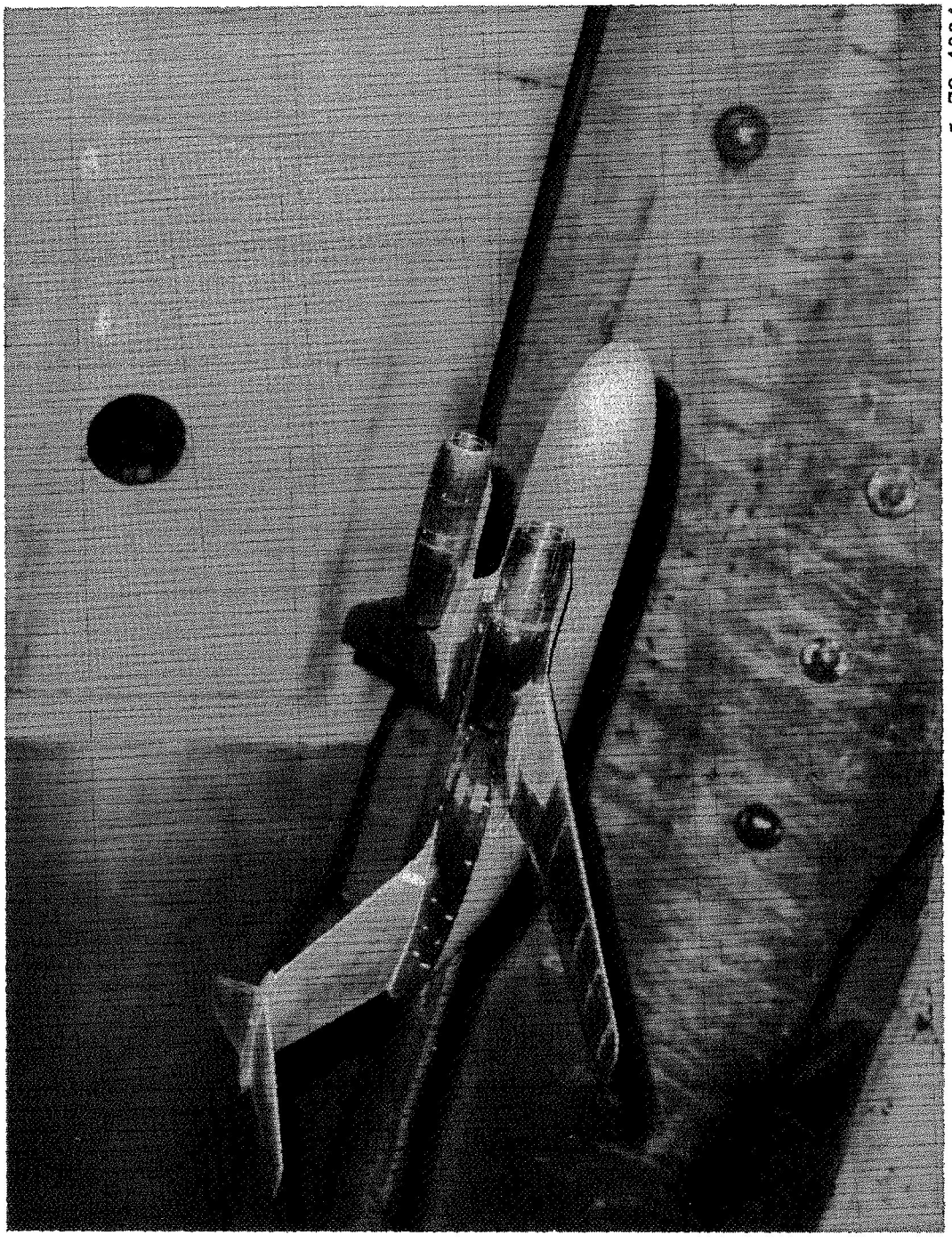

L-79-4004

Figure 2.- Model in Langley 16-Foot Transonic Tunnel.

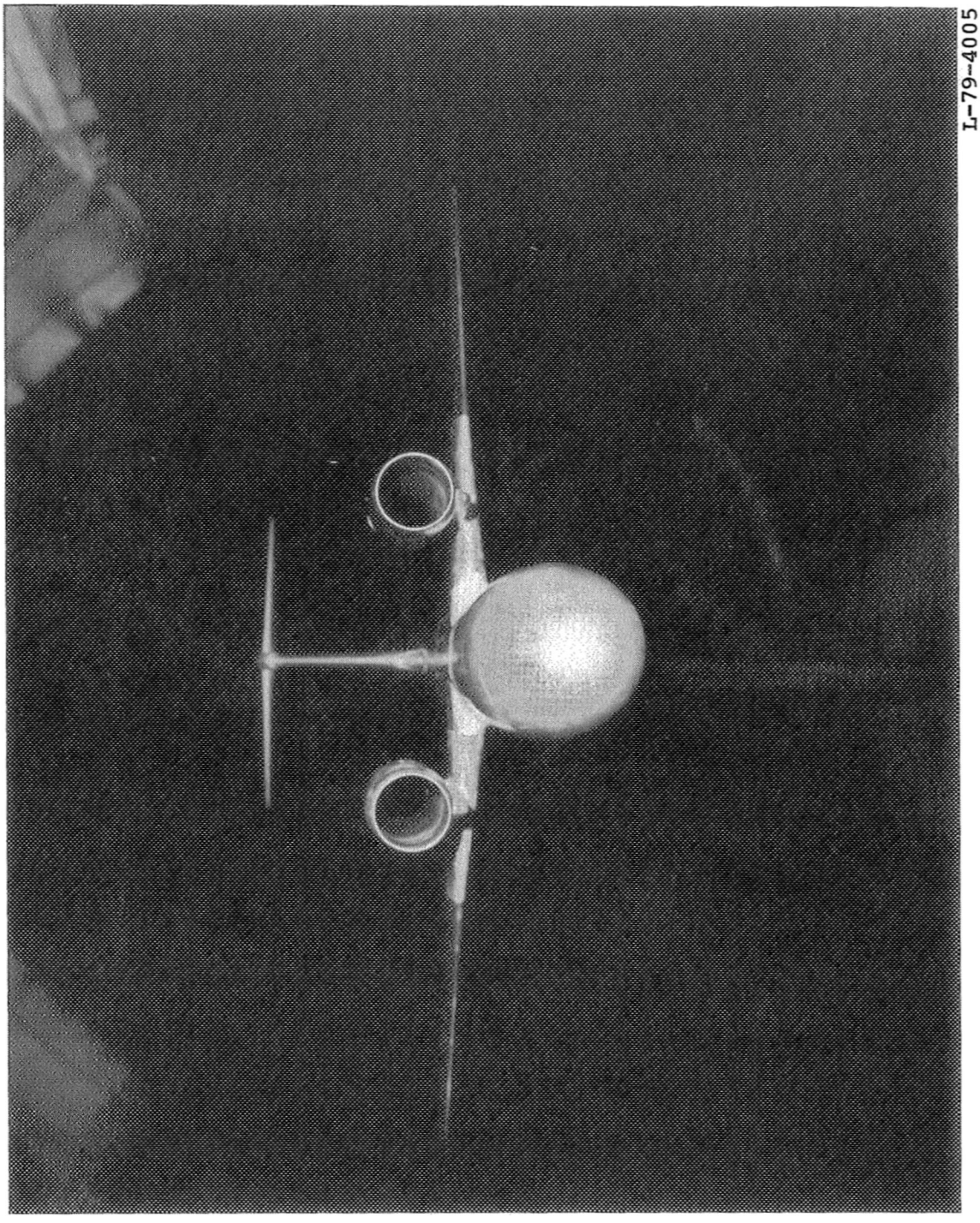

L-79-4005

Figure 2.- Continued.

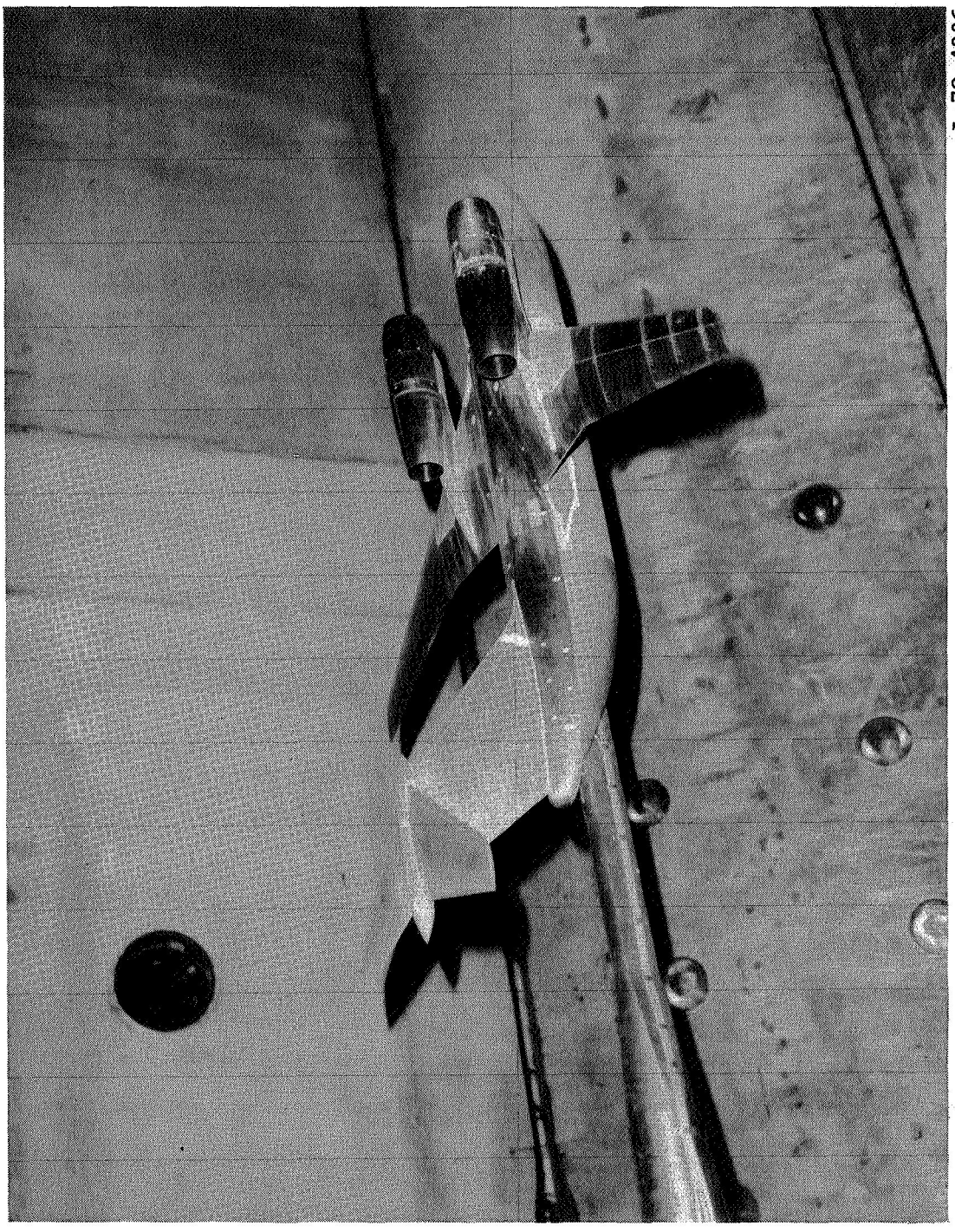

L-79-4006

Figure 2.- Concluded.

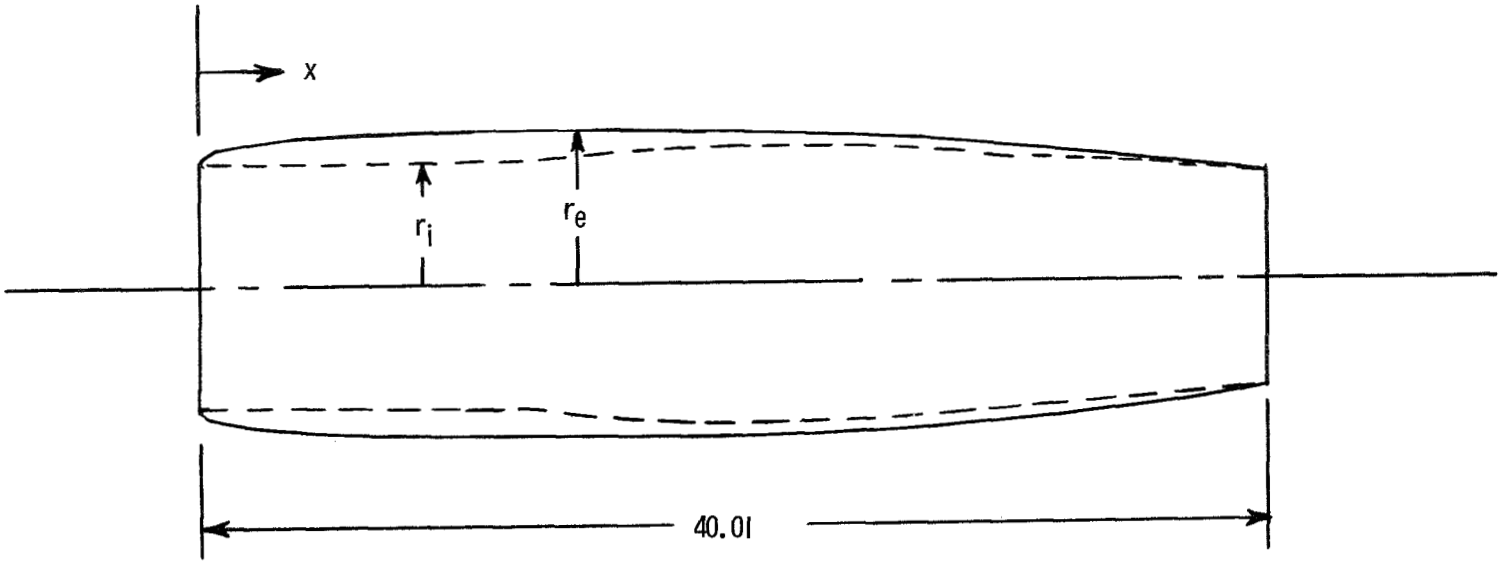


| x, cm | $r_e$, cm | $r_i$, cm | x, cm | $r_e$, cm | $r_i$, cm |
|---|---|---|---|---|---|
| 0.130 | 4.882 | 4.608 | 6.858 | 5.690 | 4.559 |
| .257 | 4.935 | 4.569 | 7.717 | 5.710 | 4.559 |
| .429 | 4.994 | 4.559 | 8.573 | 5.715 | 4.559 |
| .599 | 5.042 | ↓ | 9.749 | ↓ | 4.577 |
| .859 | 5.105 | ↓ | 10.922 | ↓ | 4.628 |
| 1.285 | 5.192 | ↓ | 12.098 | ↓ | 4.699 |
| 1.715 | 5.263 | ↓ | 13.272 | ↓ | 4.788 |
| 2.144 | 5.324 | ↓ | 14.448 | ↓ | 4.884 |
| 2.570 | 5.380 | ↓ | 15.621 | ↓ | 4.978 |
| 3.000 | 5.431 | ↓ | 16.797 | ↓ | 5.067 |
| 3.429 | 5.474 | ↓ | 17.971 | ↓ | 5.138 |
| 3.858 | 5.514 | ↓ | 19.147 | ↓ | 5.189 |
| 4.288 | 5.550 | ↓ | 20.320 | ↓ | 5.207 |
| 5.144 | 5.611 | ↓ | 25.362 | ↓ | 5.207 |
| 5.999 | 5.657 | ↓ | 40.005 | 4.077 | 4.001 |

(a) Axisymmetric nacelle.

Figure 3.- Geometric details for symmetrical nacelle-pylon arrangement. Dimensions are in centimeters.

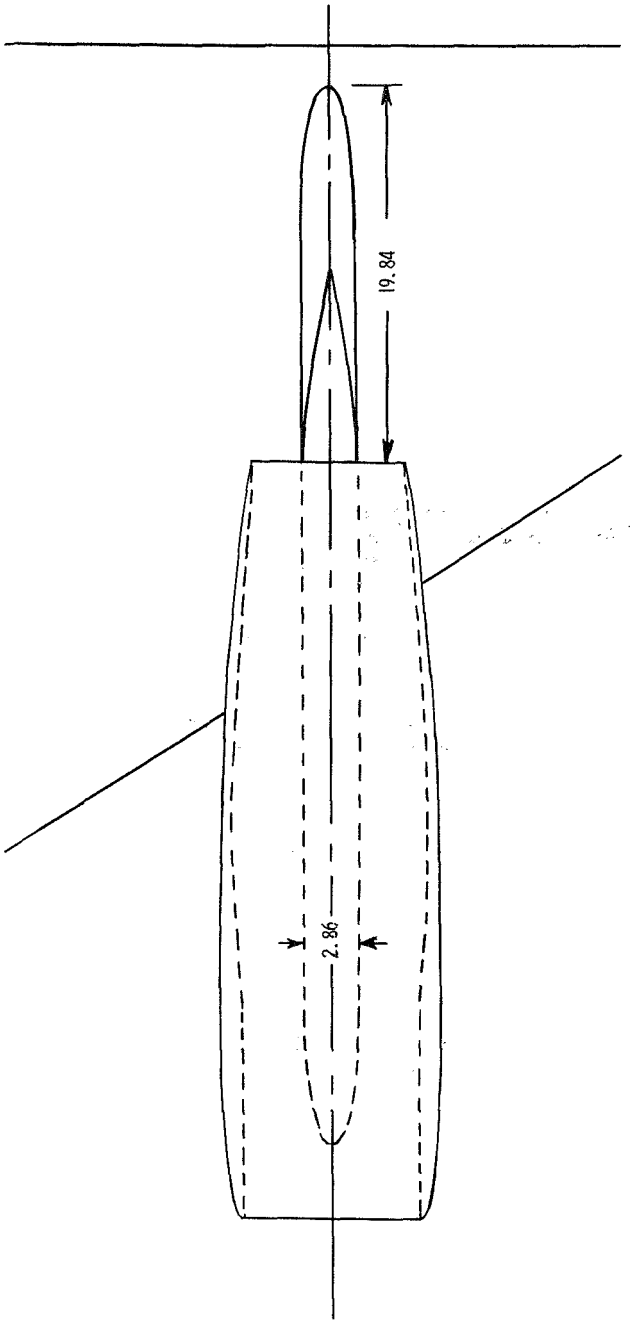


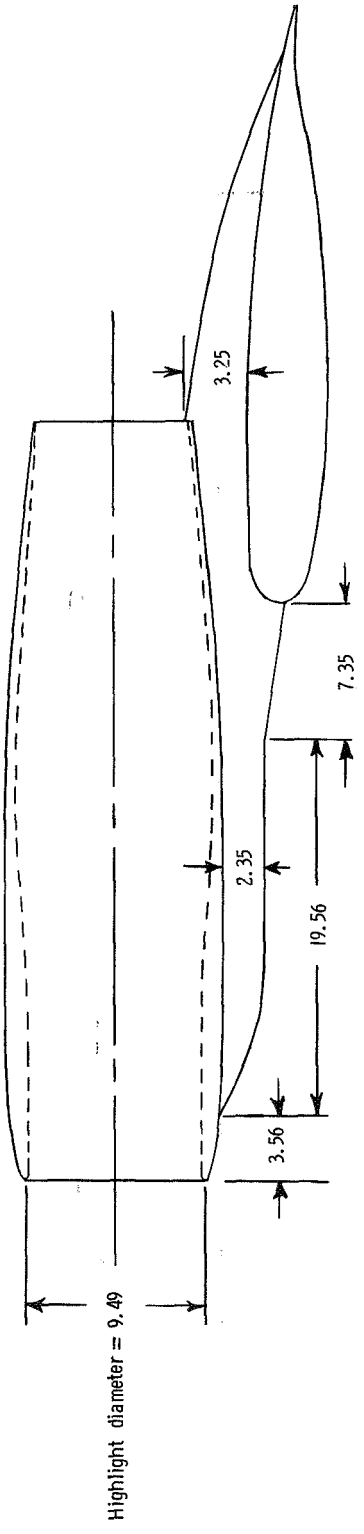


(b) Symmetrical pylon.

Figure 3.- Concluded.

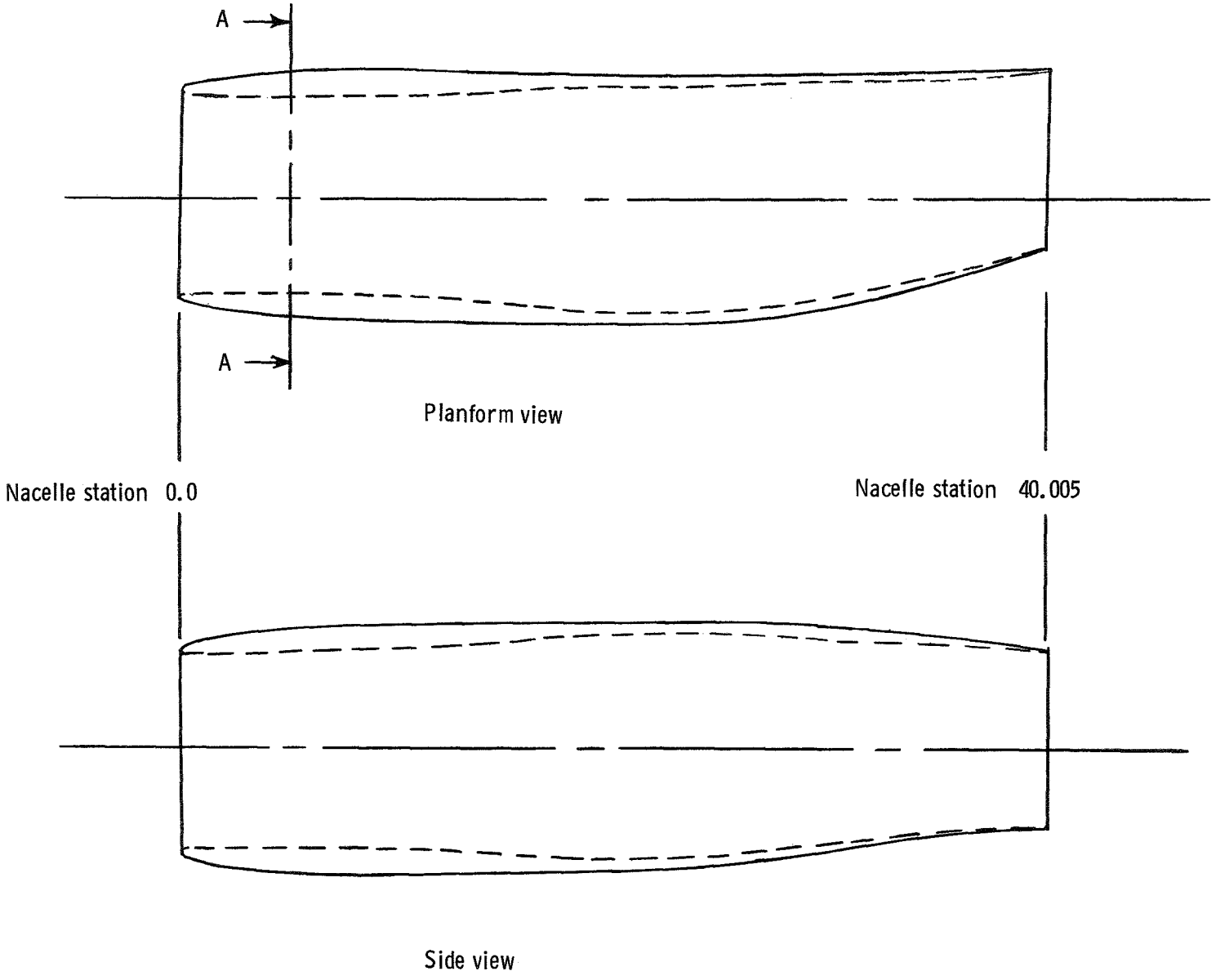


Figure 4.- Details of contoured nacelles.

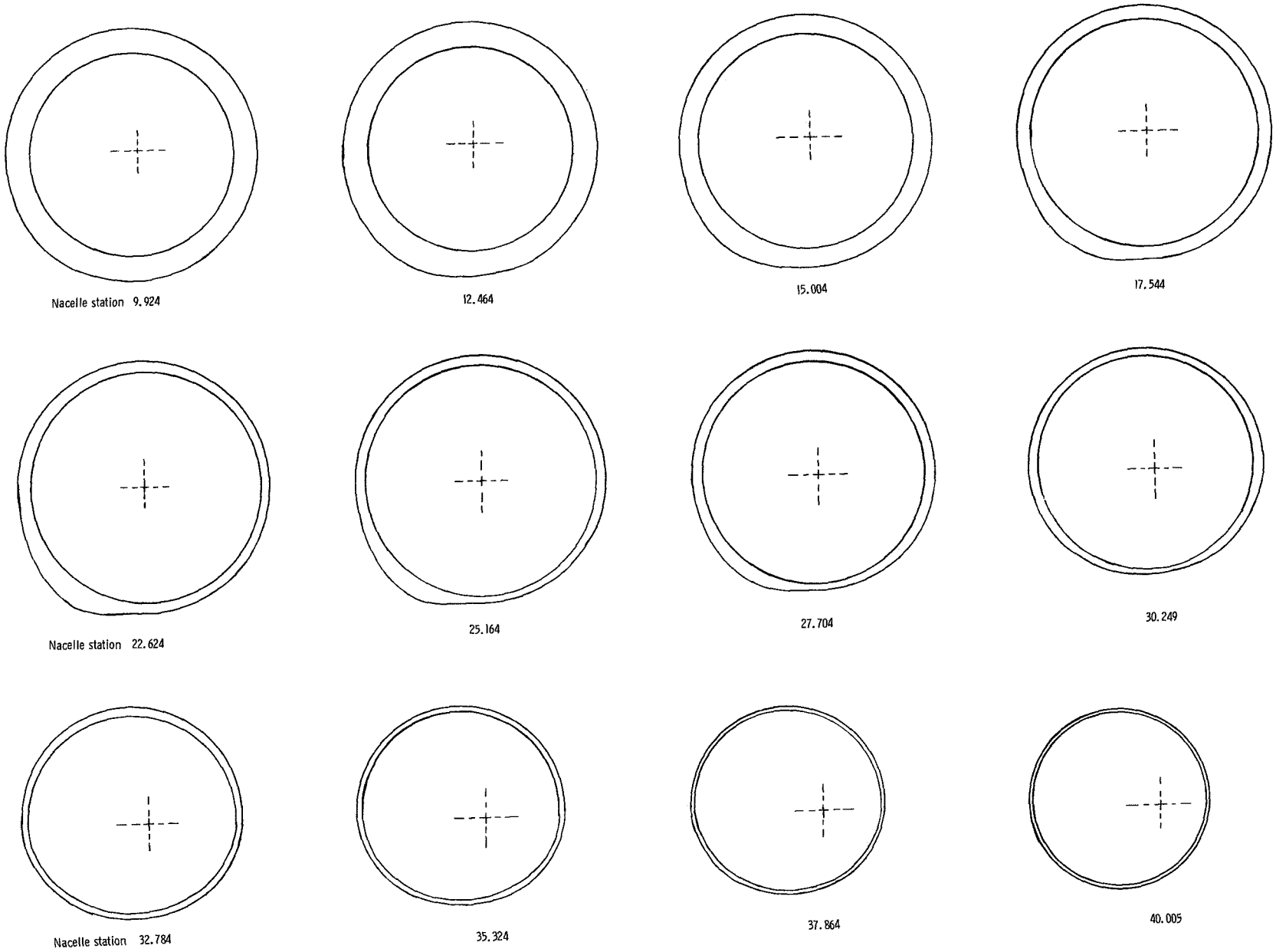


Figure 5.- Cross sections of contoured nacelles.

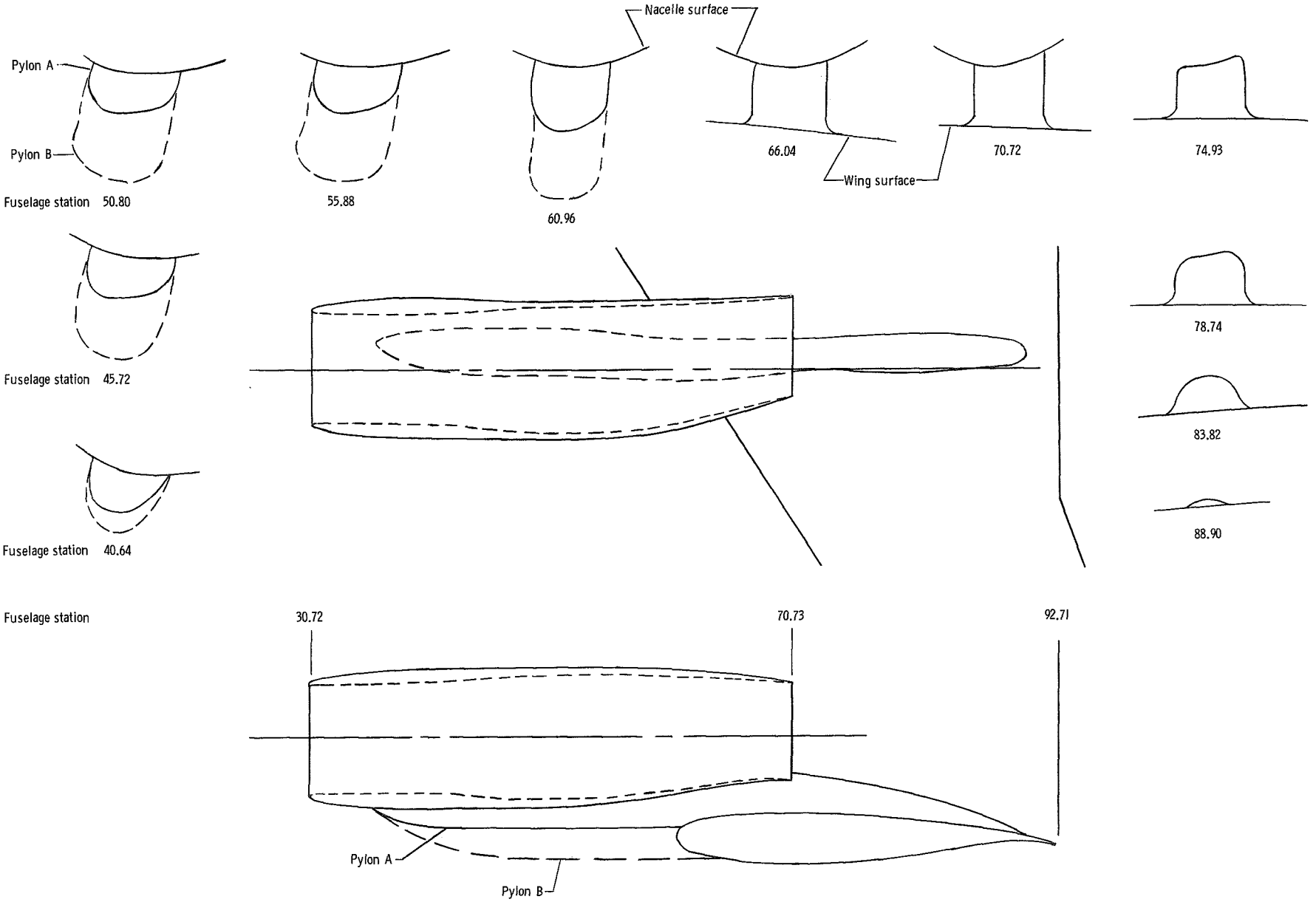


Figure 6.- Details of contoured pylons. Linear dimensions are in centimeters.

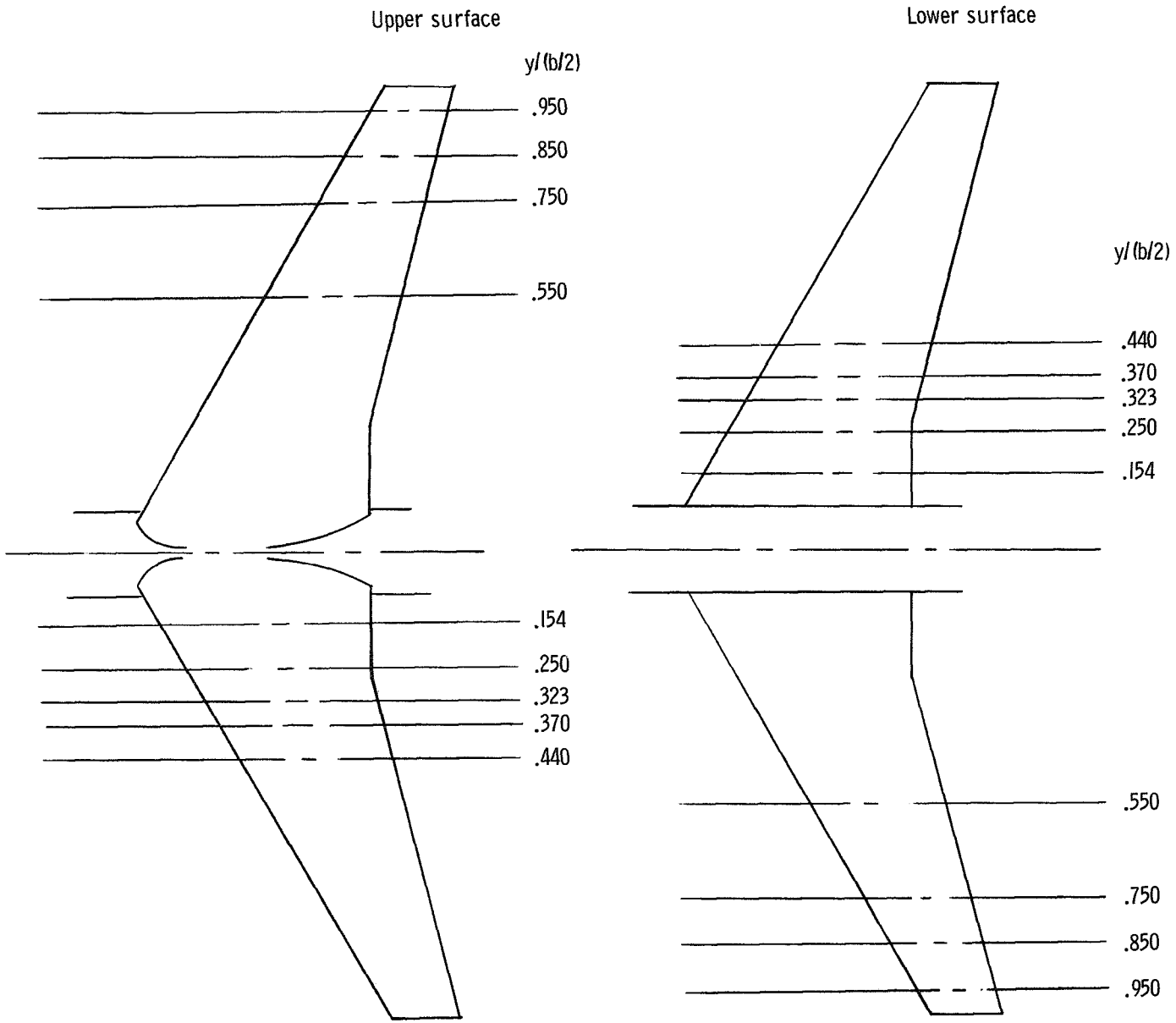


Figure 7.- Locations of pressure orifices on wings.

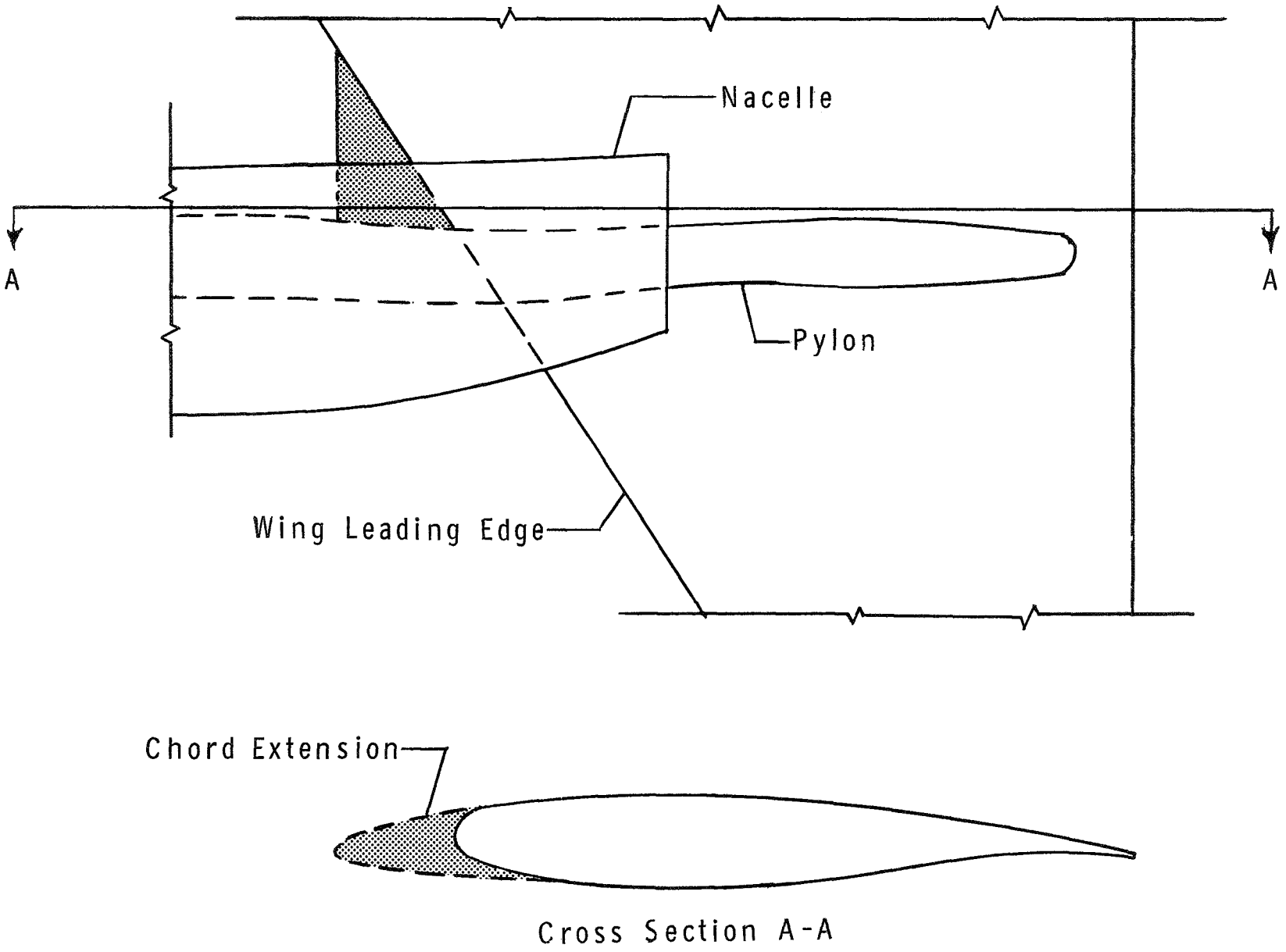


Figure 8.- Wing leading-edge modification for contoured nacelle-pylon arrangement.

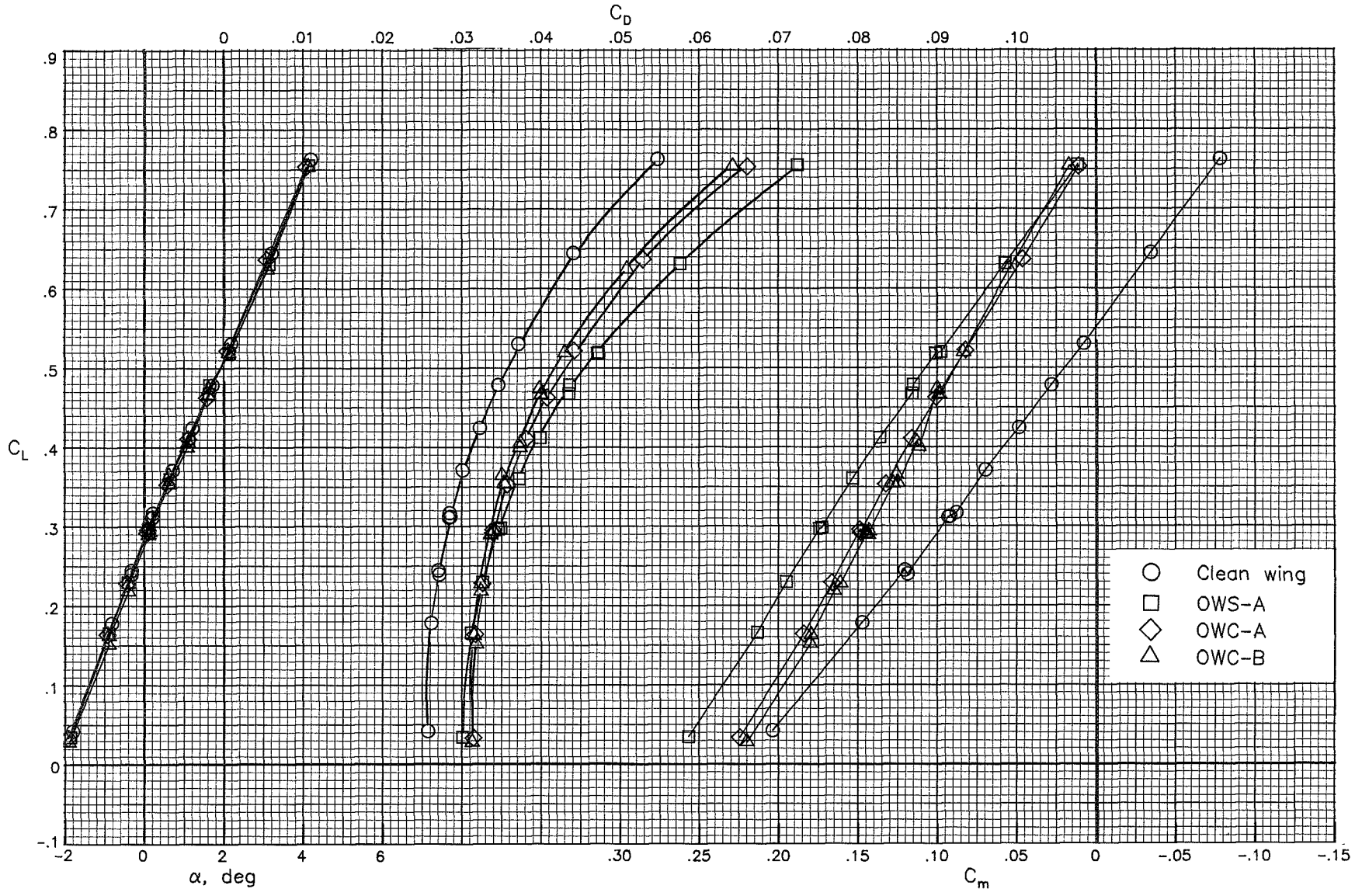


(a) M = 0.70.

Figure 9.- Effect of nacelle contouring and pylon shape on aerodynamic characteristics.

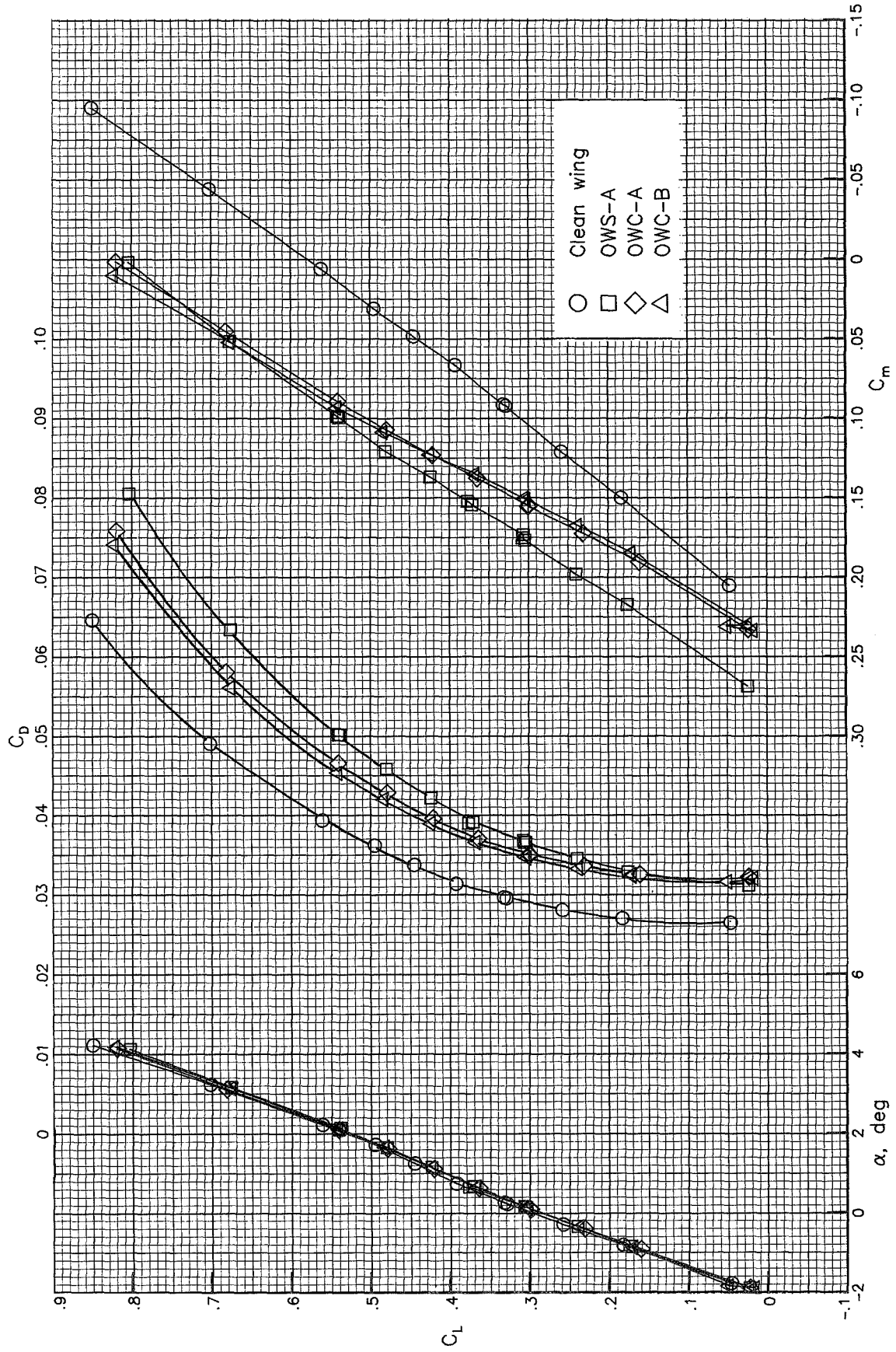


(b) M = 0.75.

Figure 9.- Continued.

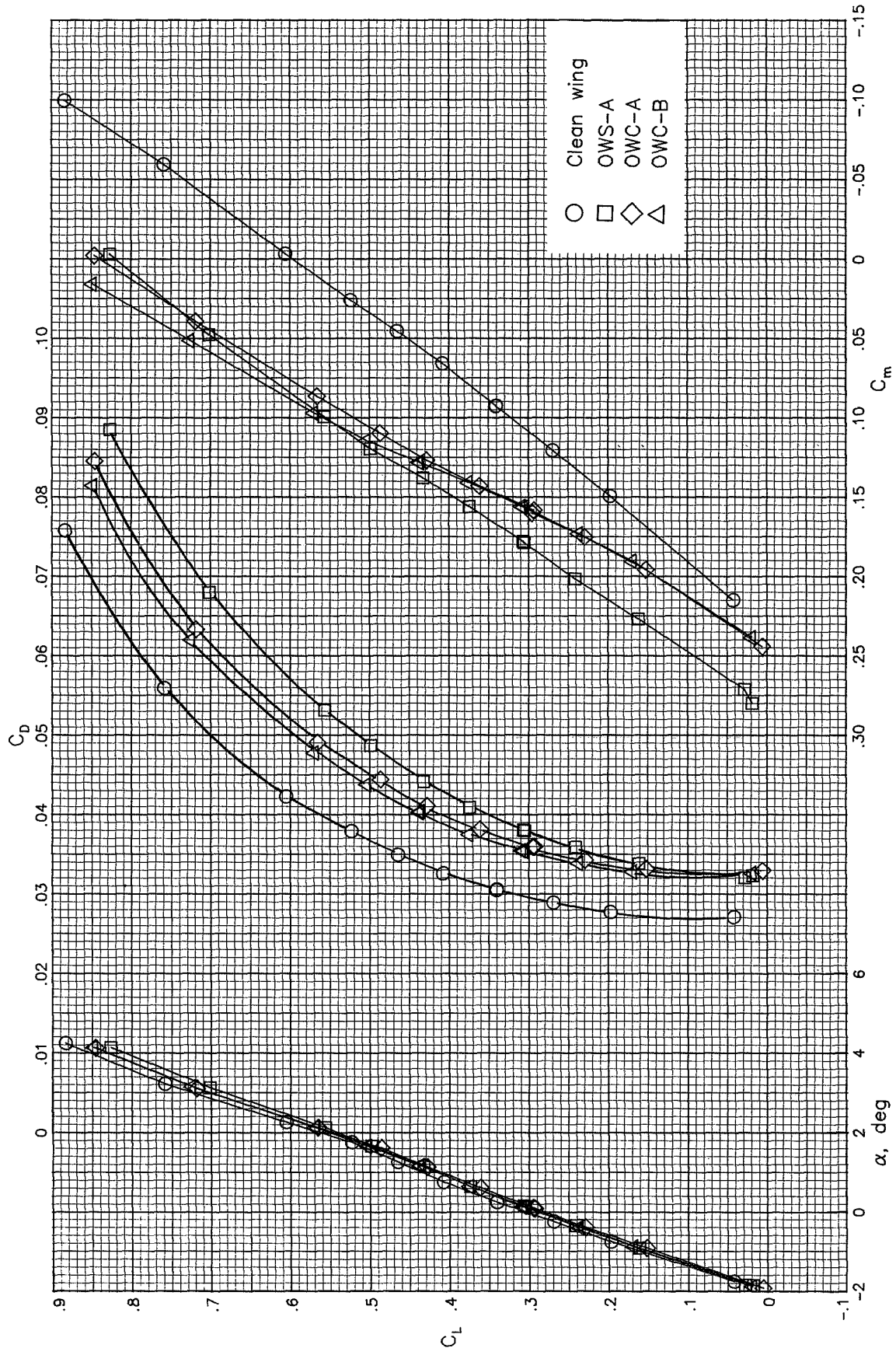


(c) M = 0.78.

Figure 9.- Continued.

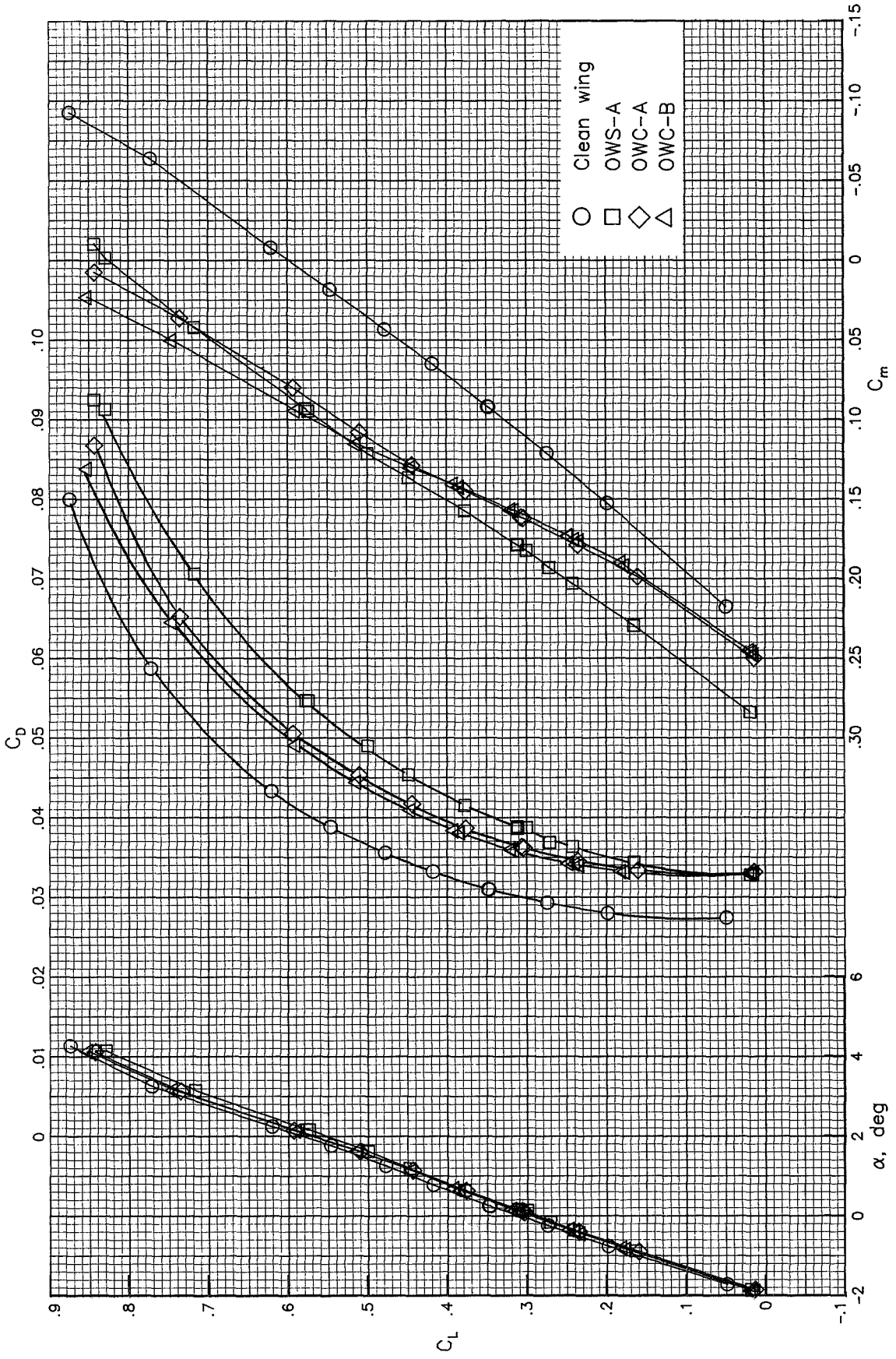


(d) M = 0.79.

Figure 9.- Continued.

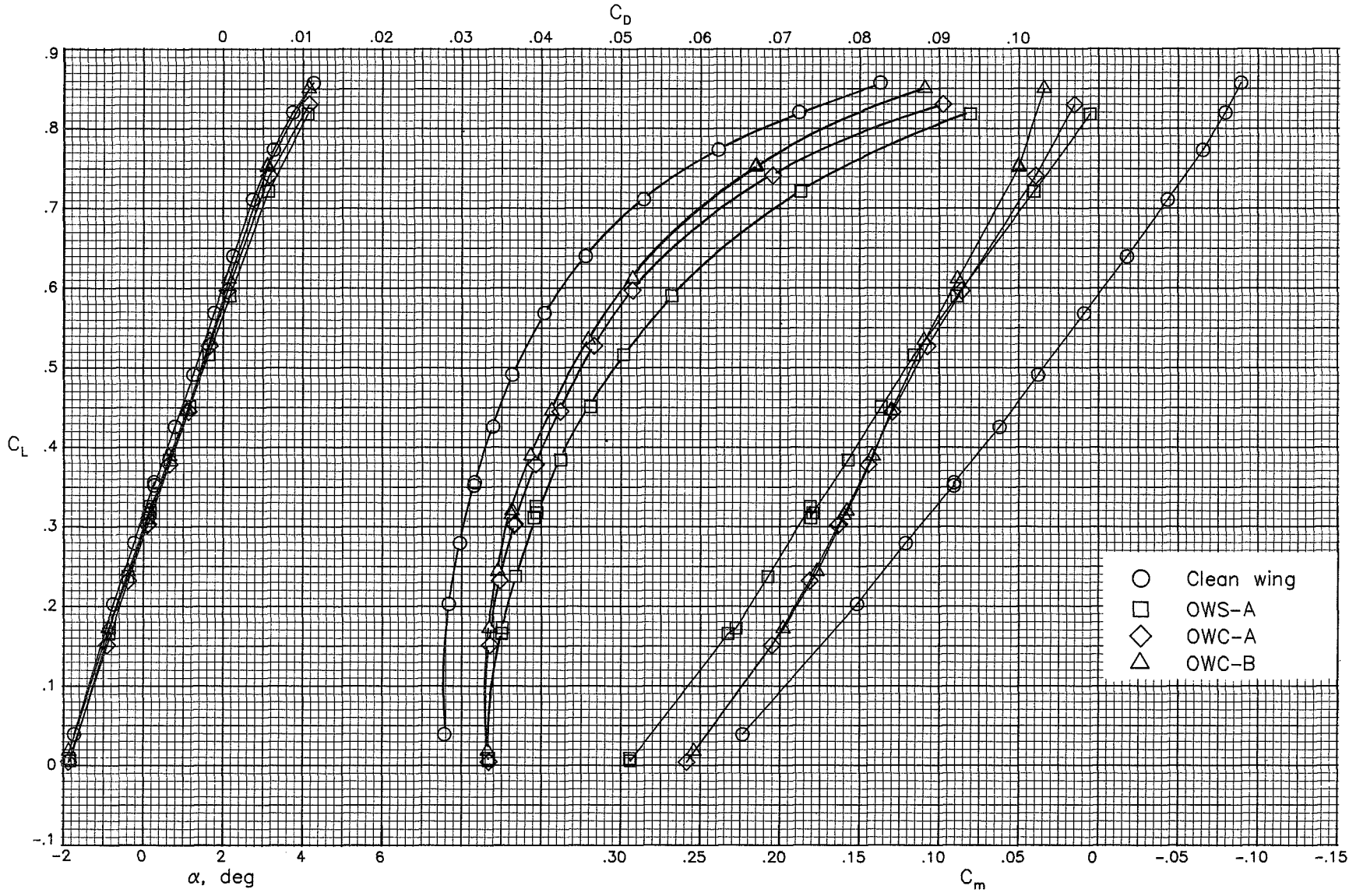


(e) M = 0.80.

Figure 9.- Continued.

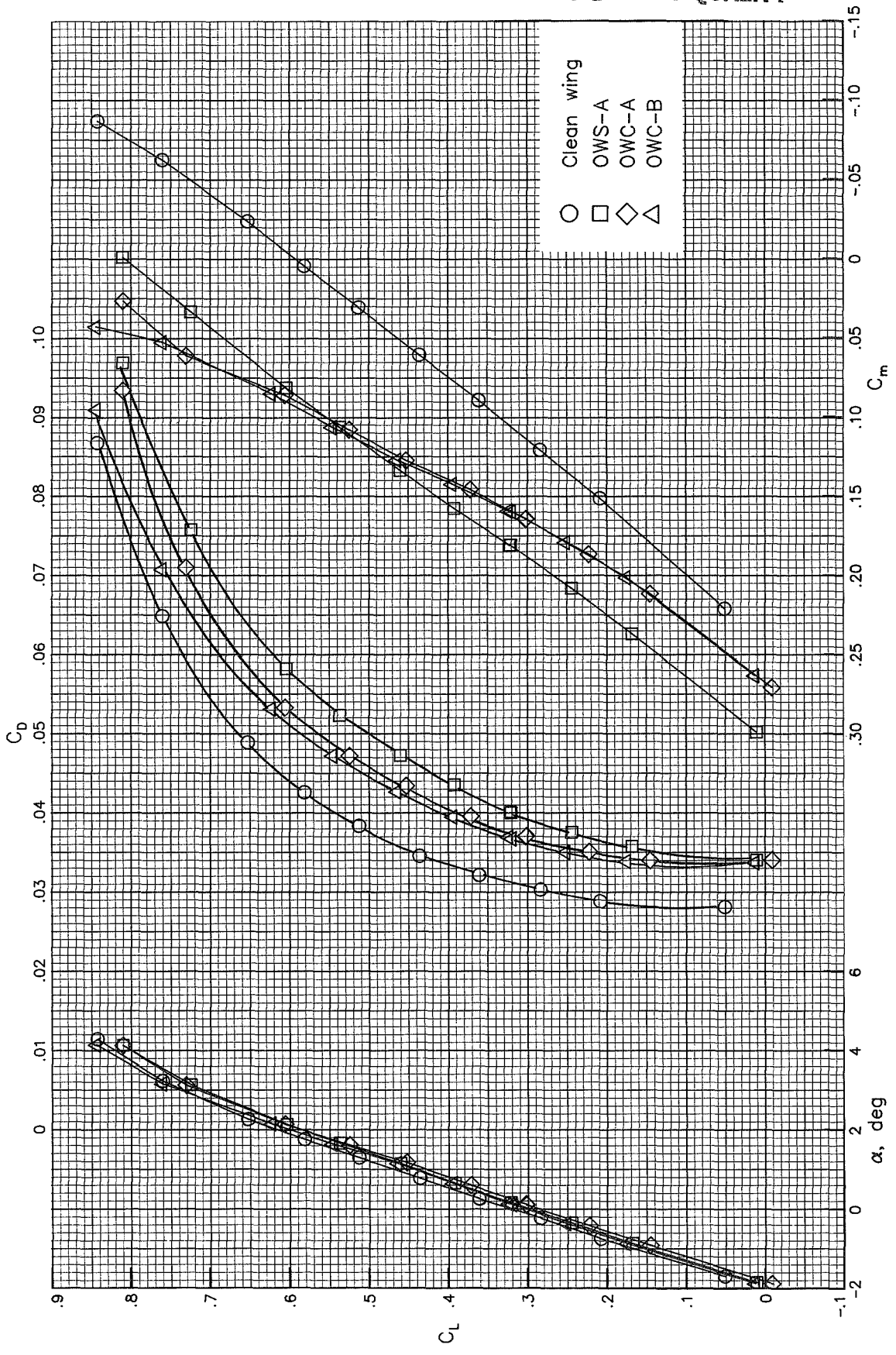


(f) M = 0.81.

Figure 9.- Continued.

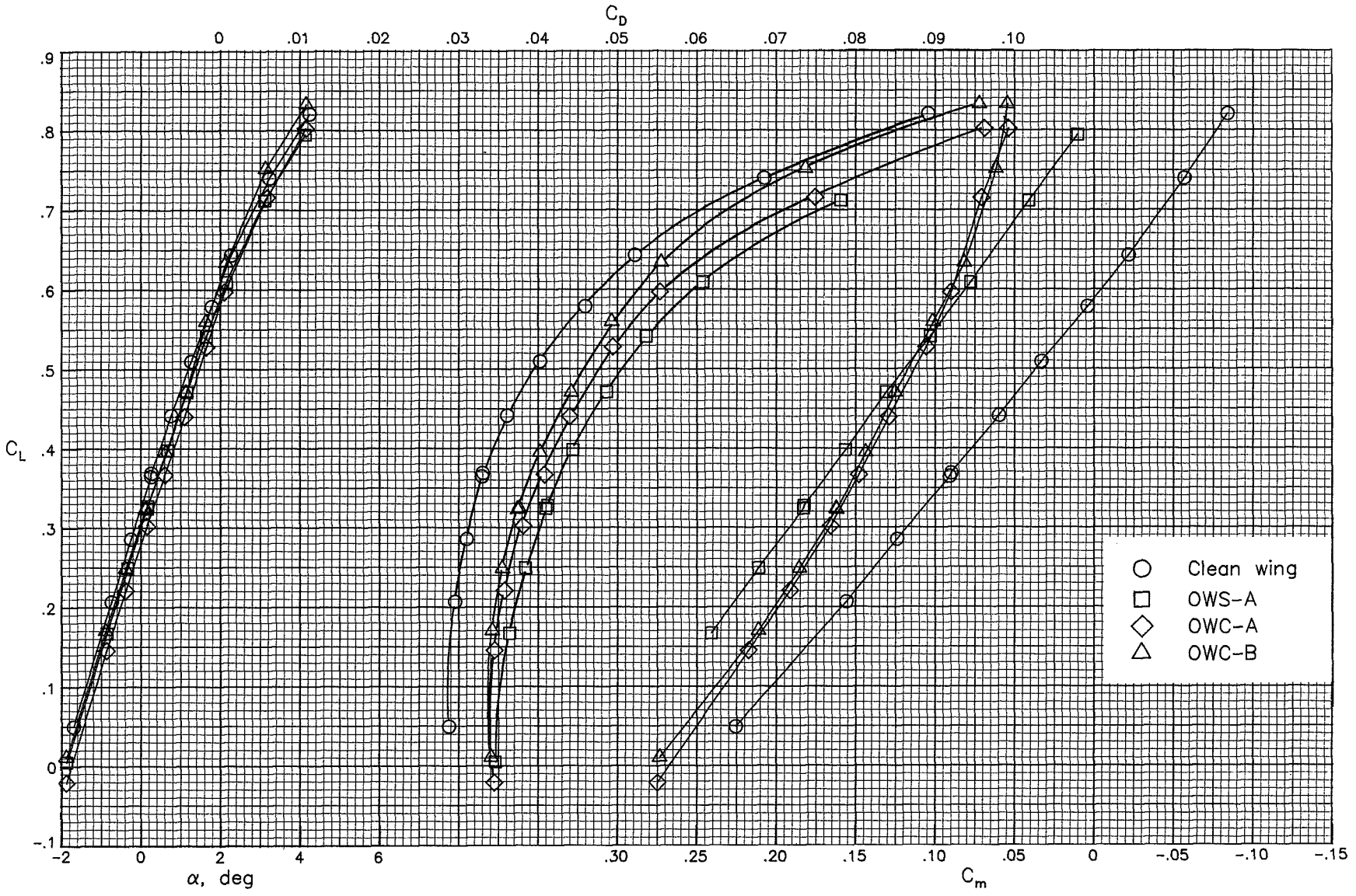


(g) M = 0.82.

Figure 9.- Concluded.

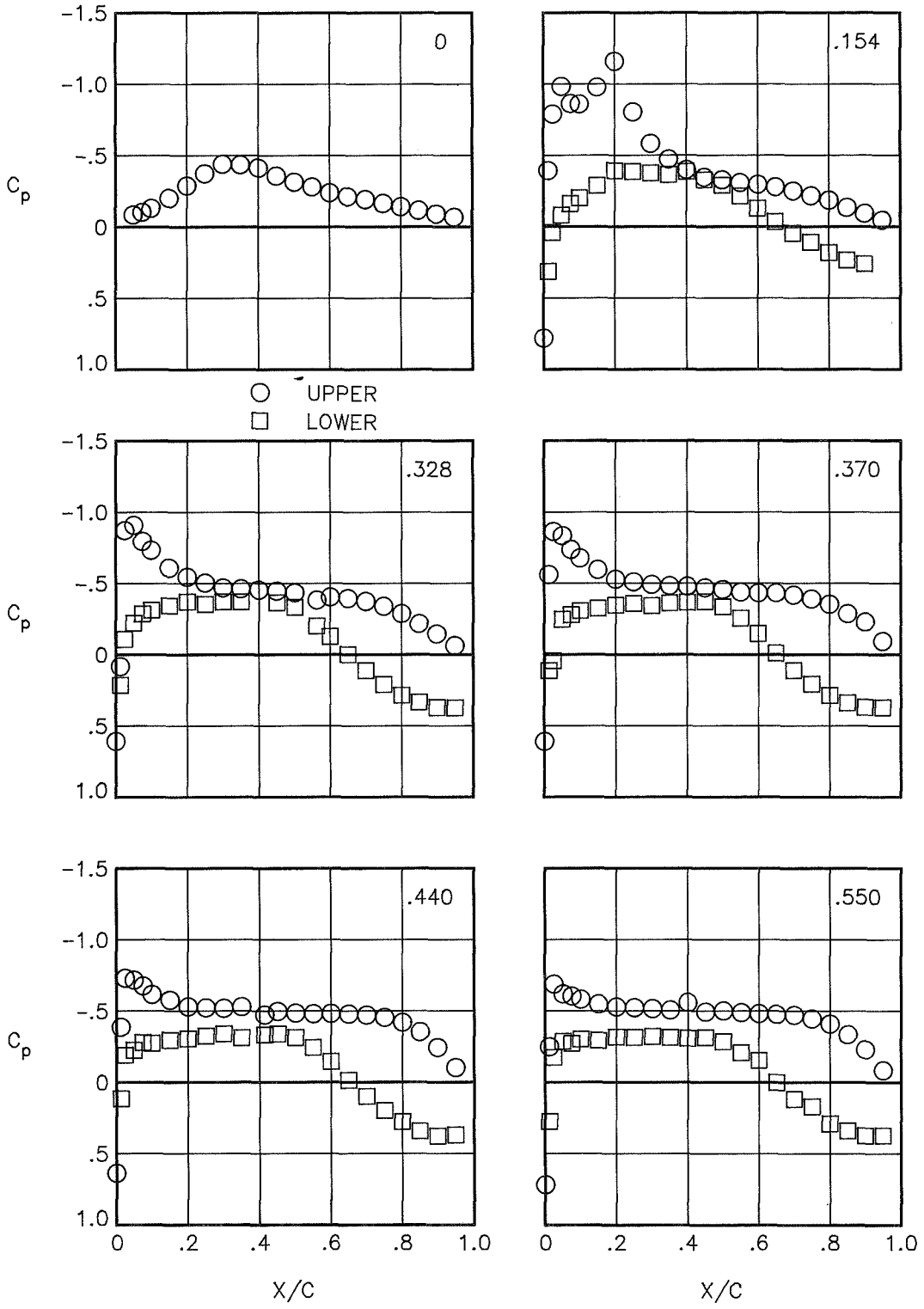


(a) $\alpha = 0.101°$.

Figure 10.- Pressure distributions for configuration with symmetrical nacelles (OWS-A) at M = 0.70. Semispan station y/(b/2) given in upper right-hand corner of each plot.

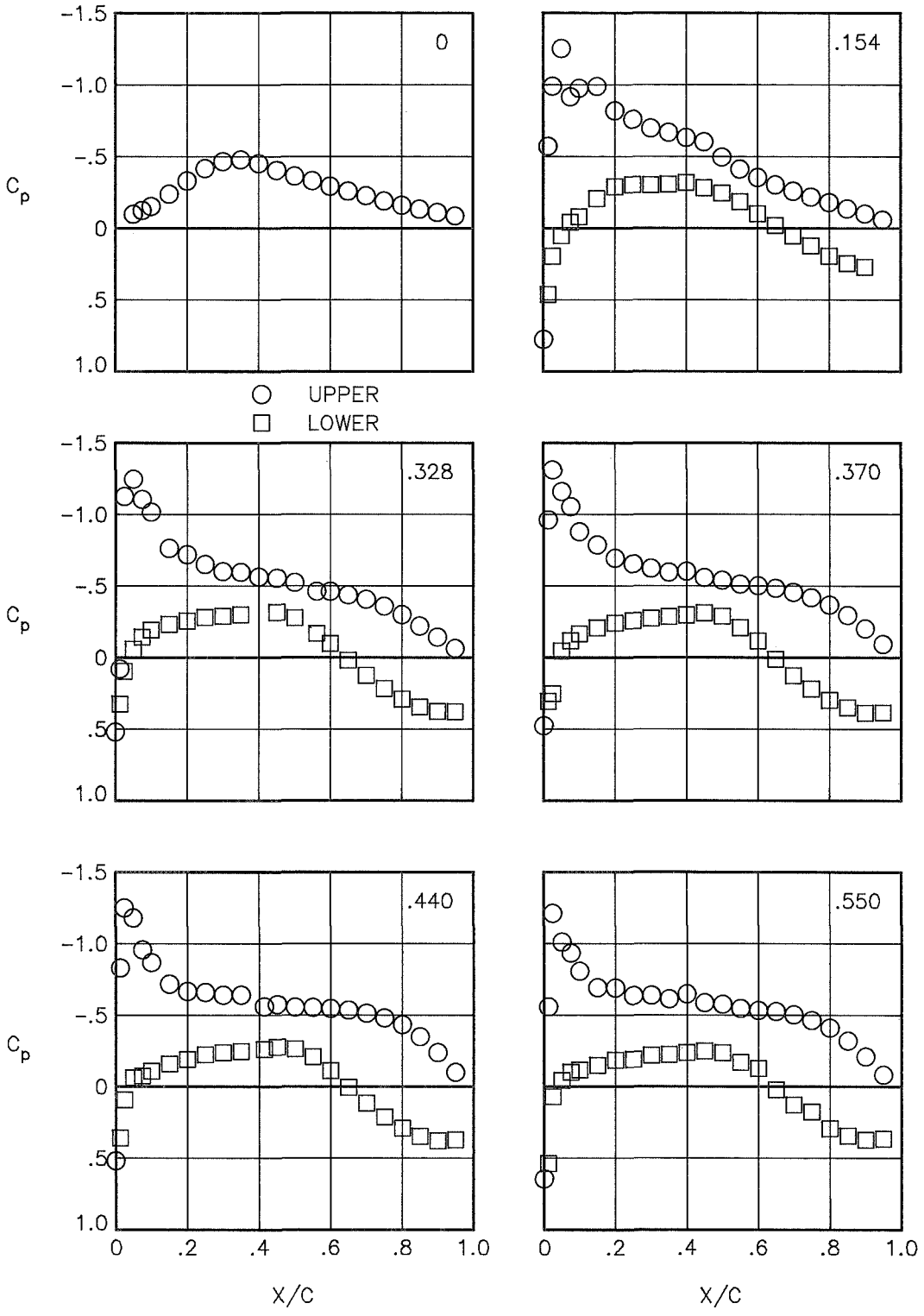


(b) $\alpha = 1.114°$.

Figure 10.- Continued.

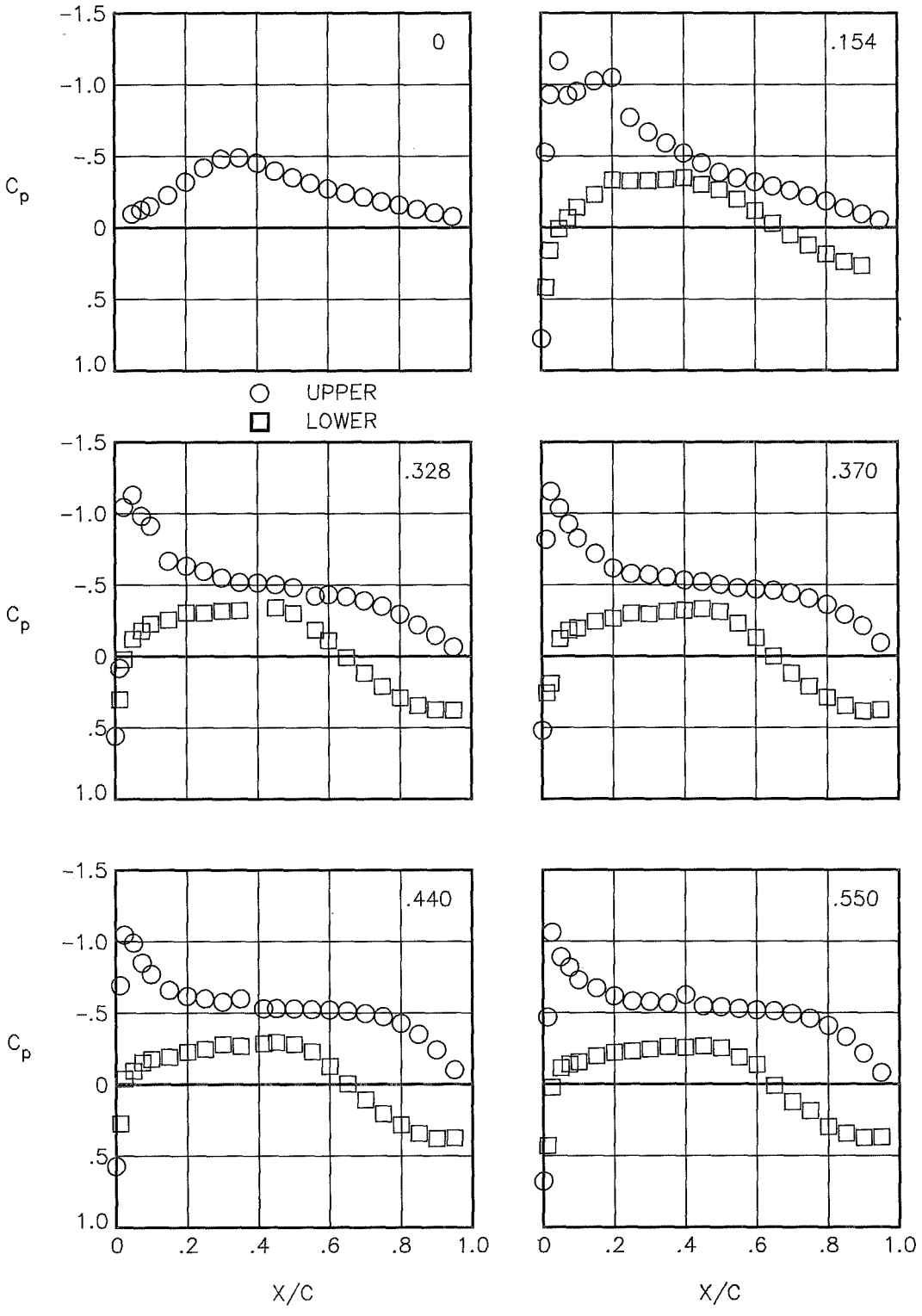


(c) $\alpha = 1.631°$.

Figure 10.– Continued.

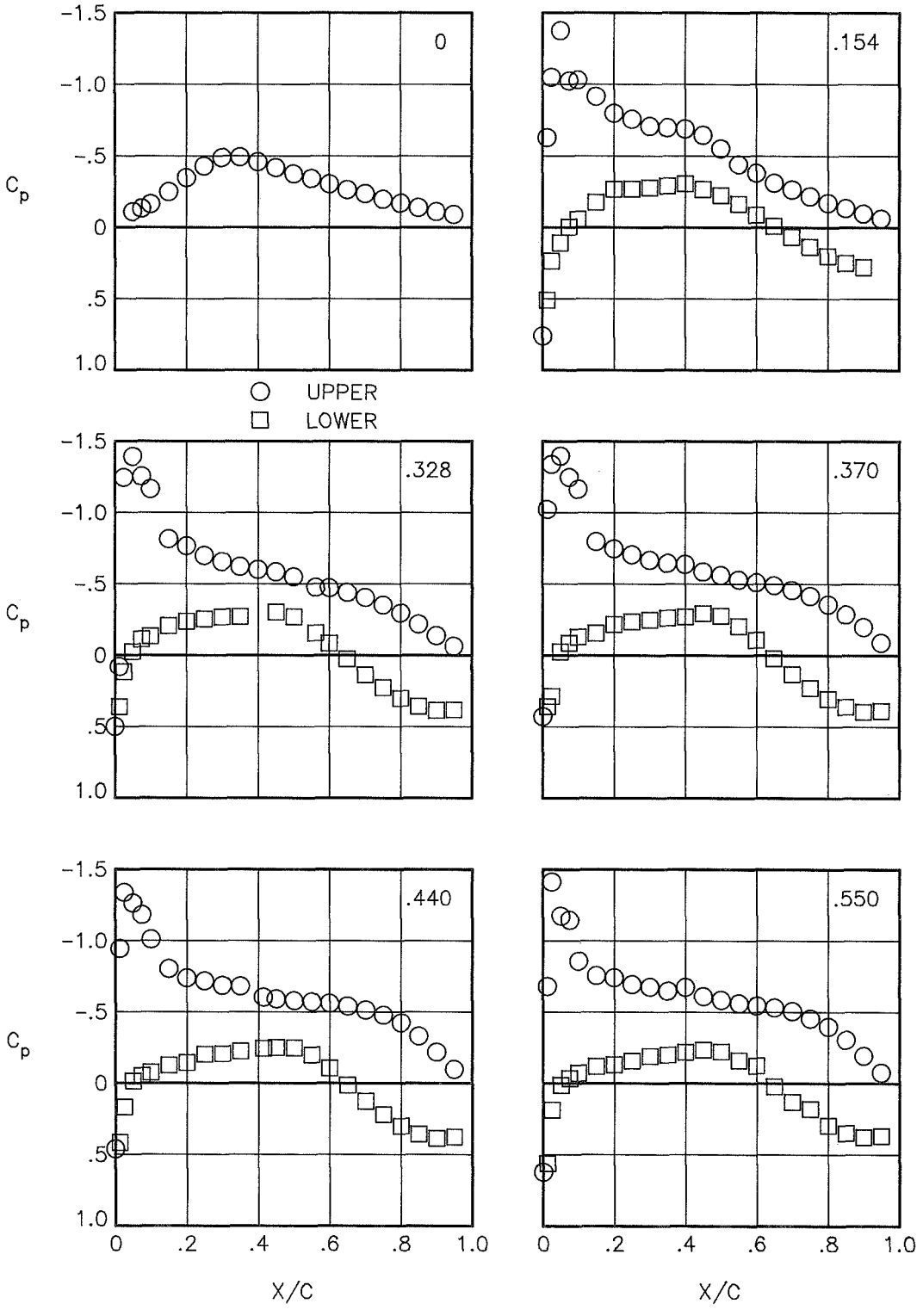


(d) $\alpha = 2.131°$.

Figure 10.- Continued.

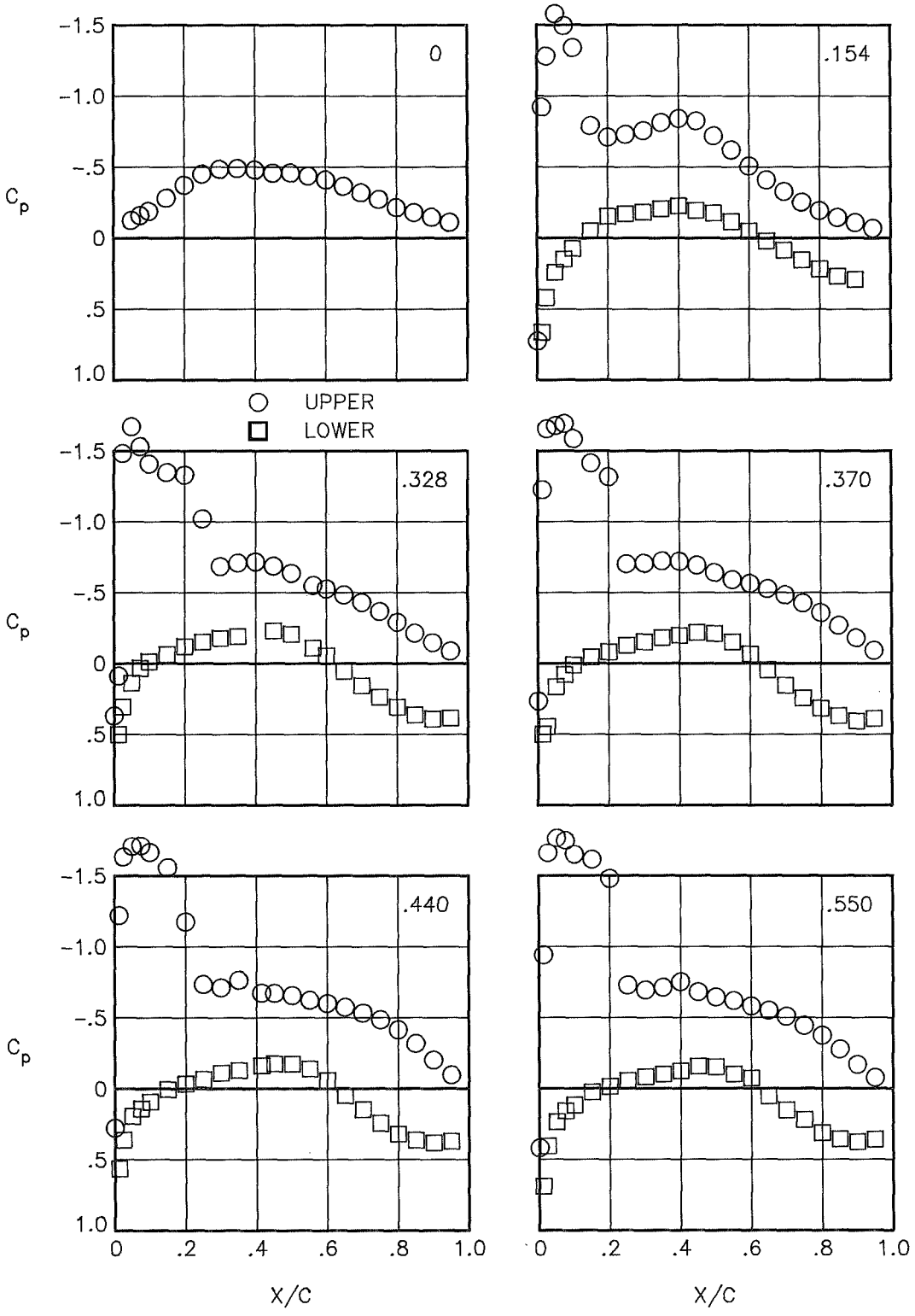


(e) $\alpha = 4.133°$.

Figure 10.- Concluded.

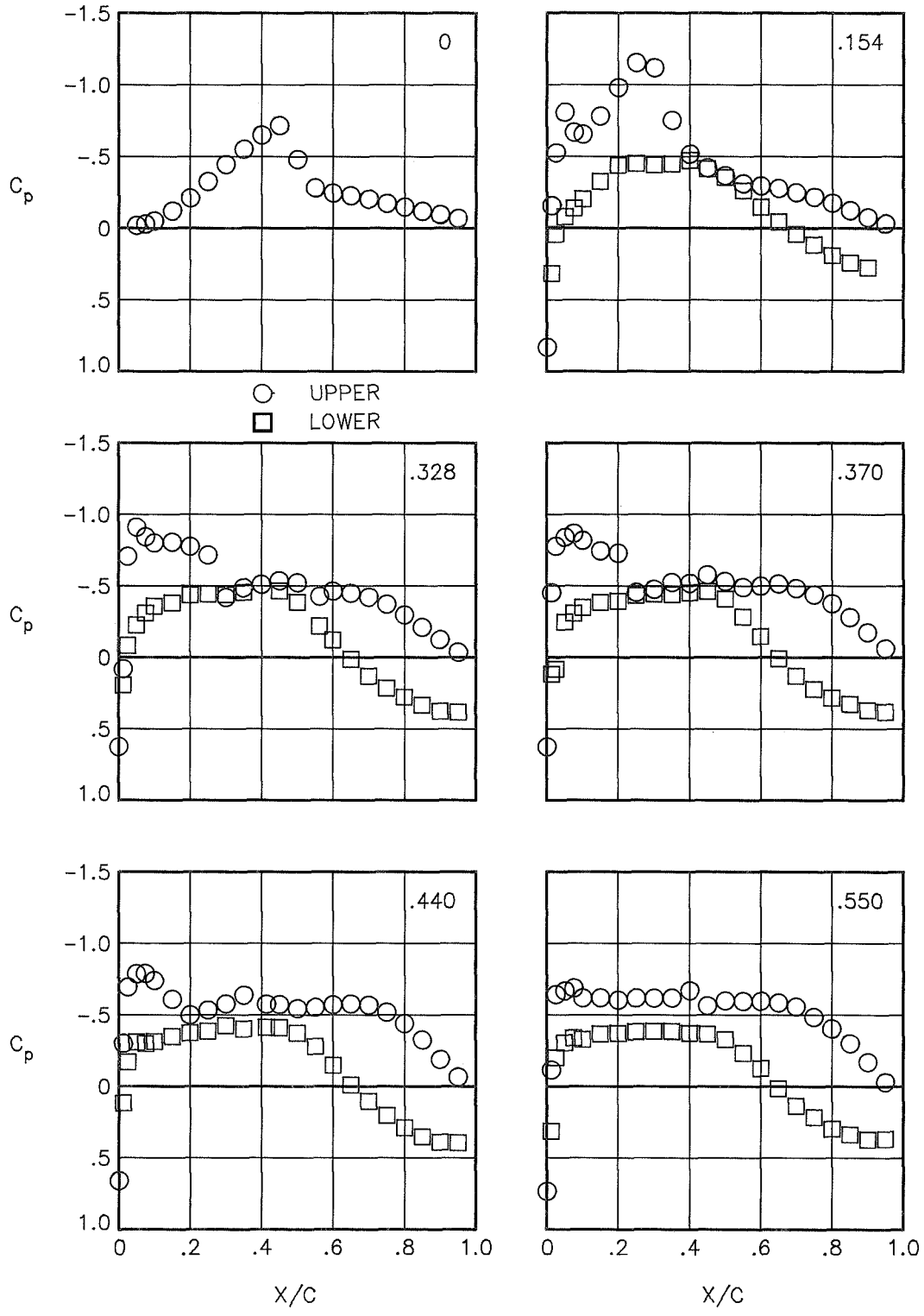


(a) $\alpha = 0.159°$.

Figure 11.- Pressure distributions for configuration with symmetrical nacelles (OWS-A) at M = 0.80. Semispan station y/(b/2) given in upper right-hand corner of each plot.

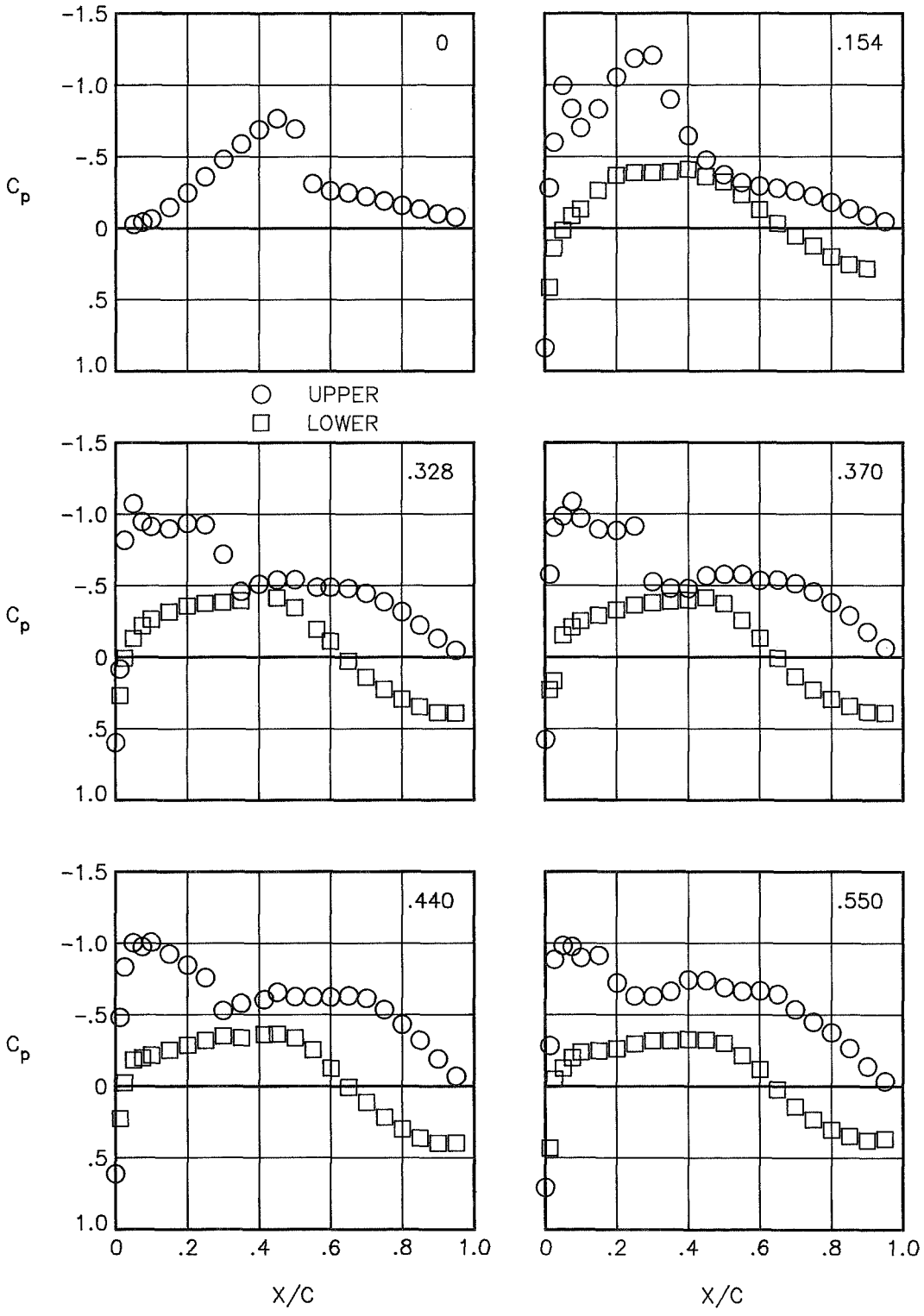


(b) $\alpha = 1.141°$.

Figure 11.- Continued.

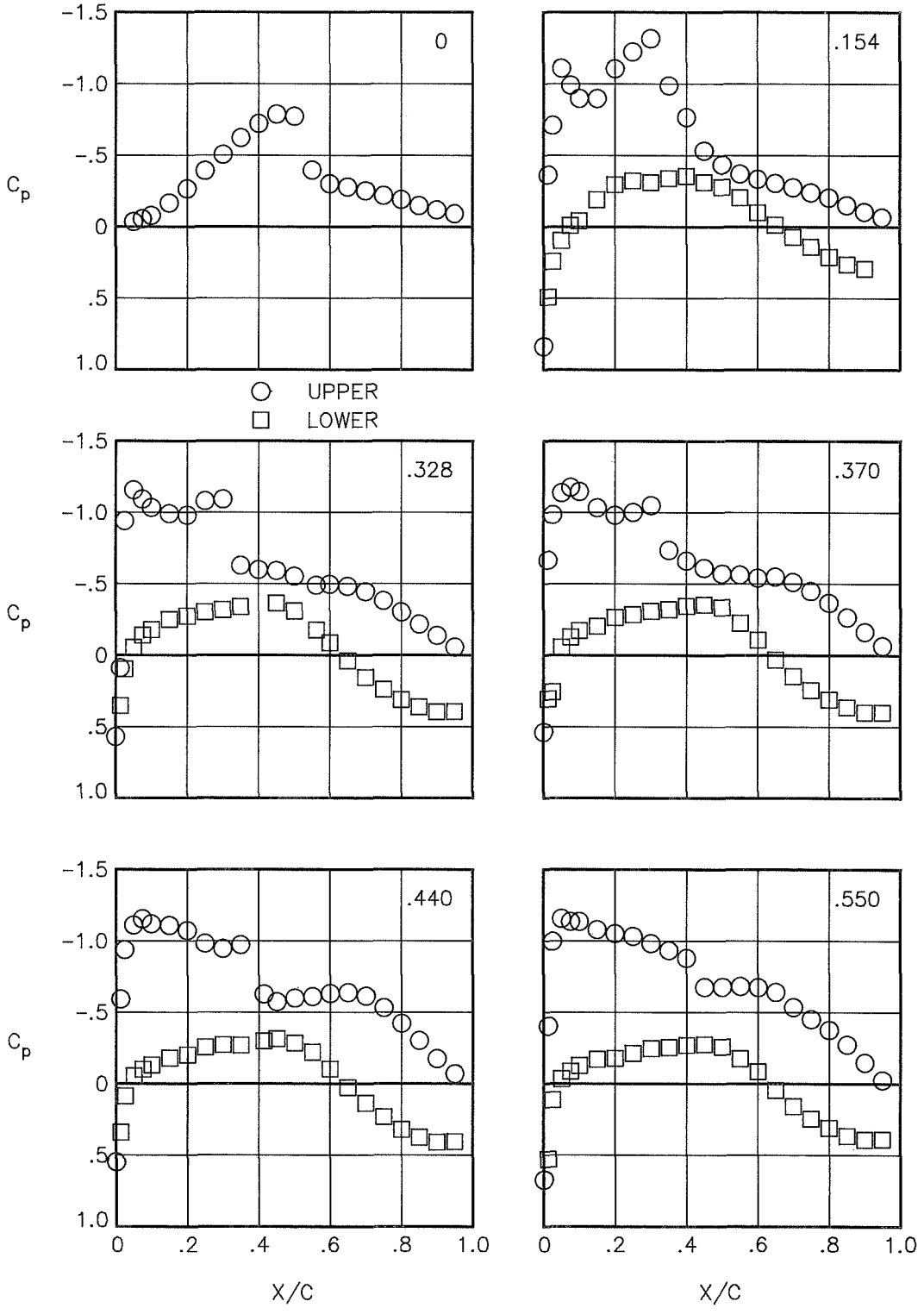


(c) $\alpha = 2.153°$.

Figure 11.- Continued.

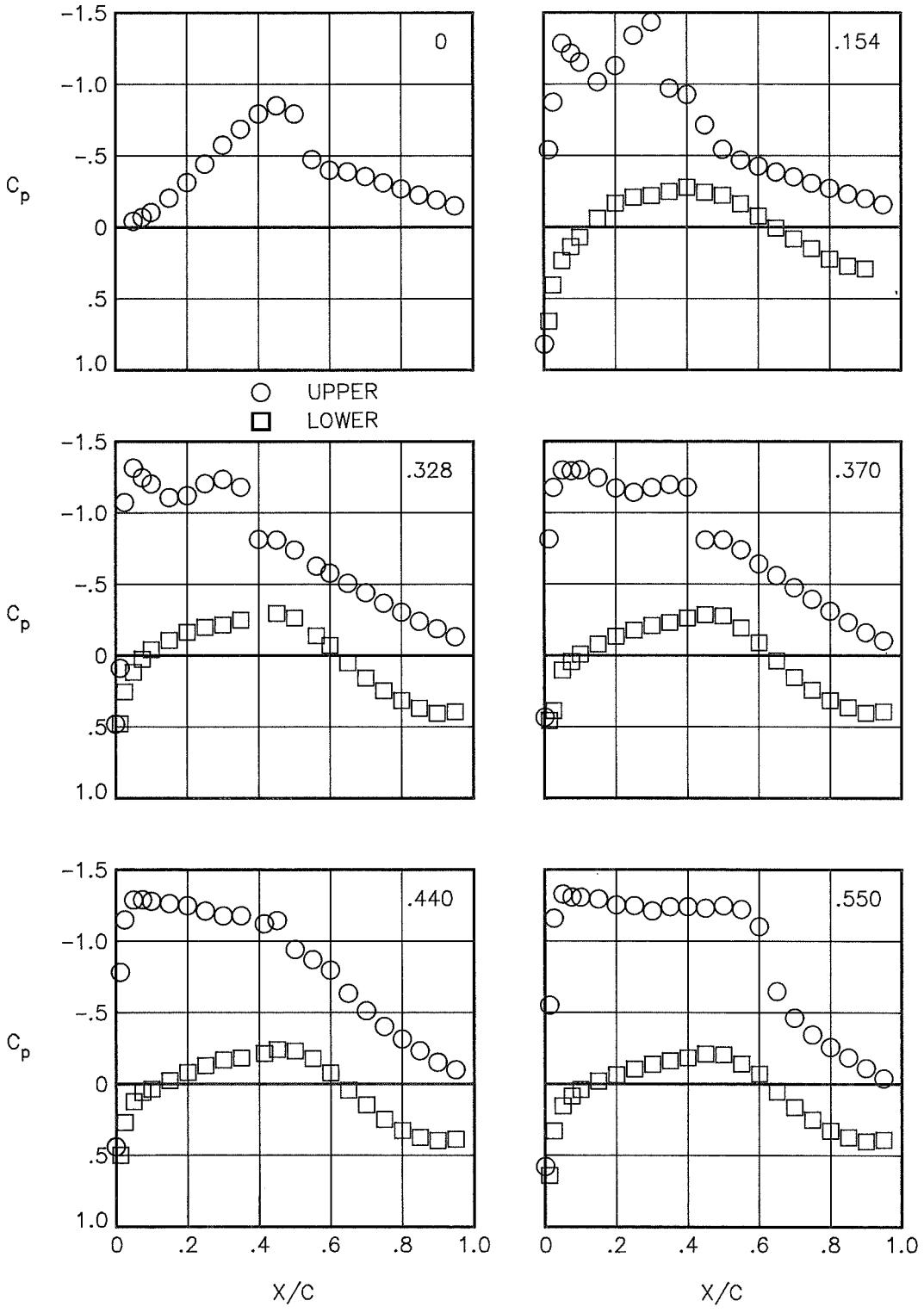


(d) $\alpha = 4.106°$.

Figure 11.- Concluded.

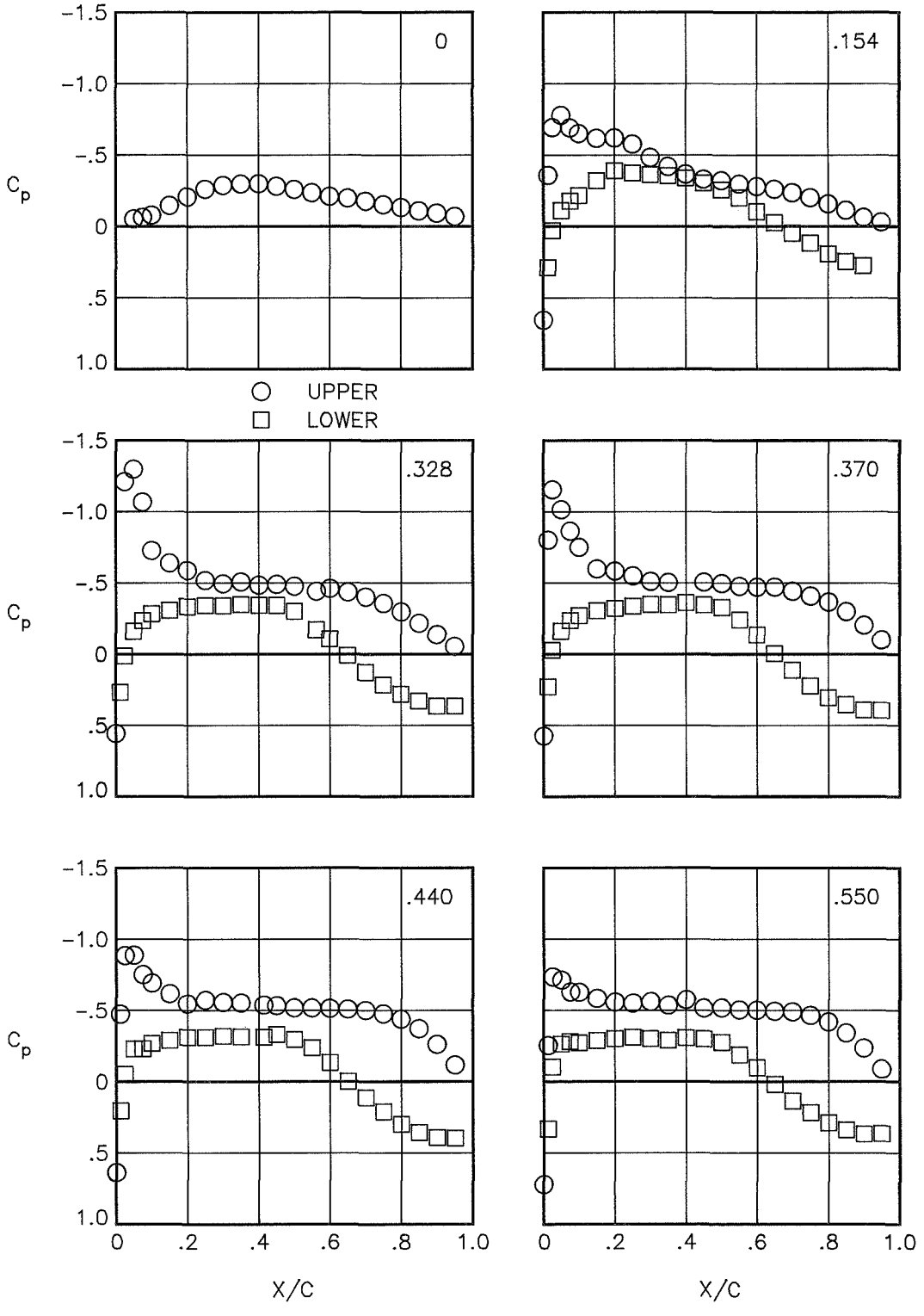


(a) $\alpha = 0.069°$.

Figure 12.- Pressure distributions for configuration with contoured nacelles (OWC-A) at M = 0.70. Semispan station y/(b/2) given in upper right-hand corner of each plot.

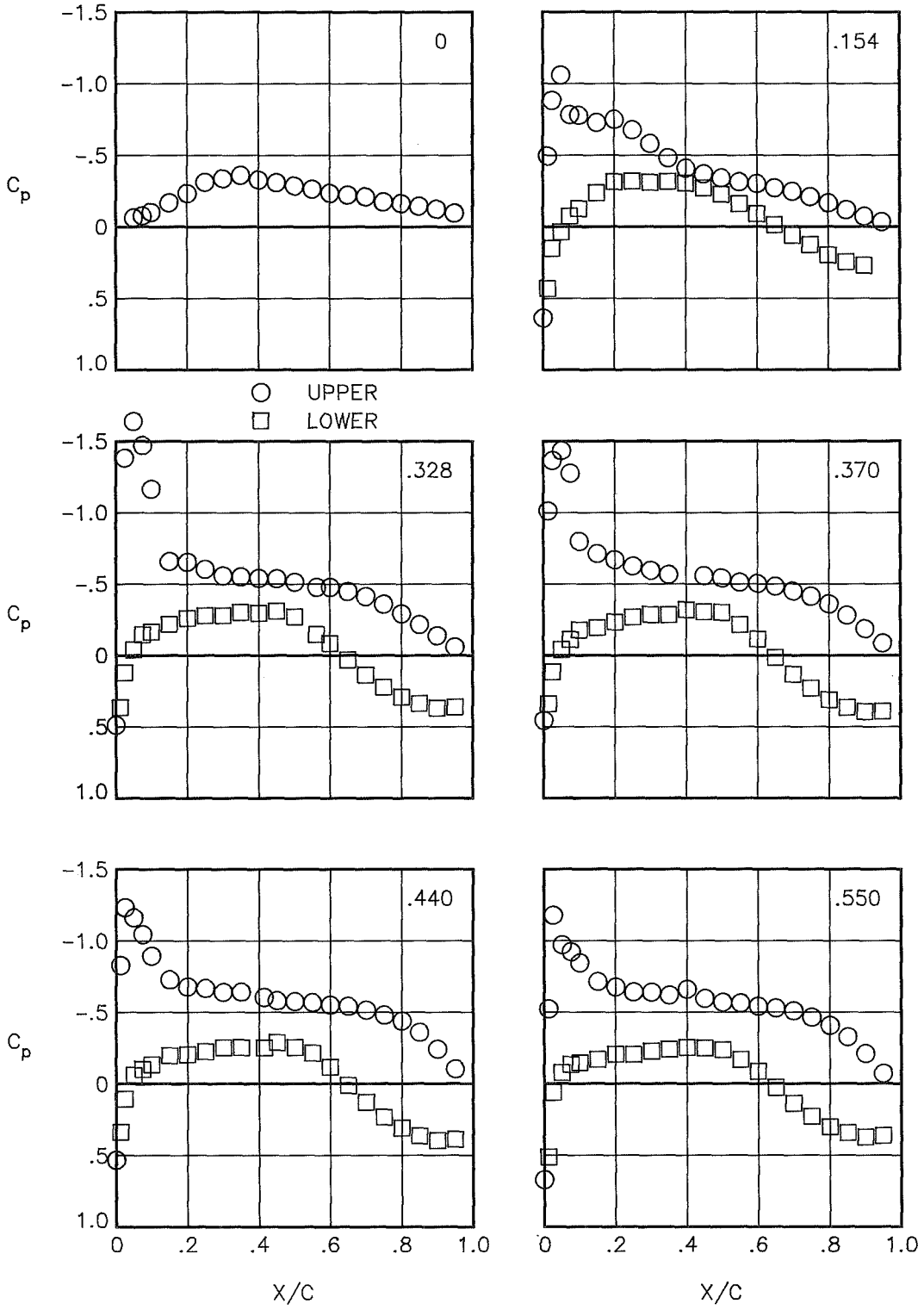


(b) $\alpha = 1.096°$.

Figure 12.- Continued.

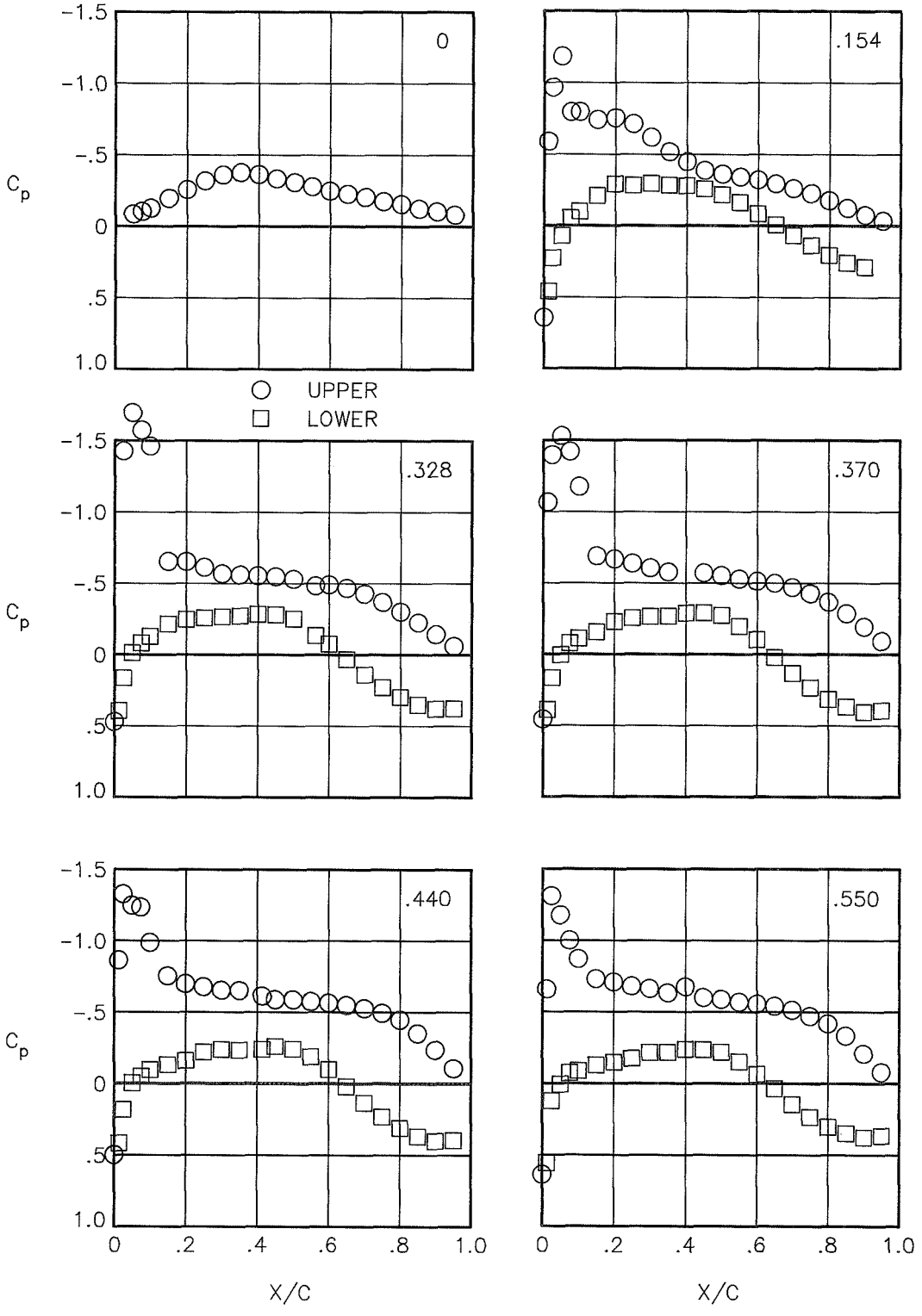


(c) $\alpha = 1.575°$.

Figure 12.- Continued.

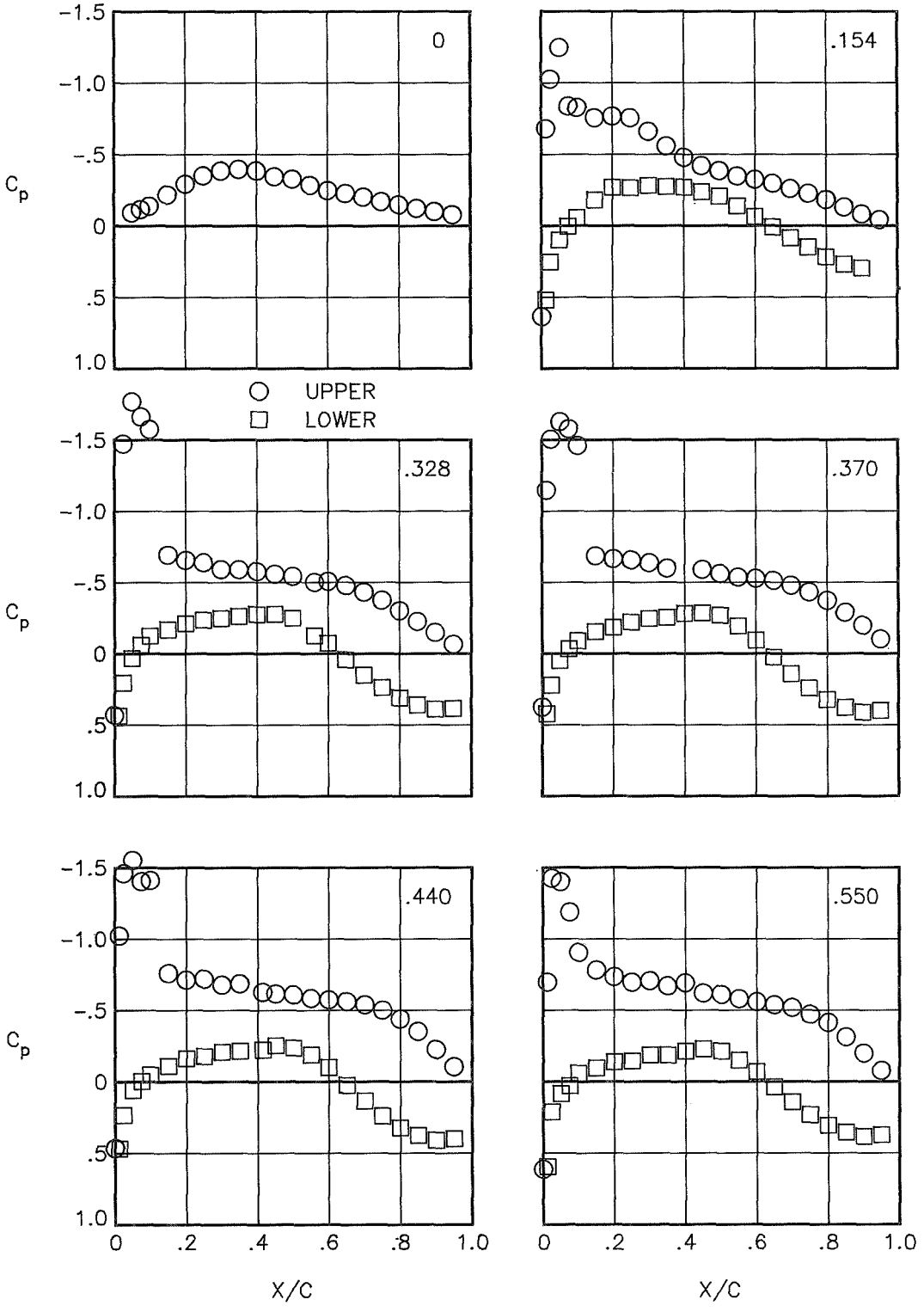


(d) $\alpha = 2.095°$.

Figure 12.- Continued.

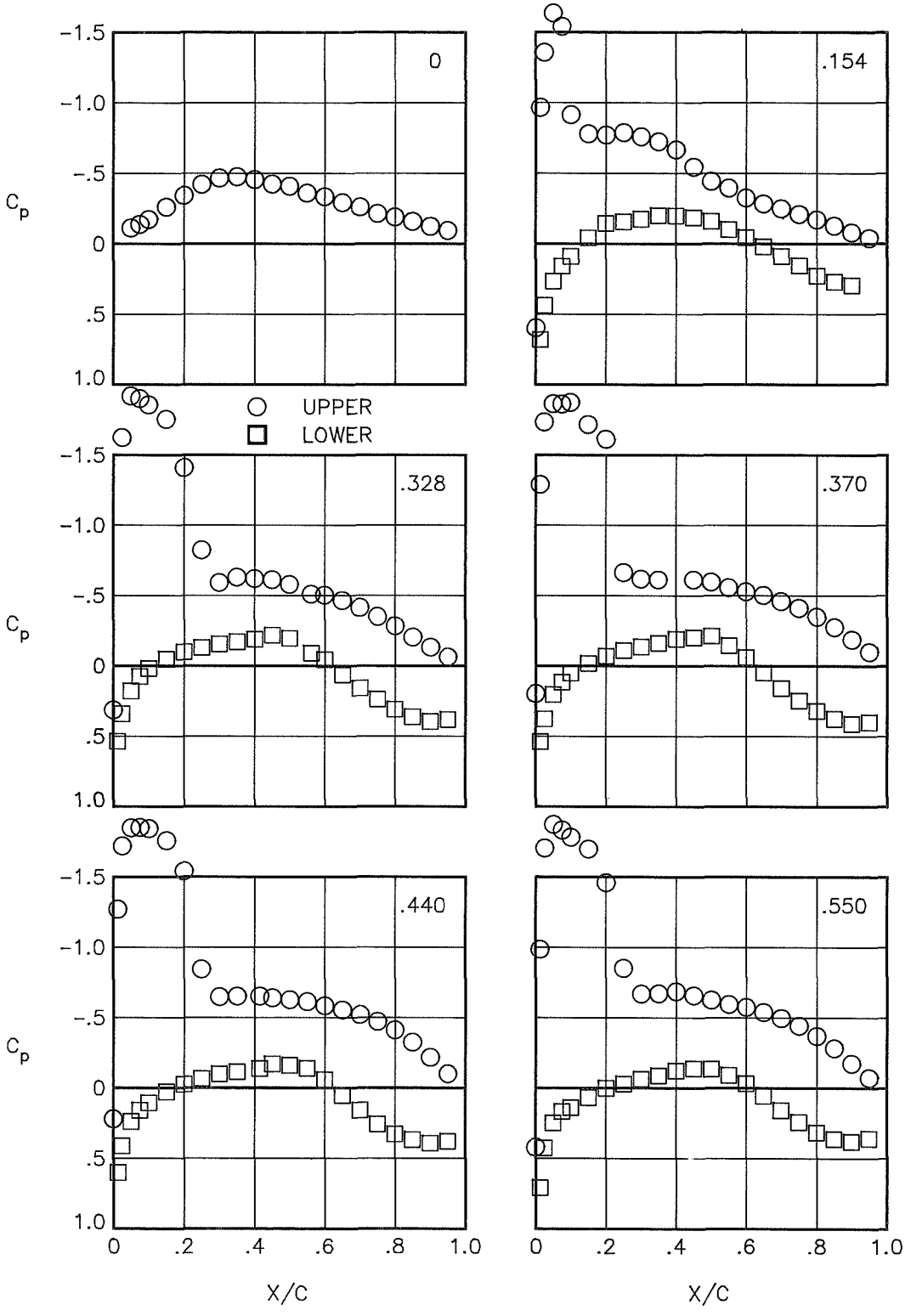


(e) $\alpha = 4.070°$.

Figure 12.- Concluded.

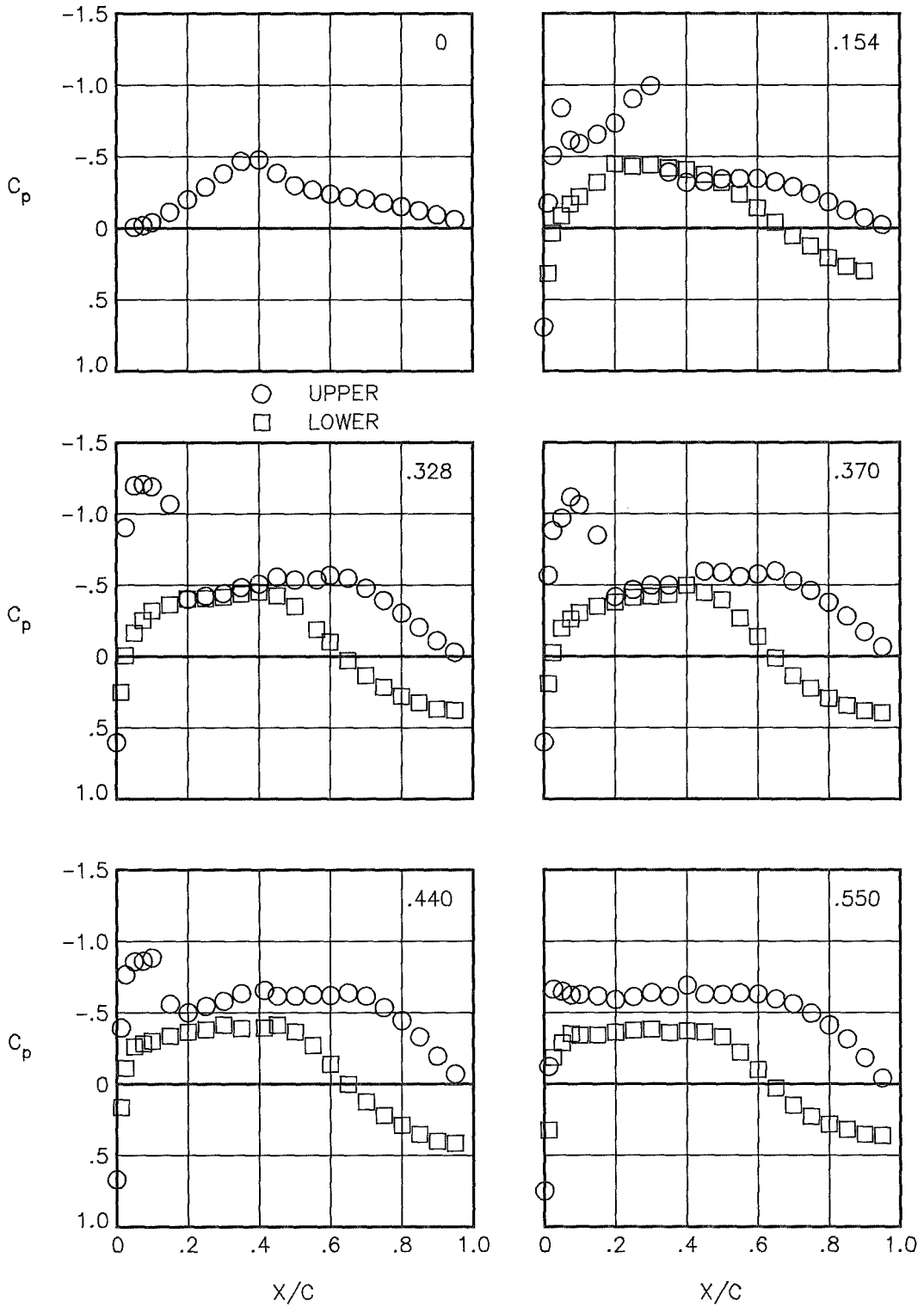


(a) $\alpha = 0.110°$.

Figure 13.- Pressure distributions for configuration with contoured nacelles (OWC-A) at M = 0.80. Semispan station y/(b/2) given in upper right-hand corner of each plot.

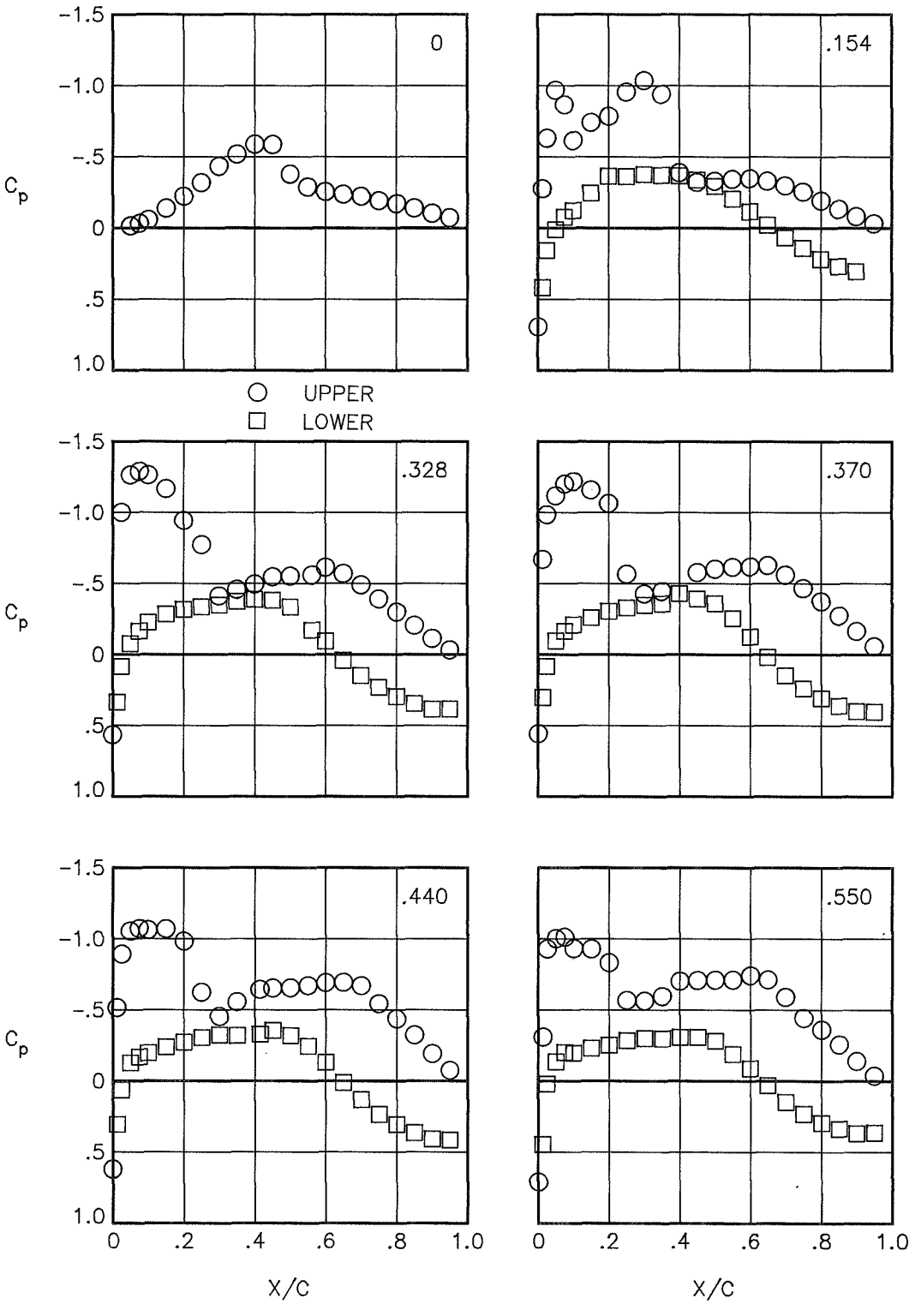


(b) $\alpha = 1.116°$.

Figure 13.- Continued.

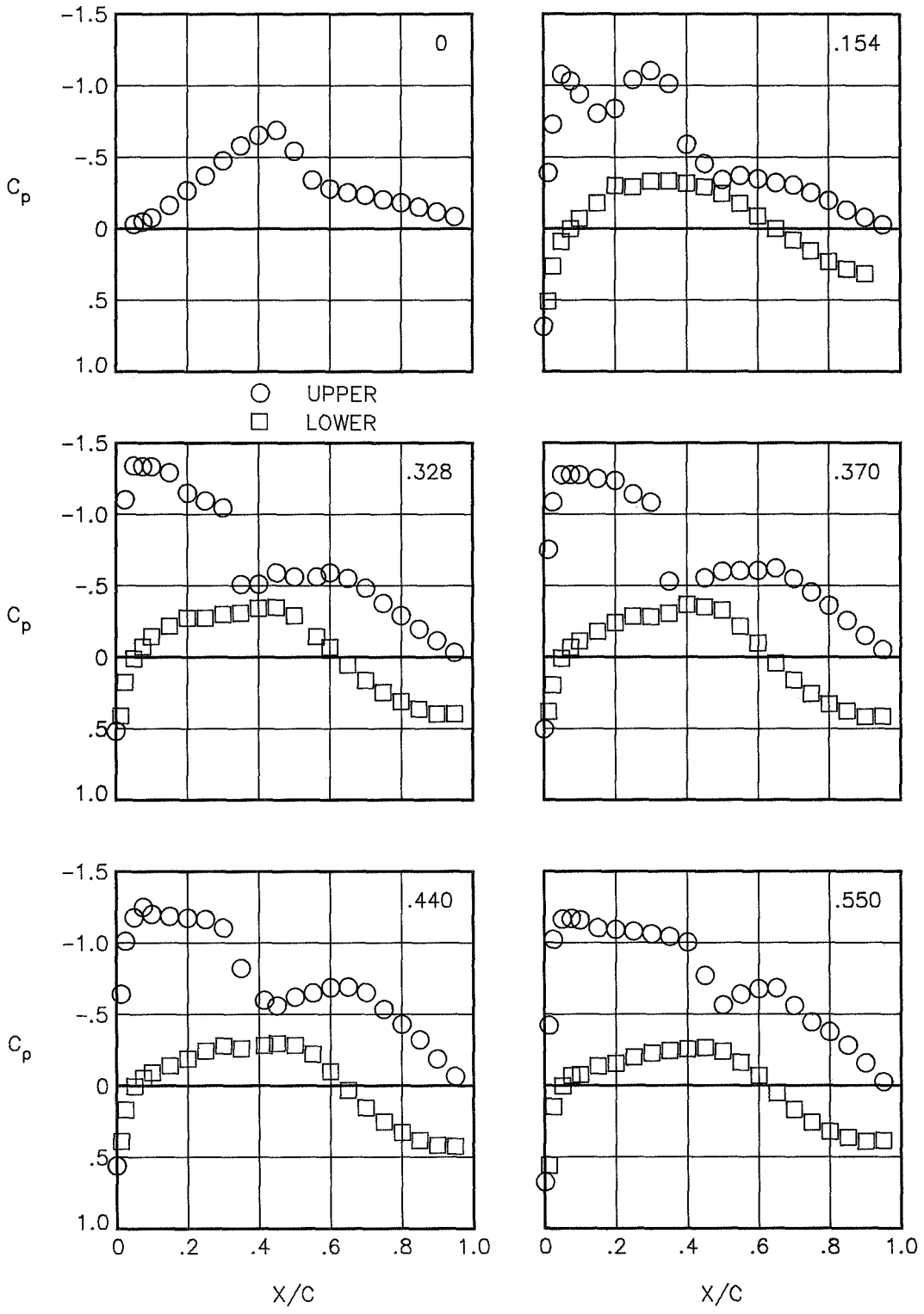


(c) $\alpha = 2.101°$.

Figure 13.- Continued.

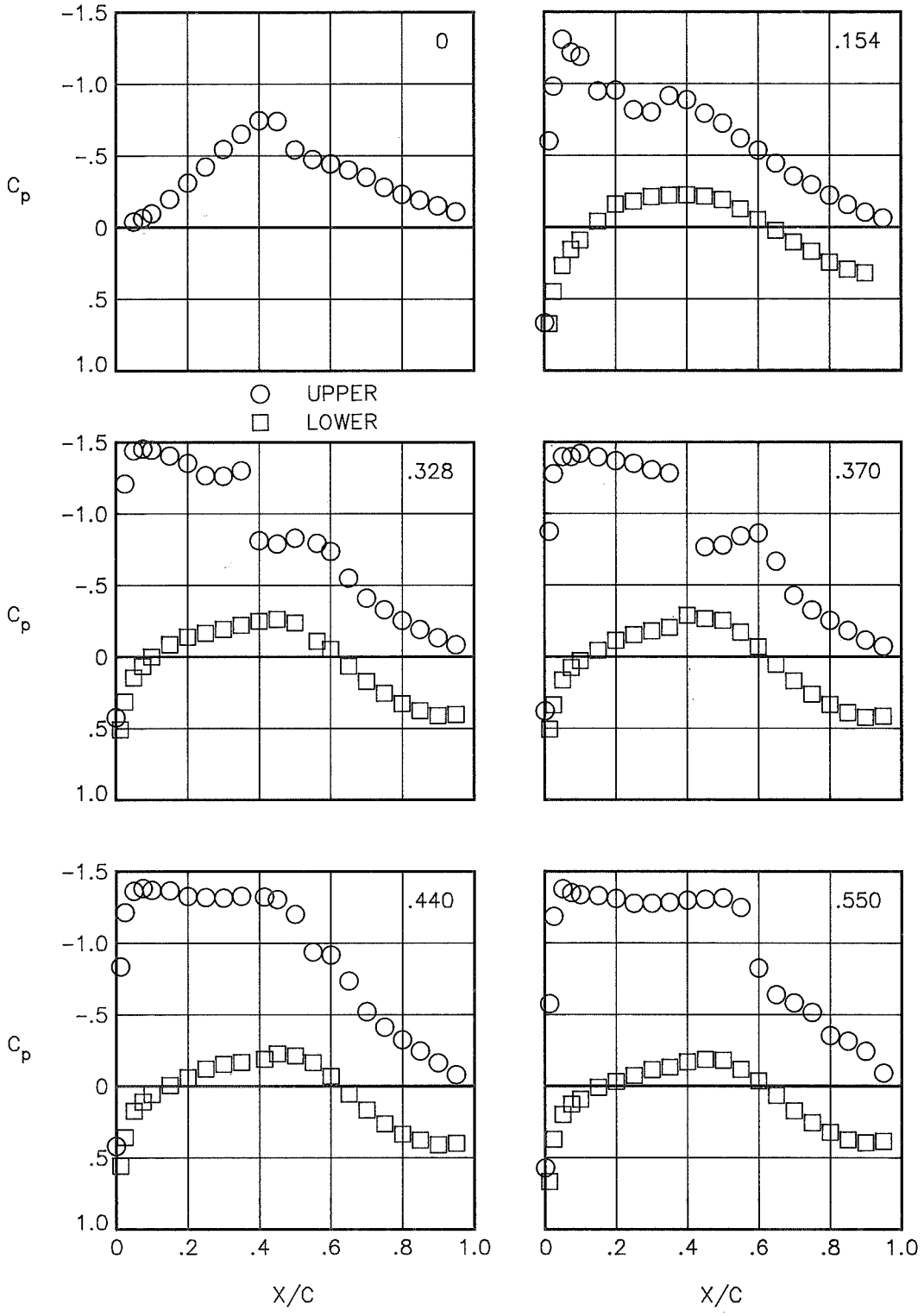


(d) $\alpha = 4.141°$.

Figure 13.– Concluded.

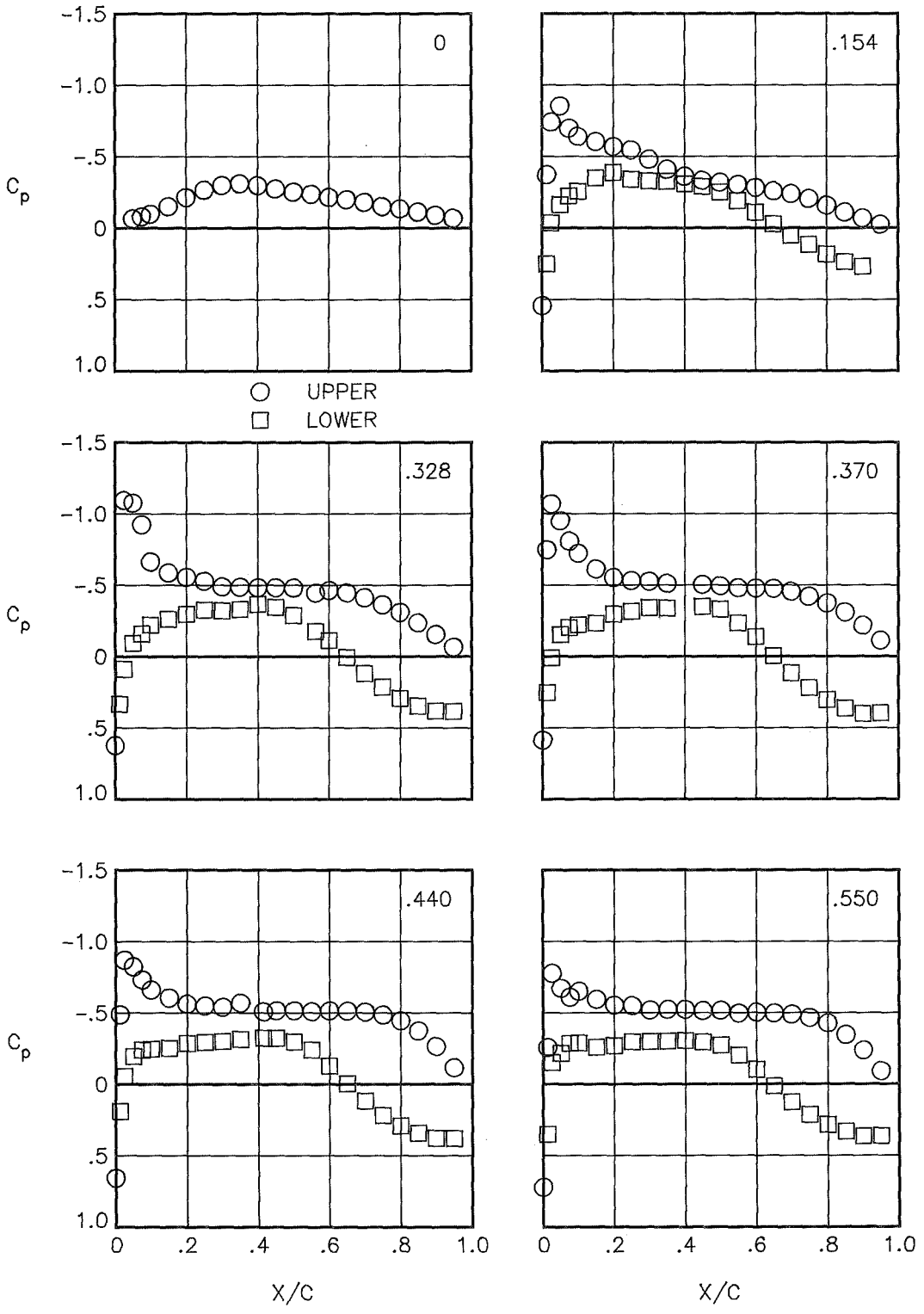


(a) $\alpha = 0.109°$.

Figure 14.- Pressure distributions for configuration with contoured nacelles and alternate pylons (OWC-B) at M = 0.70. Semispan station y/(b/2) given in upper right-hand corner of each plot.

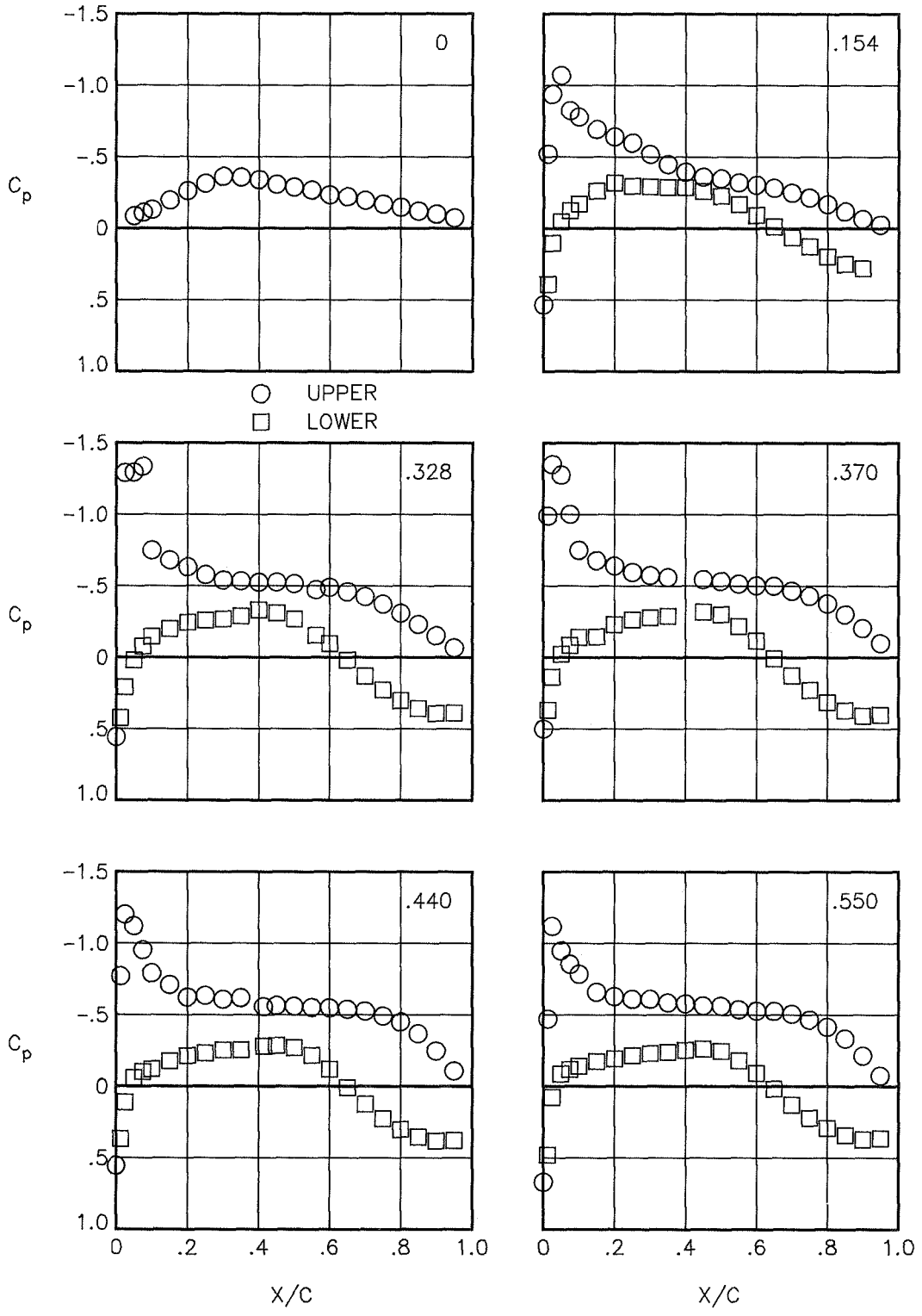


(b) $\alpha = 1.107°$.

Figure 14.- Continued.

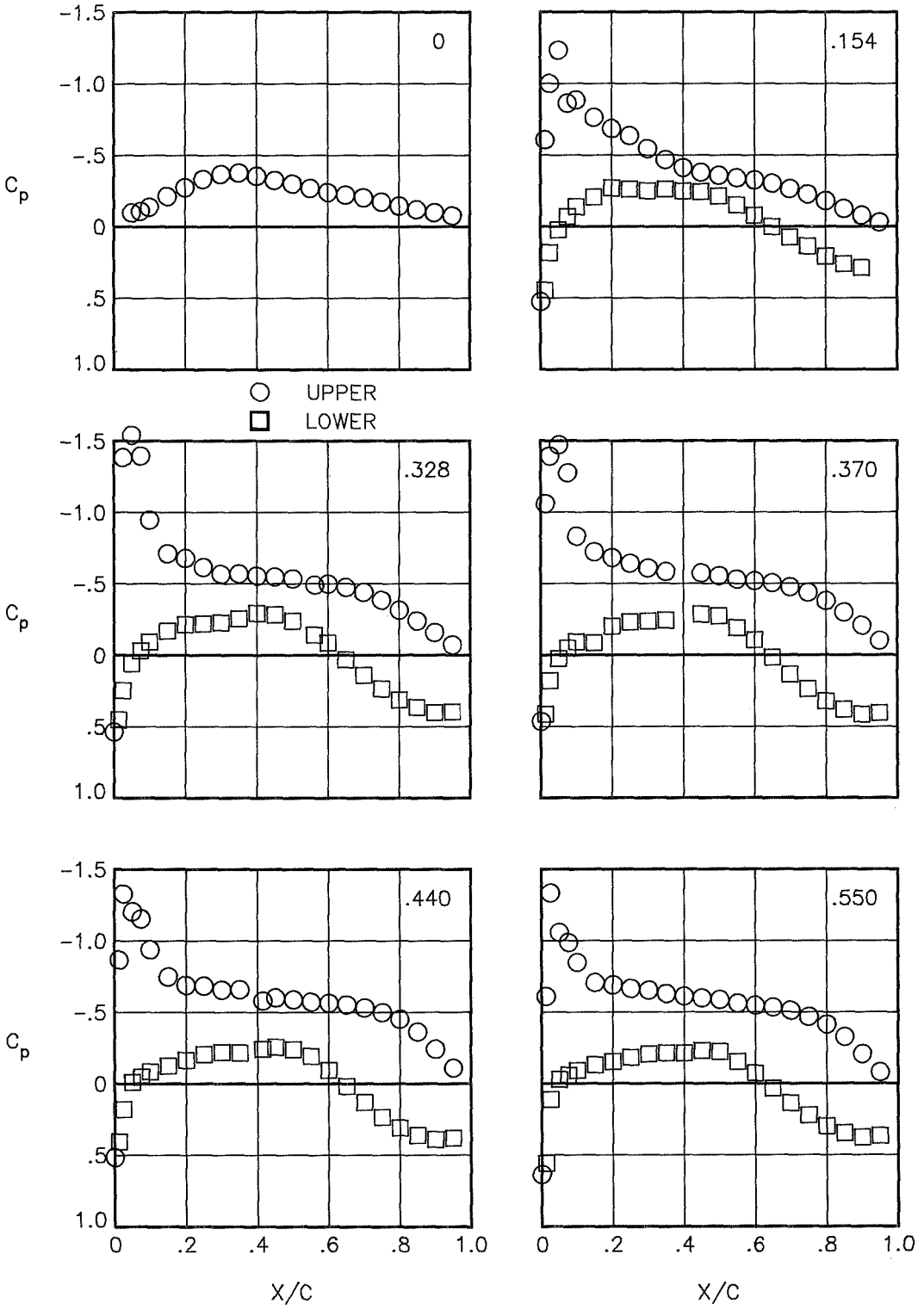


(c) $\alpha = 1.617°$.

Figure 14.- Continued.

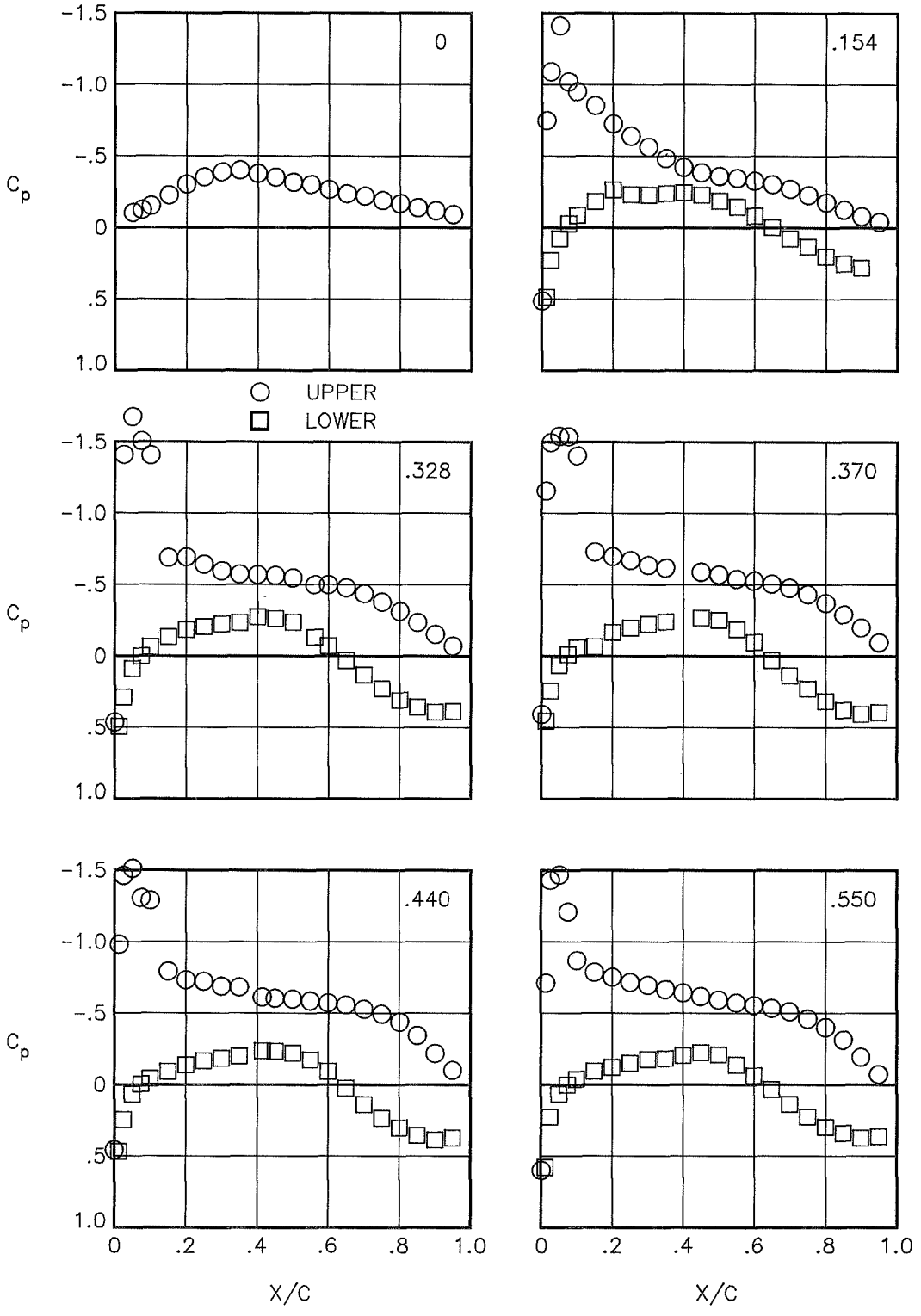


(d) $\alpha = 2.122°$.

Figure 14.- Continued.

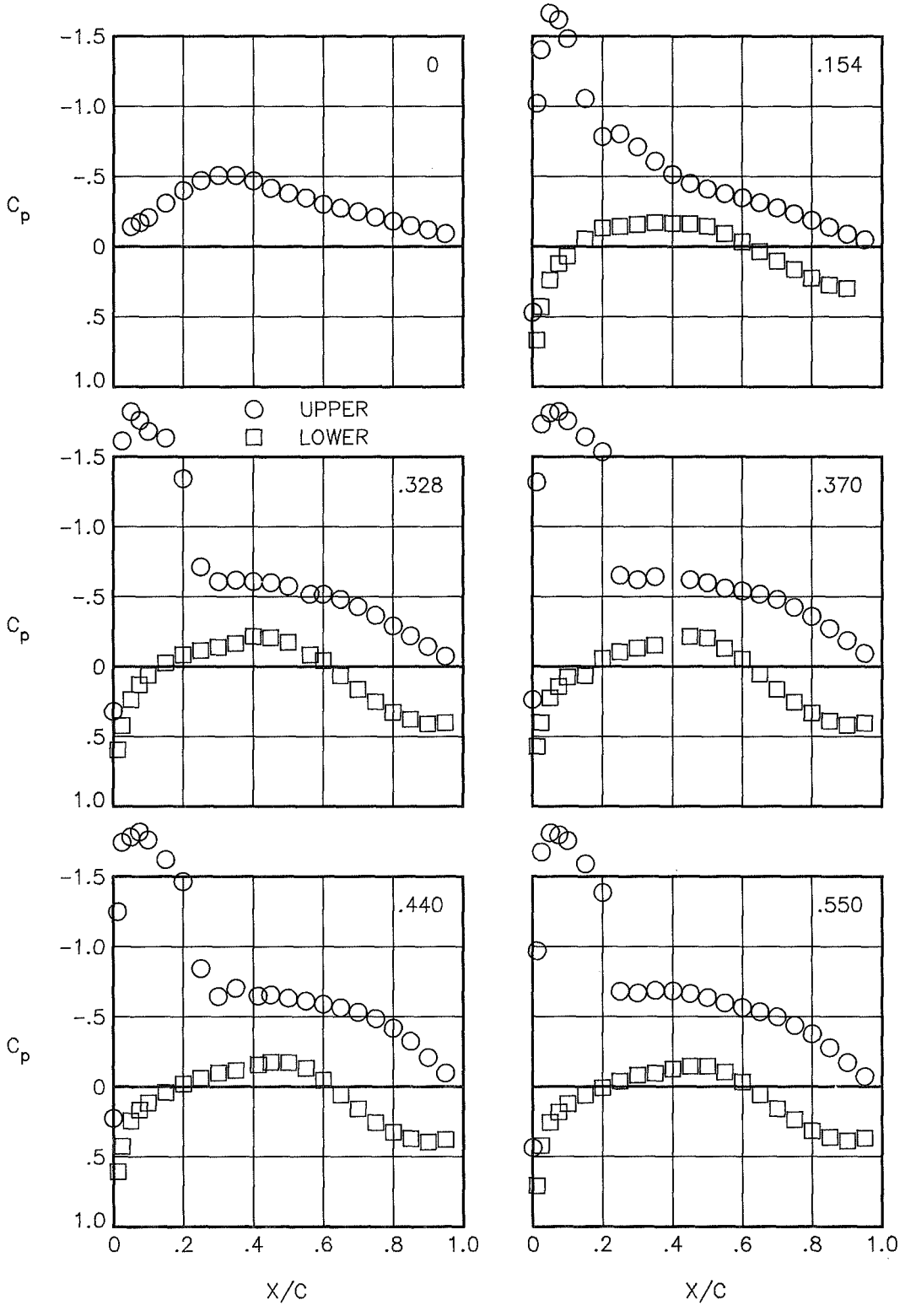


(e) $\alpha = 4.132°$.

Figure 14.- Concluded.

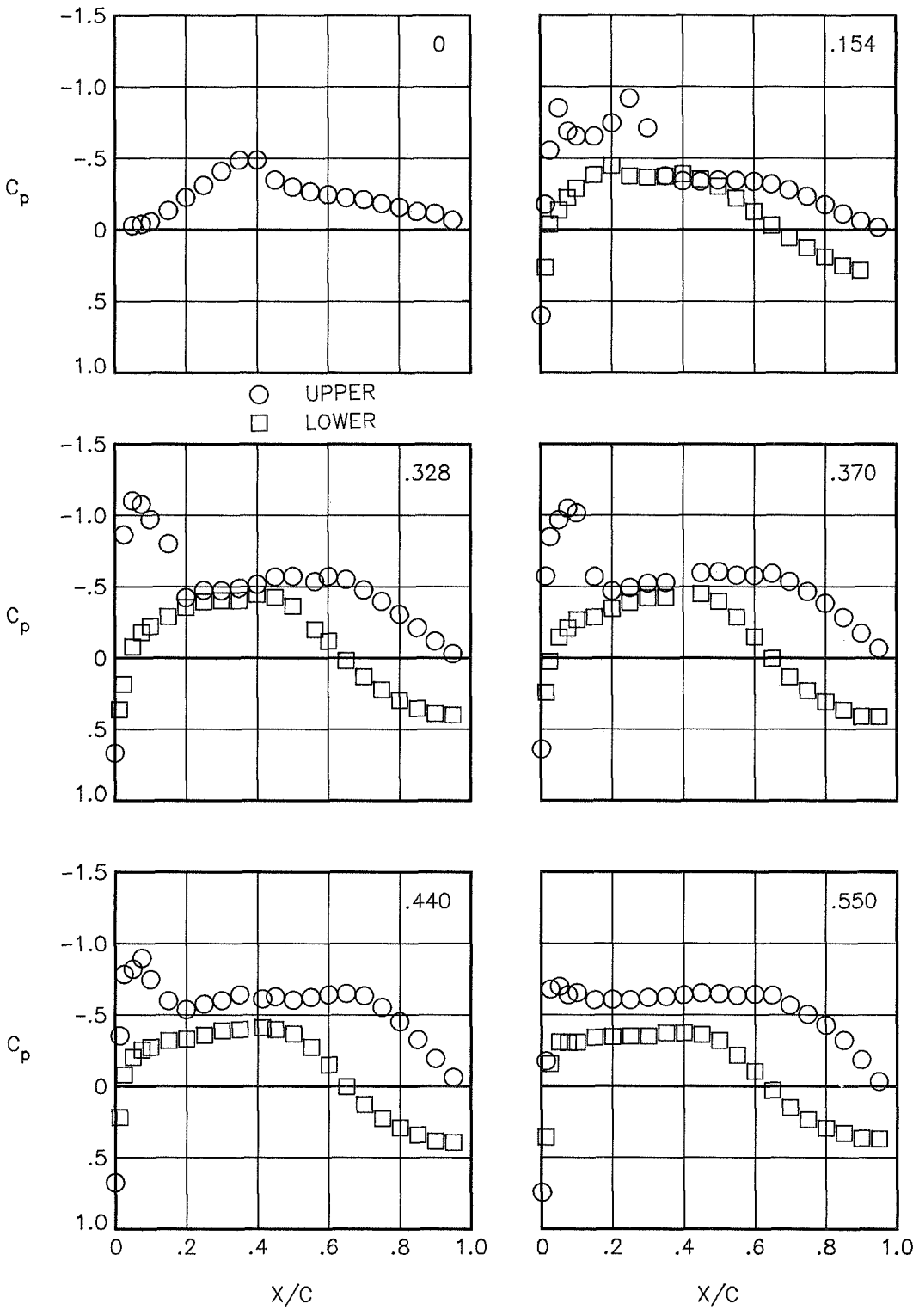


(a) $\alpha = 0.146°$.

Figure 15.- Pressure distributions for configuration with contoured nacelles and alternate pylons (OWC-B) at M = 0.80. Semispan station y/(b/2) given in upper right-hand corner of each plot.

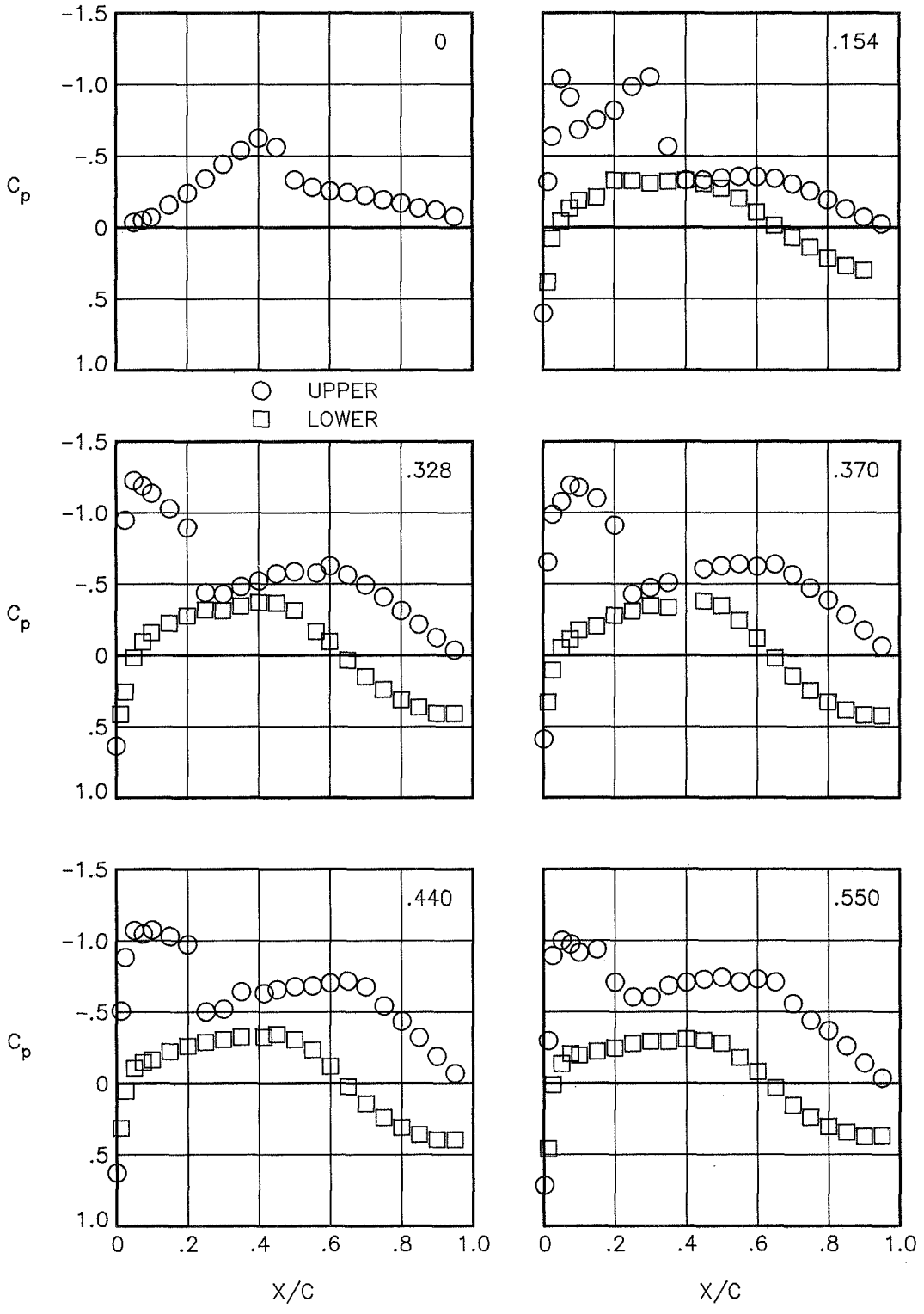


(b) $\alpha = 1.079°$.

Figure 15.- Continued.

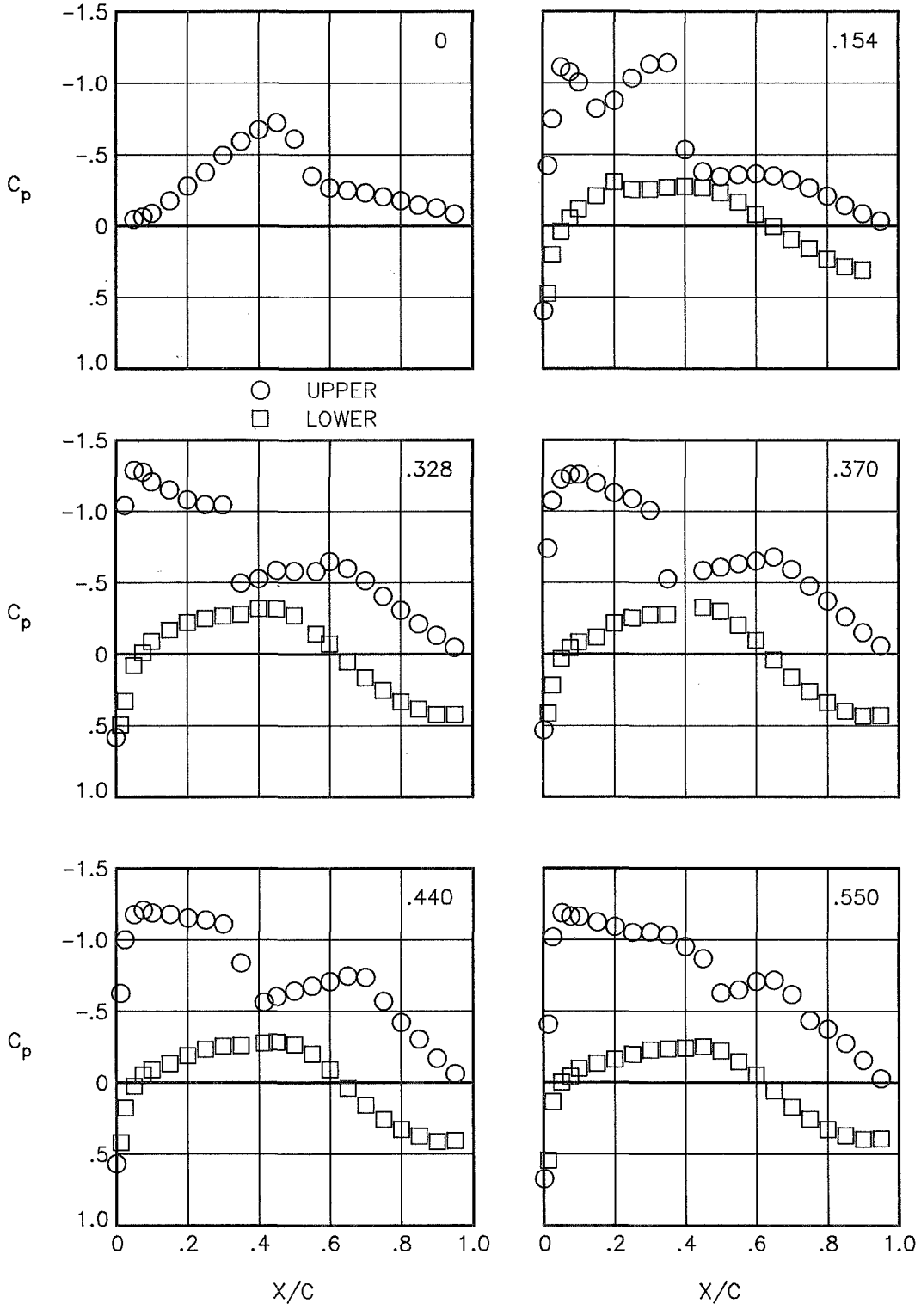


(c) $\alpha = 2.138°$.

Figure 15.- Continued.

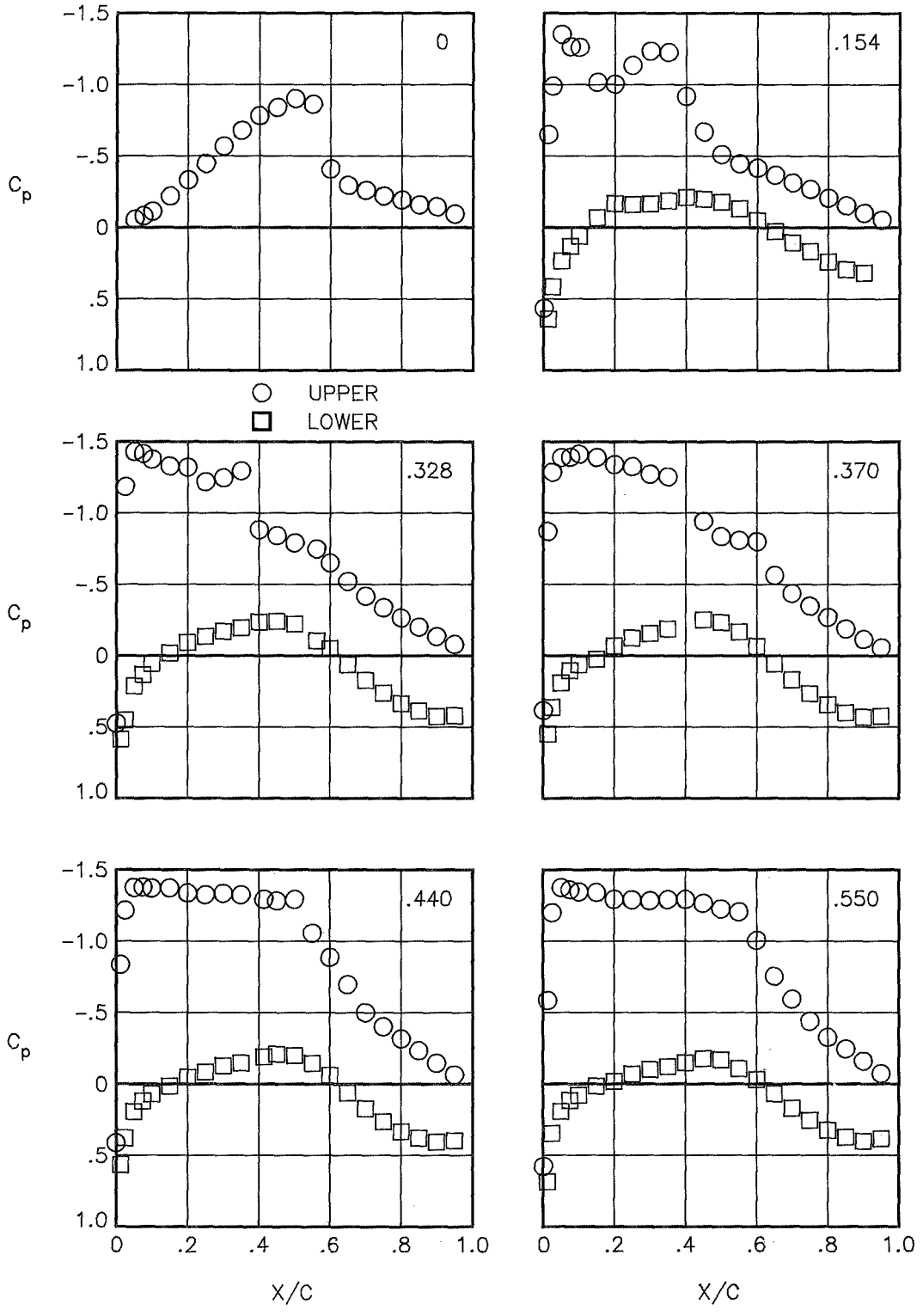


(d) $\alpha = 4.138°$.

Figure 15.- Concluded.

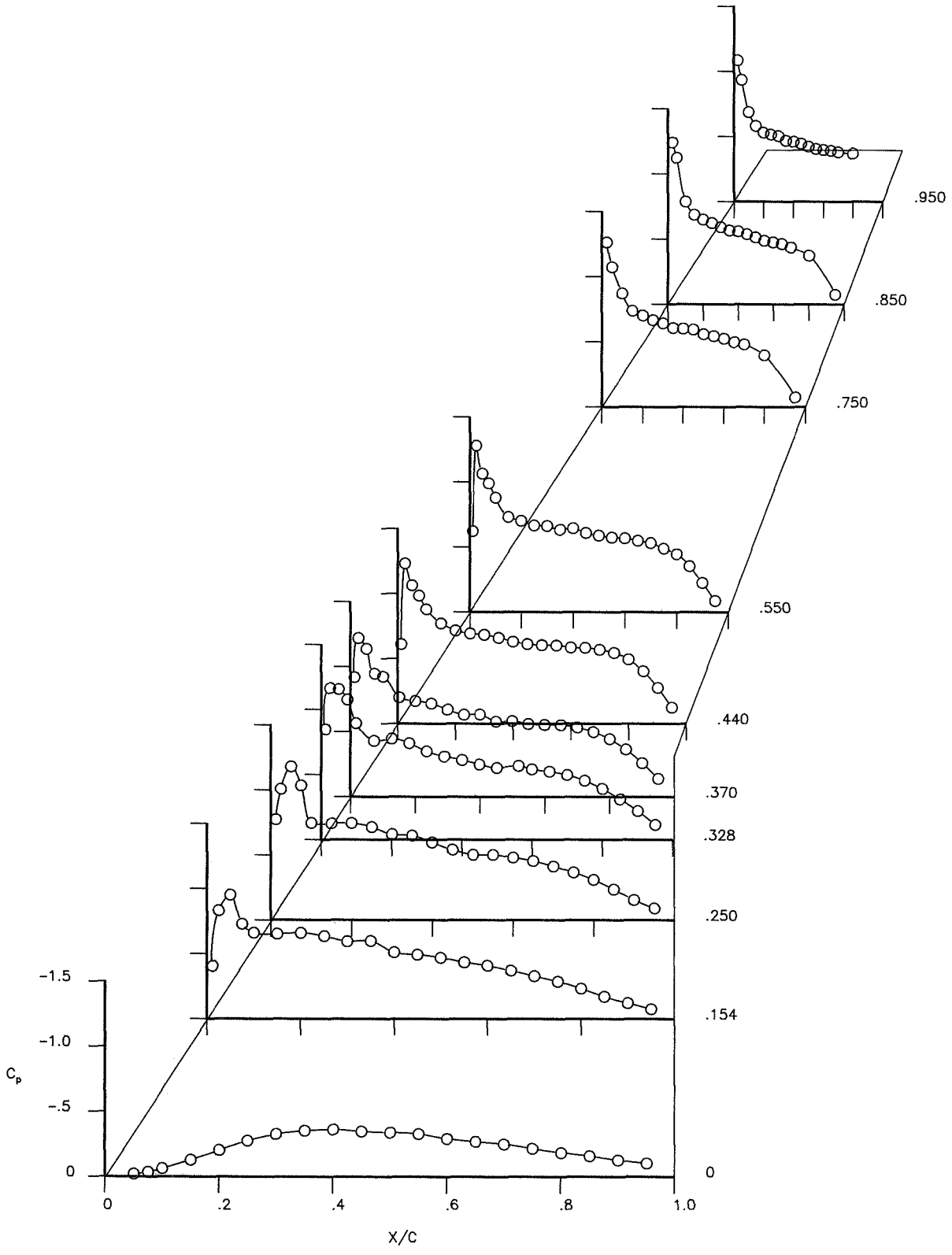


(a) Upper surface.

Figure 16.- Pressure distributions for clean wing at M = 0.70. $\alpha$ = 1.71°; $C_L$ = 0.48. Semispan stations y/(b/2) = 0 to .950 given to right of plot.

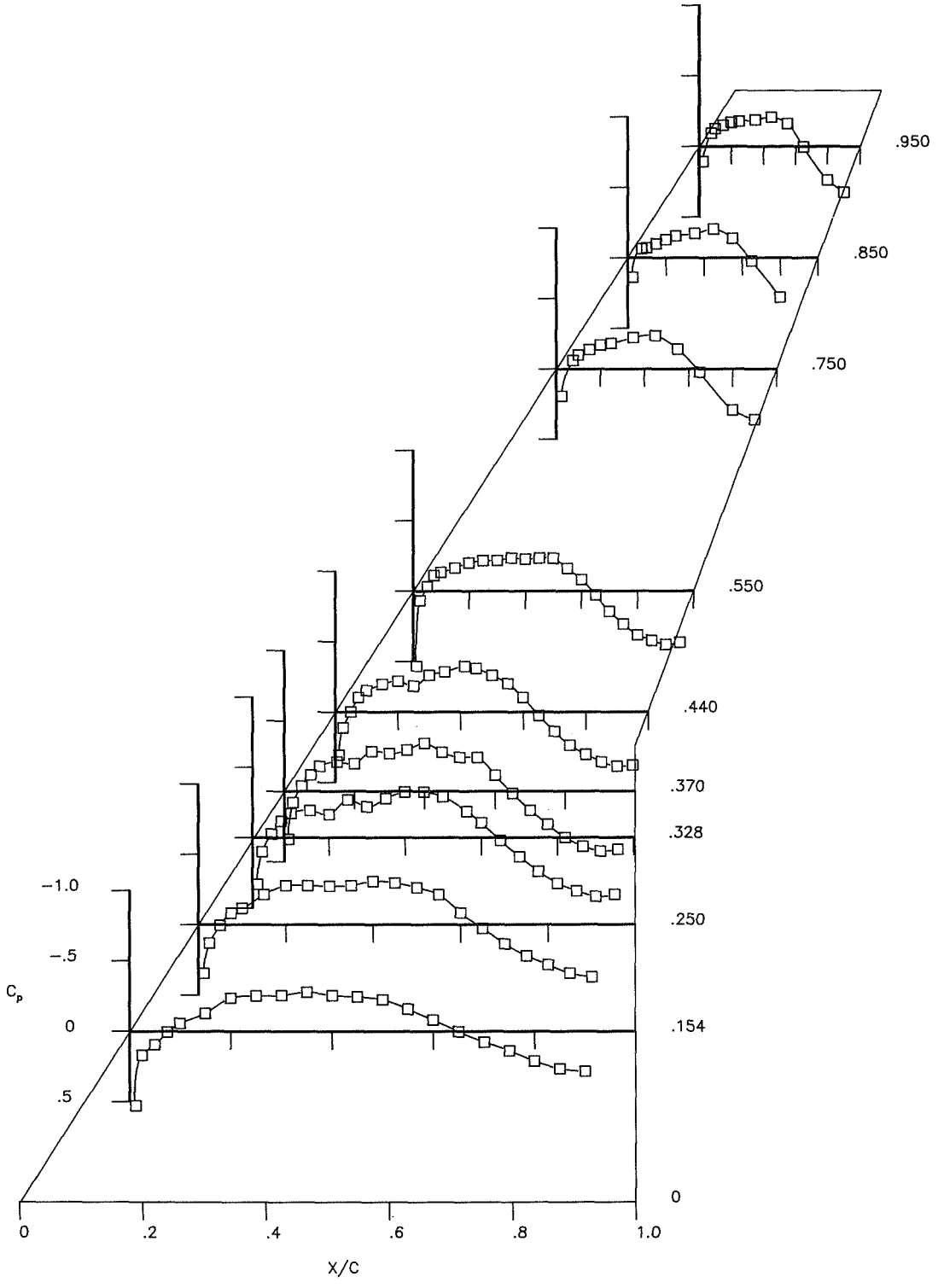


(b) Lower surface.

Figure 16.- Concluded.

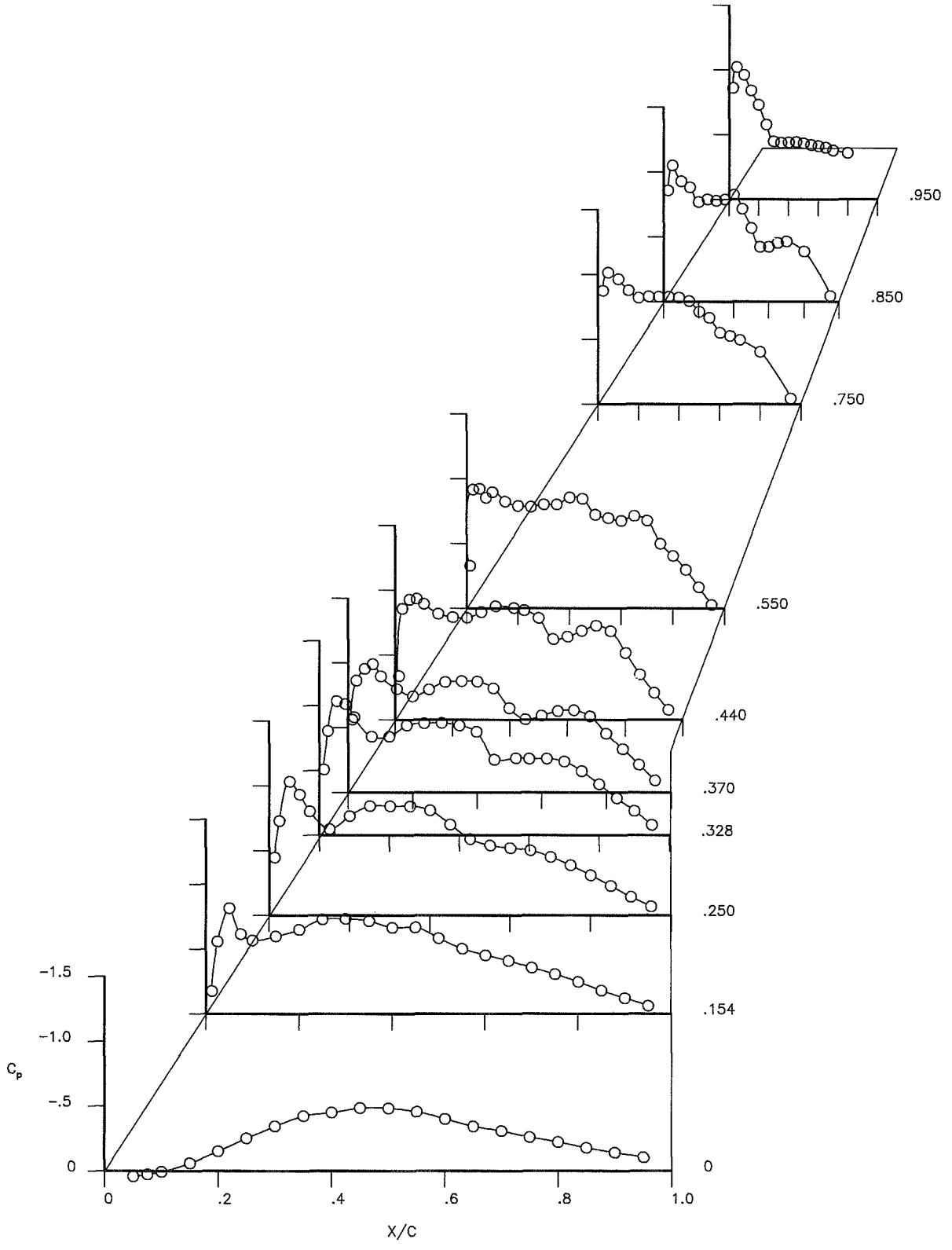


(a) Upper surface.

Figure 17.- Pressure distributions for clean wing at M = 0.80. $\alpha$ = 1.24°; $C_L$ = 0.49. Semispan stations y/(b/2) = 0 to .950 given to right of plot.

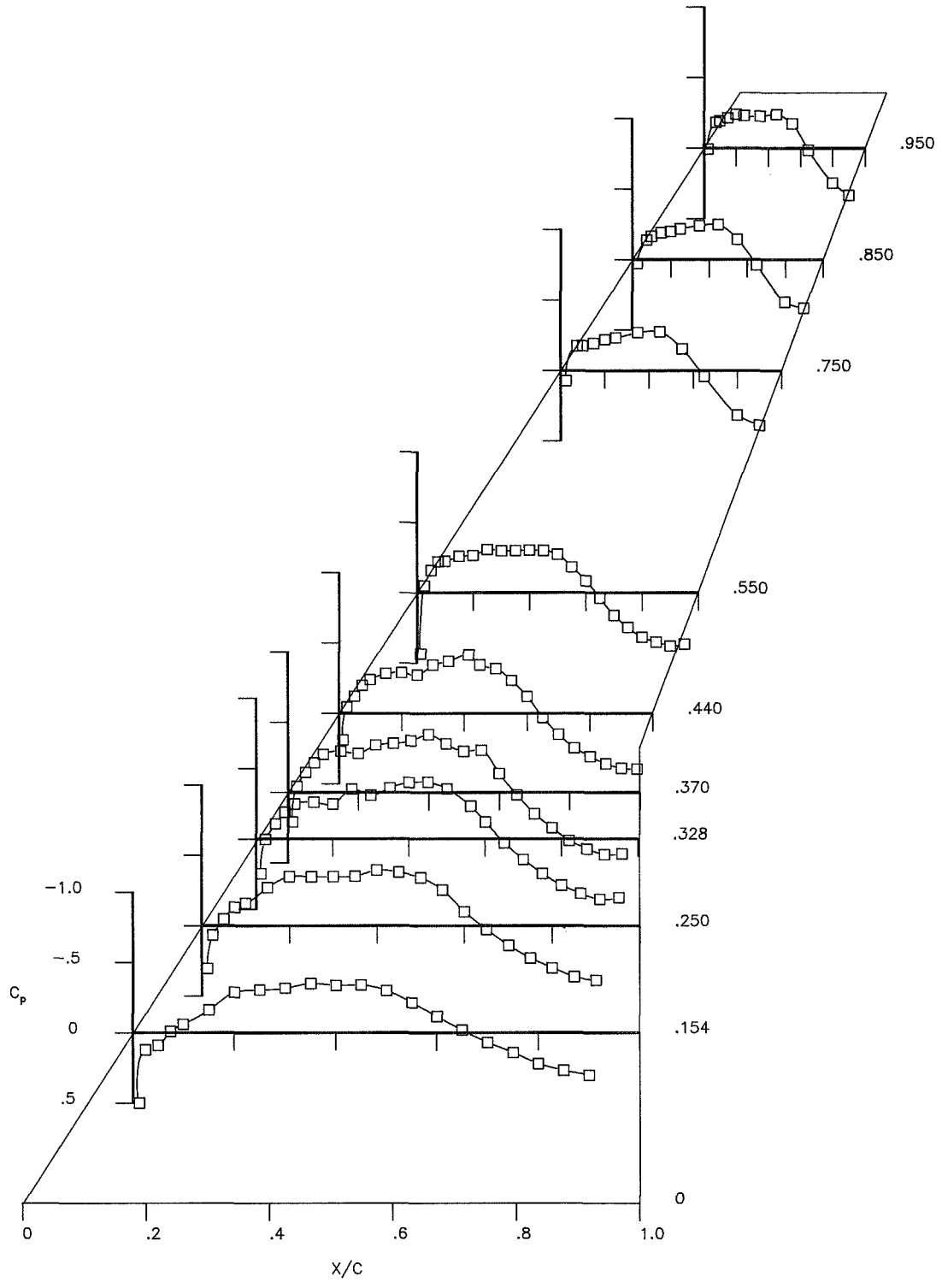


(b) Lower surface.

Figure 17.- Concluded.

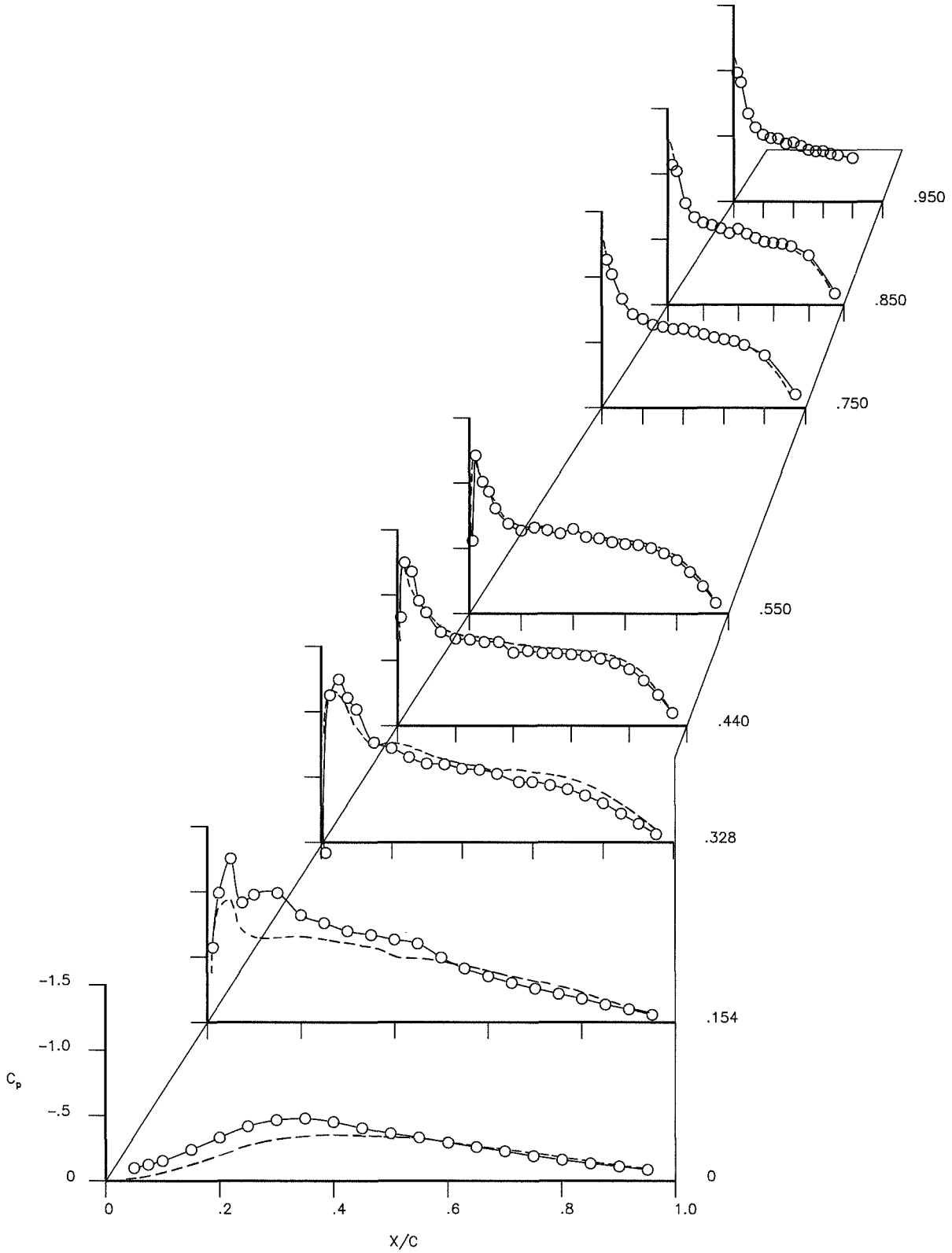


(a) Upper surface.

Figure 18.- Pressure distributions on wing for configuration with symmetrical nacelles (OWS-A) at M = 0.70. (Dashed lines for clean wing from ref. 6.) Semispan stations y/(b/2) = 0 to .950 given to right of plot. $\alpha = 1.14^\circ$; $C_L = 0.45$.

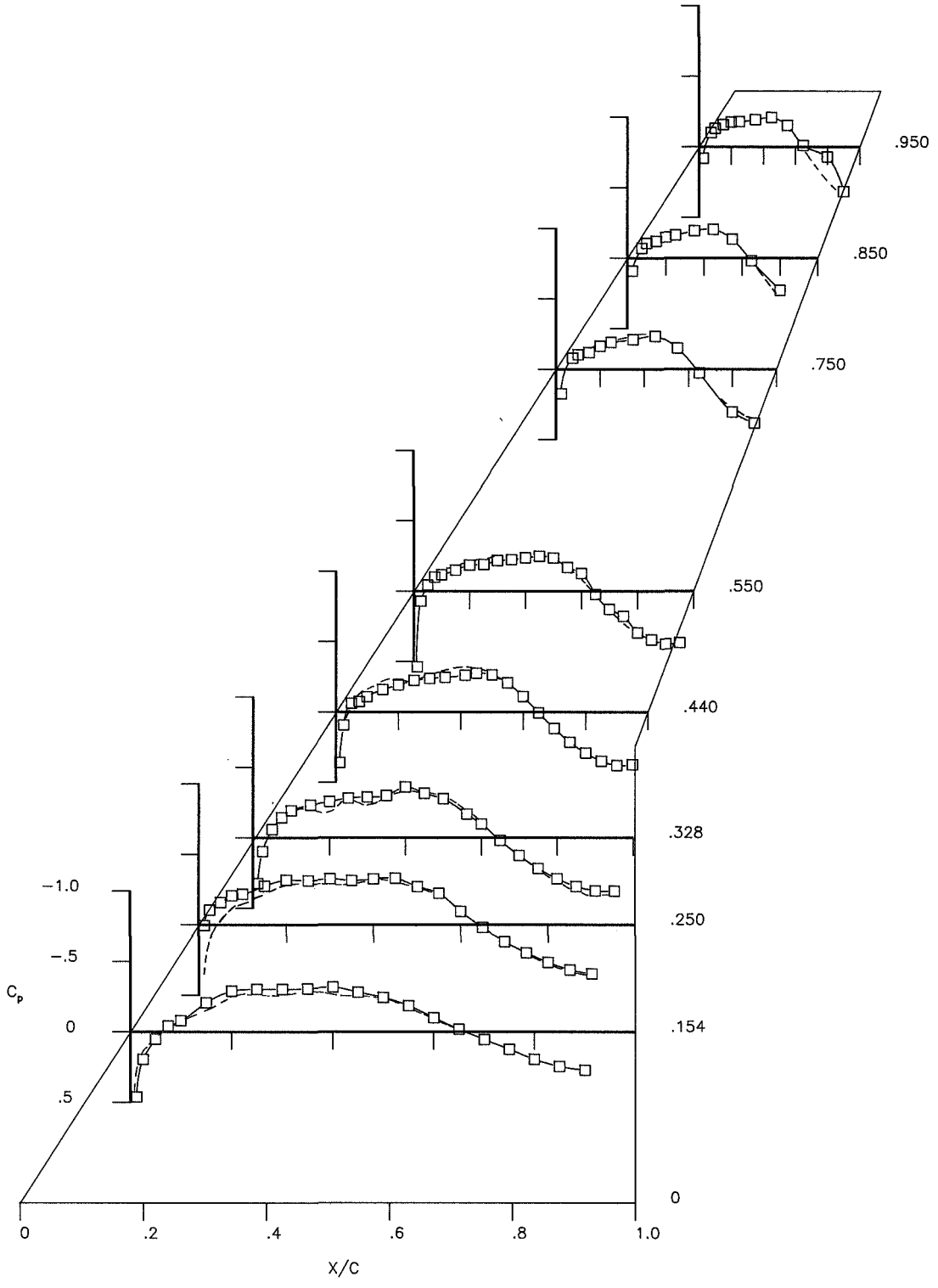


(b) Lower surface.

Figure 18.- Concluded.

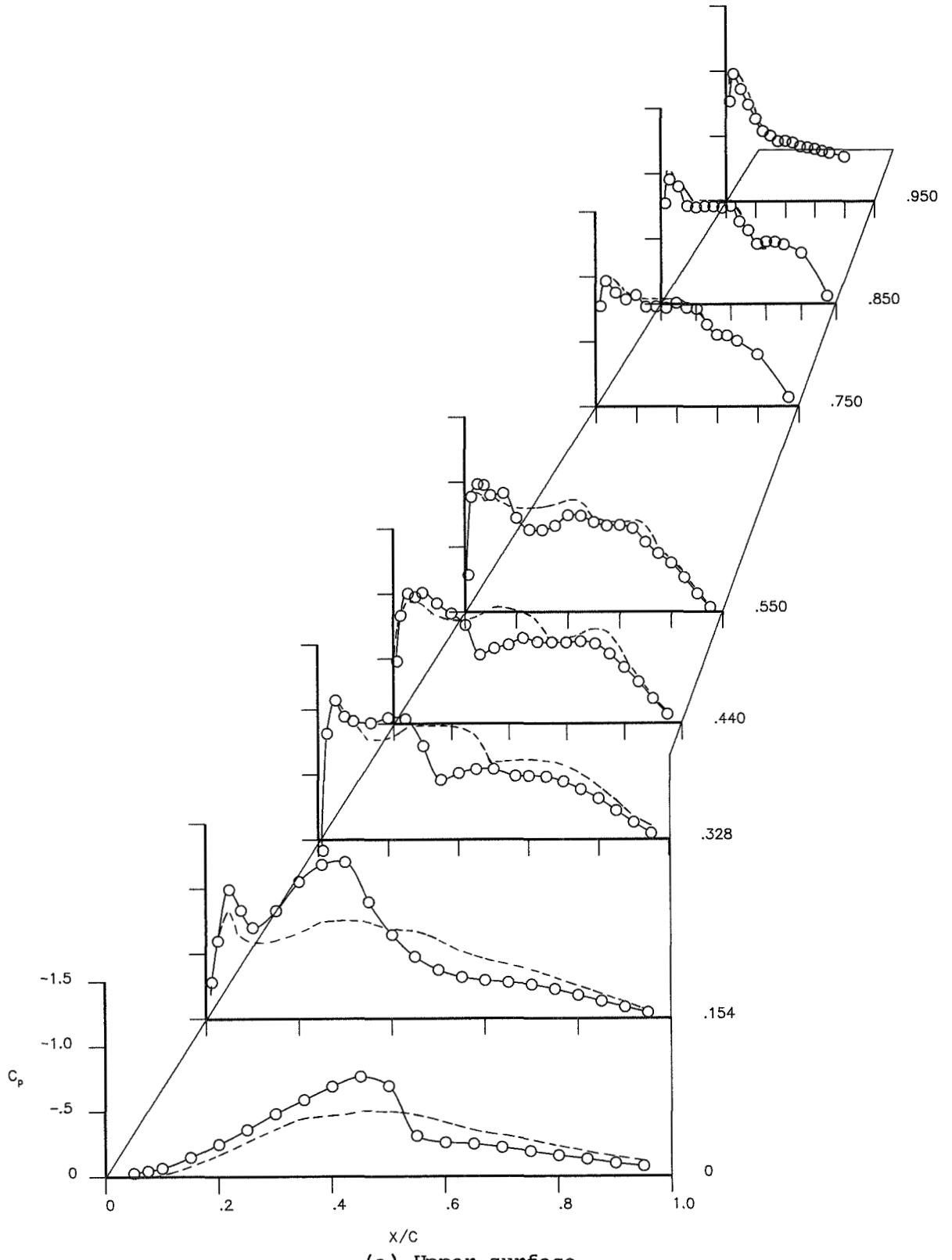


(a) Upper surface.

Figure 19.- Pressure distributions on wing for configuration with symmetrical nacelles (OWS-A) at M = 0.80. (Dashed lines for clean wing from ref. 6.) Semispan stations y/(b/2) = 0 to .950 given to right of plot. $\alpha = 1.14°$; $C_L = 0.45$.

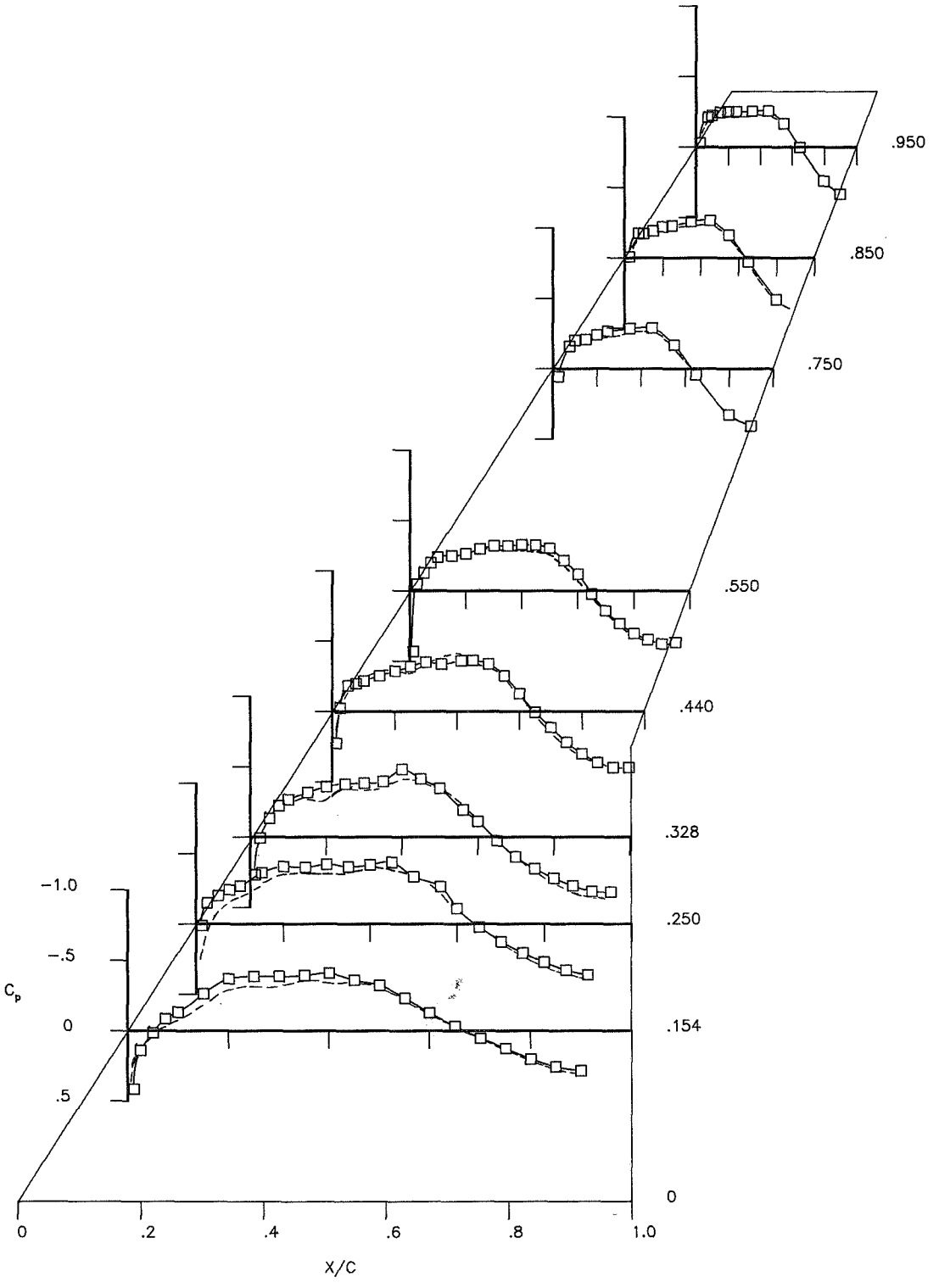


(b) Lower surface.

Figure 19.- Concluded.

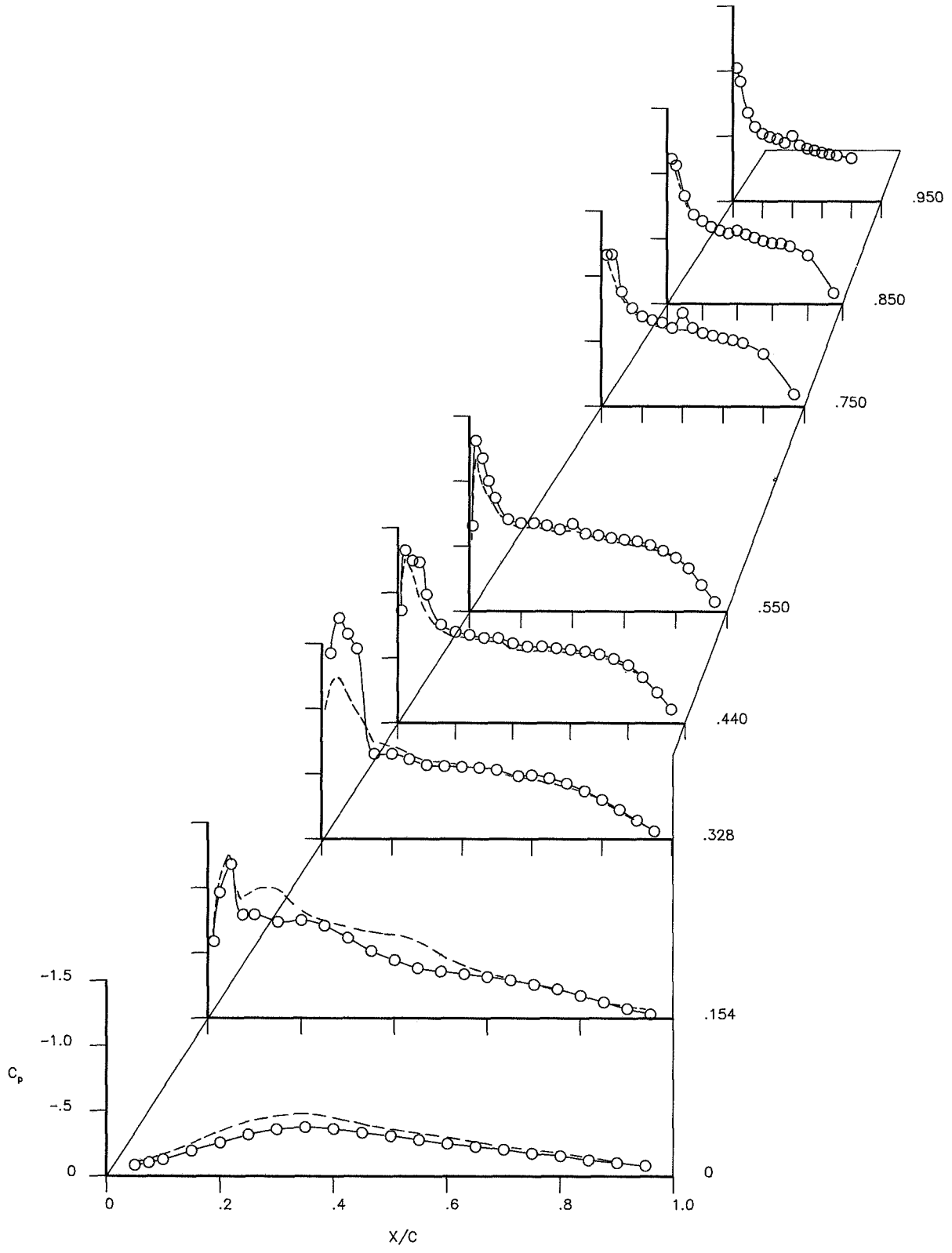


(a) Upper surface.

Figure 20.- Pressure distributions on wing for configuration with contoured nacelles (OWC-A) at M = 0.70, $\alpha = 1.57°$; $C_L = 0.46$. (Dashed lines are data on wing with symmetrical nacelles.) Semispan stations y/(b/2) = 0 to .950 given to right of plot.

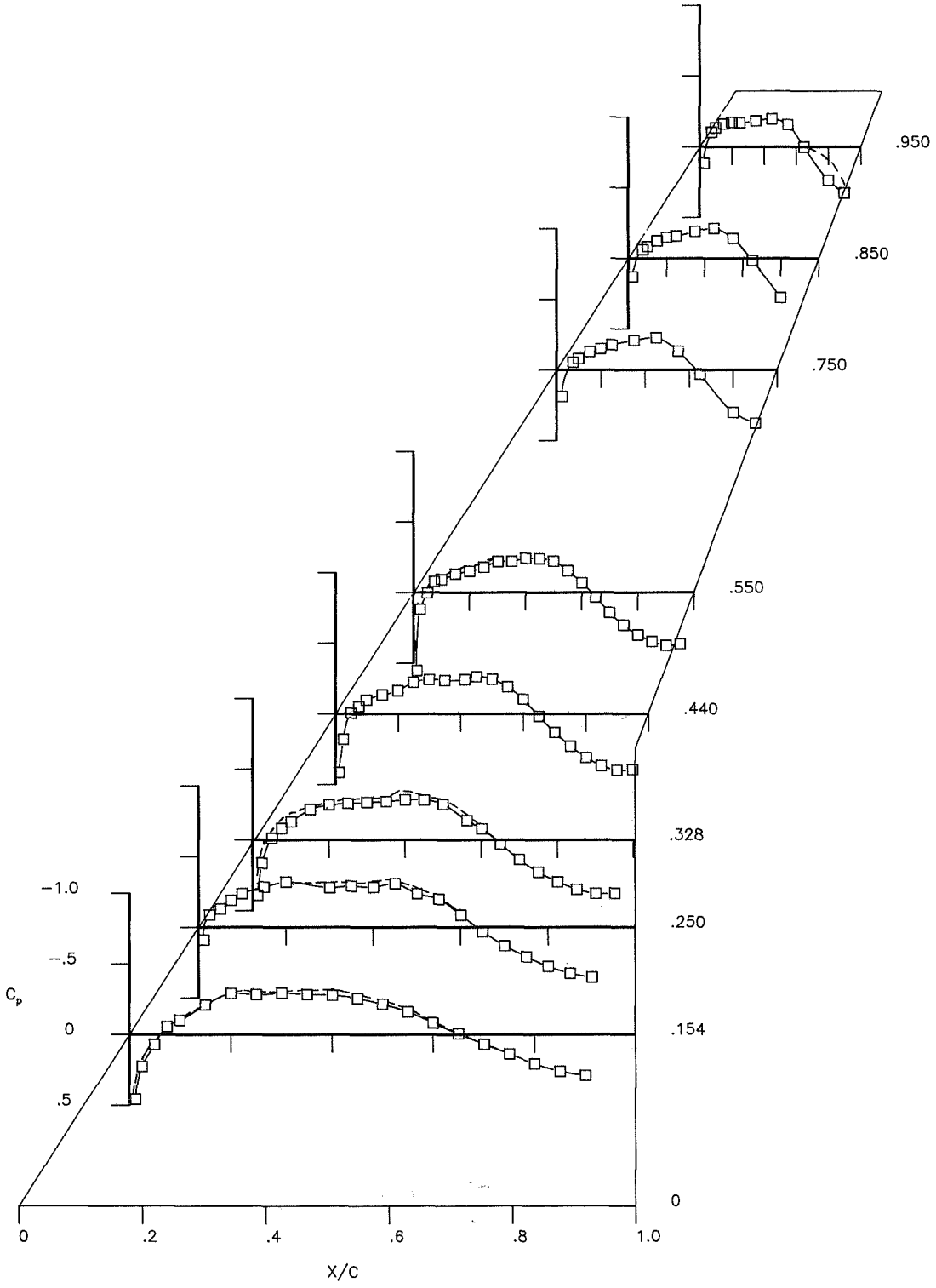


(b) Lower surface.

Figure 20.- Concluded.

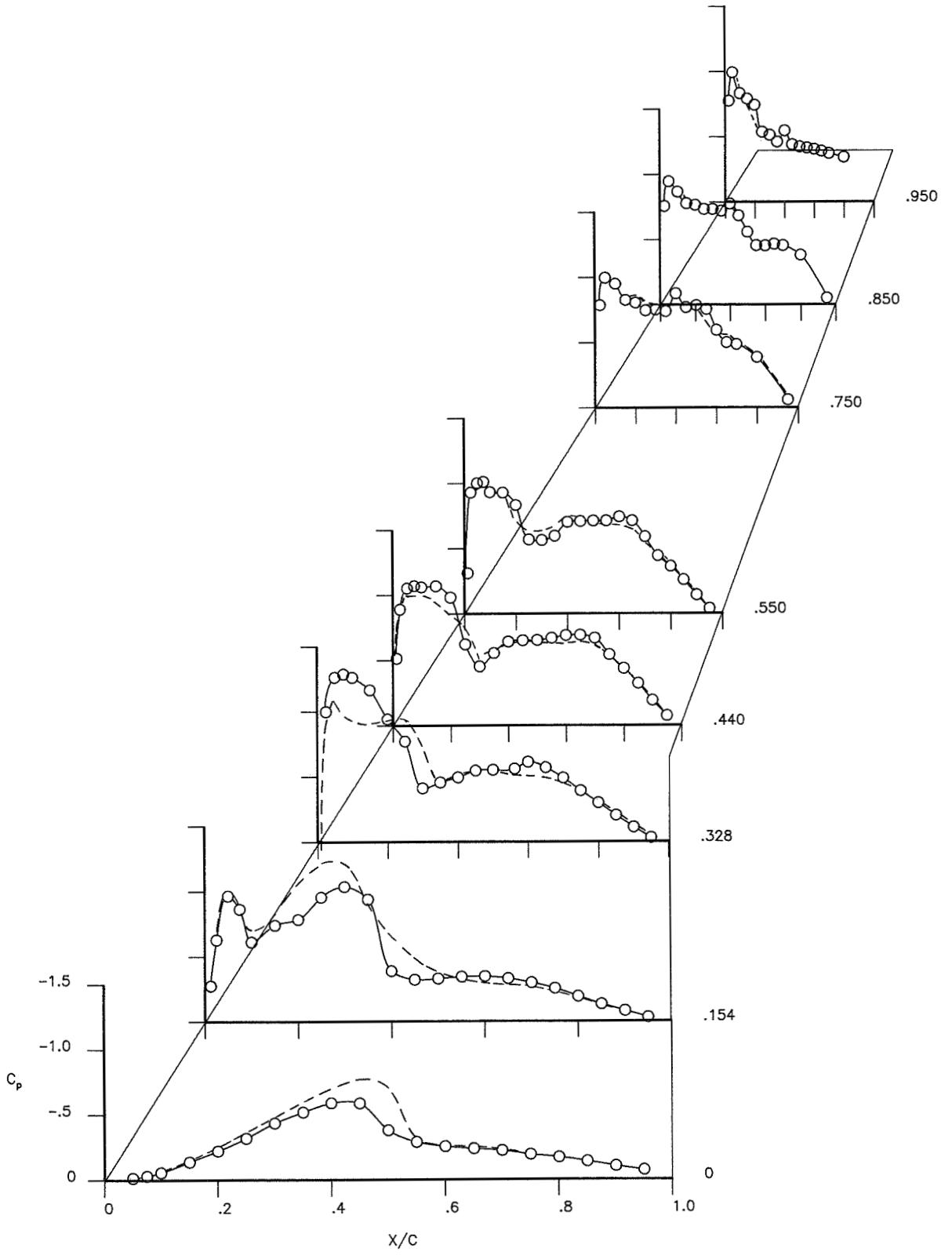


(a) Upper surface.

Figure 21.- Pressure distributions on wing for configuration with contoured nacelles (OWC-A) at $M = 0.80$, $\alpha = 1.12^\circ$; $C_L = 0.45$. (Dashed lines are data on wing with symmetrical nacelles.) Semispan stations $y/(b/2) = 0$ to .950 given to right of plot.

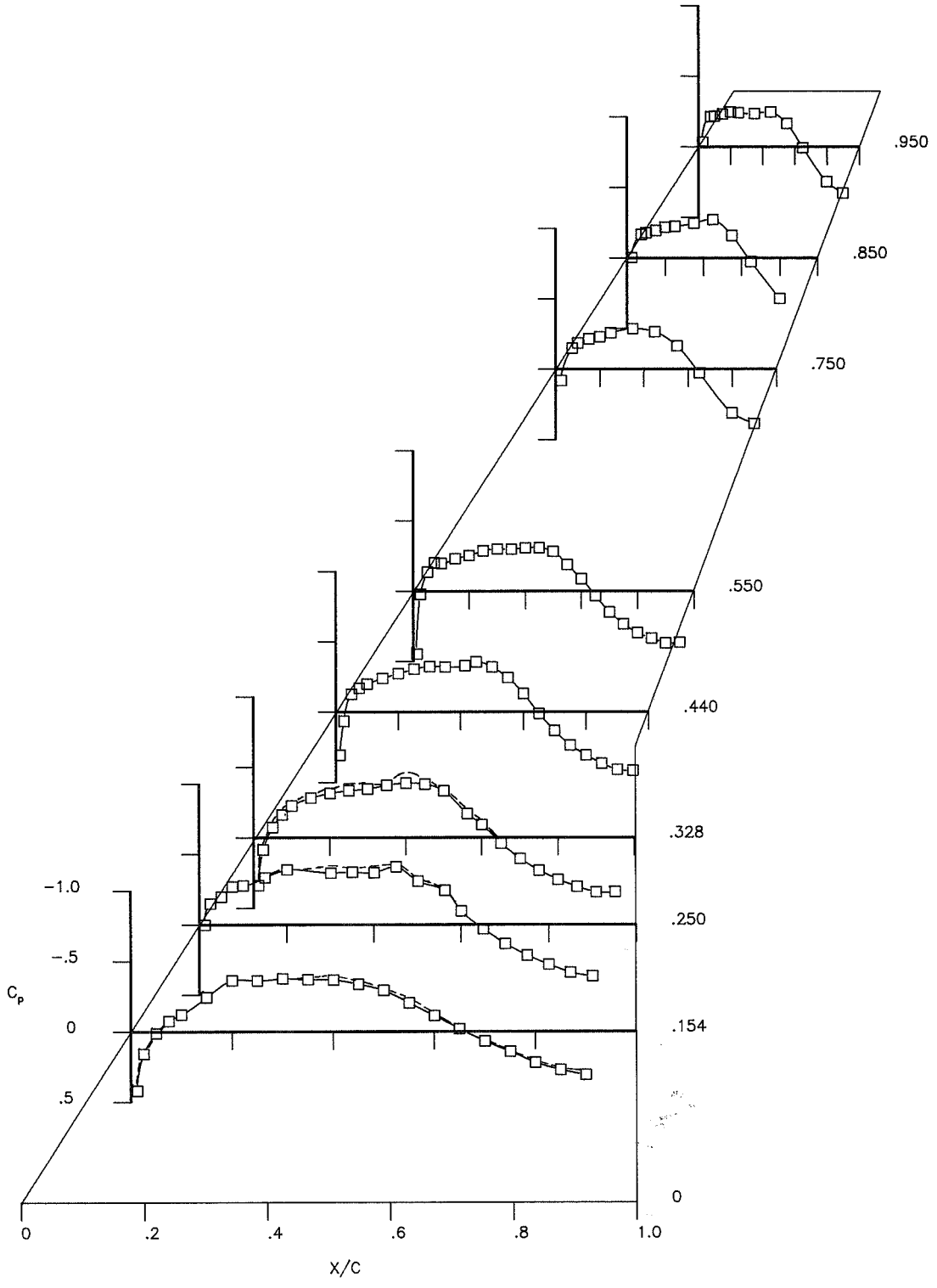


(b) Lower surface.

Figure 21.- Concluded.

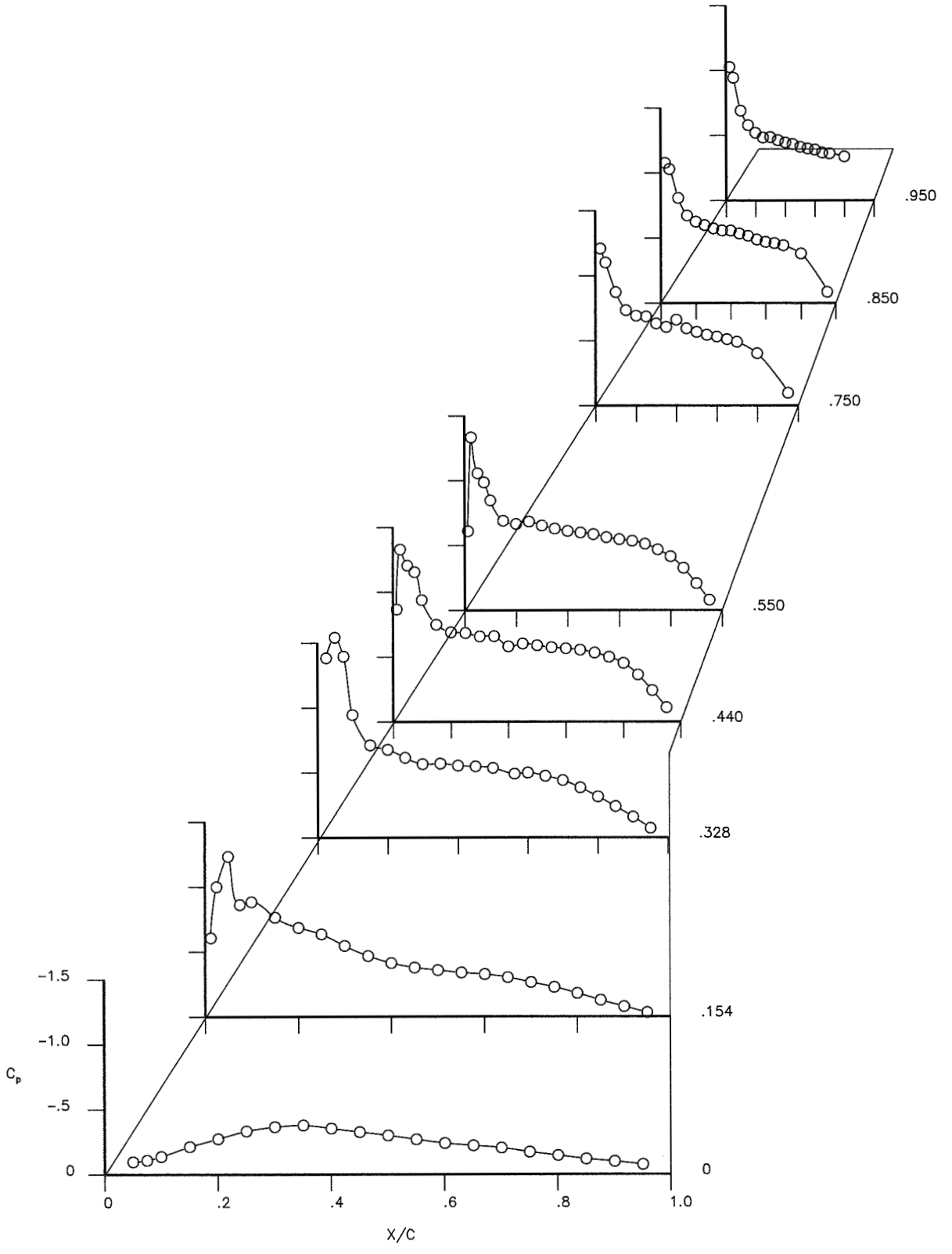


(a) Upper surface.

Figure 22.- Pressure distributions on wing for configuration with contoured nacelles and alternate pylons (OWC-B) at M = 0.70. $\alpha$ = 1.62°; $C_L$ = 0.47. Semispan stations y/(b/2) = 0 to .950 given to right of plot.

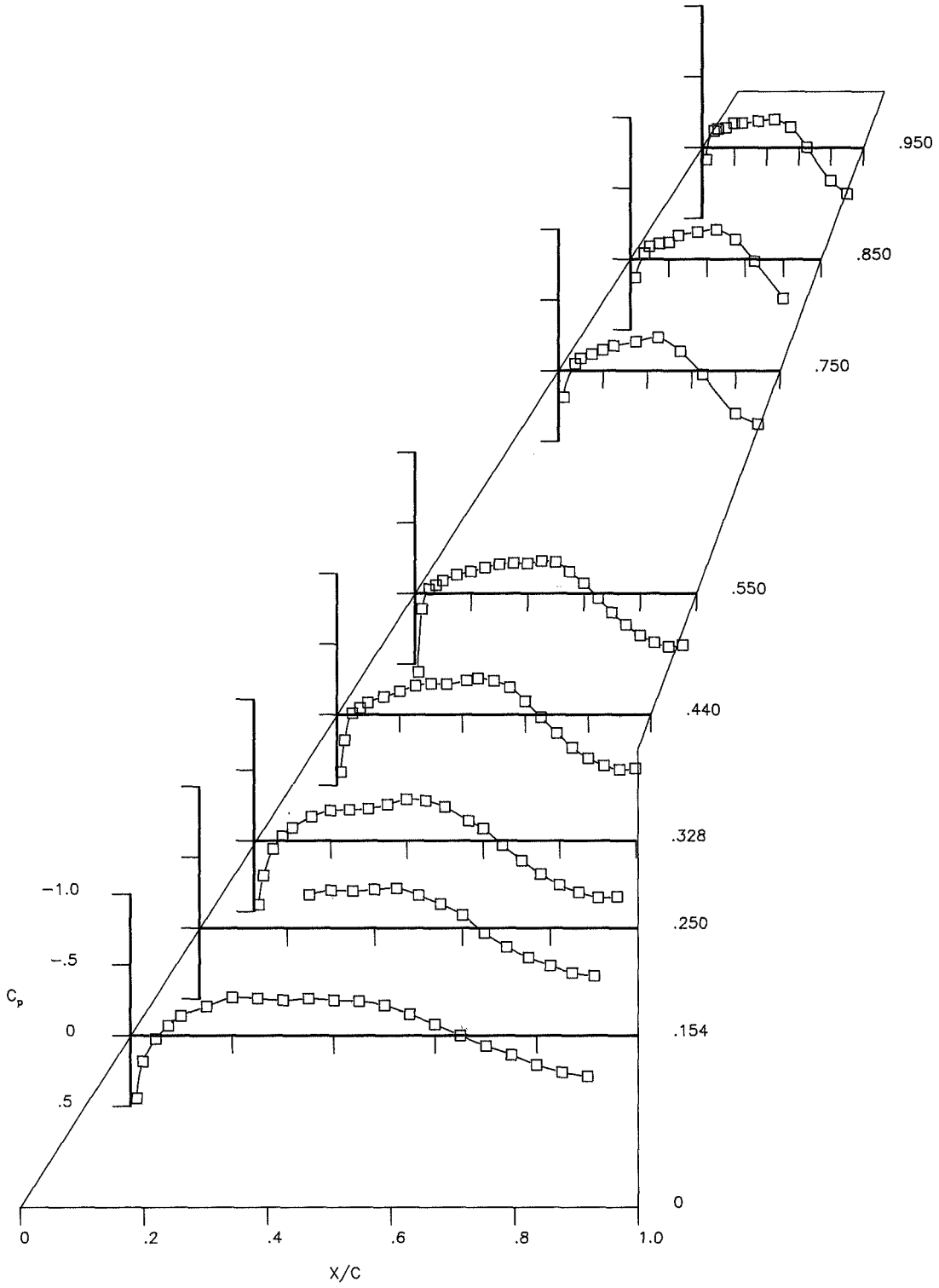


(b) Lower surface.

Figure 22.- Concluded.

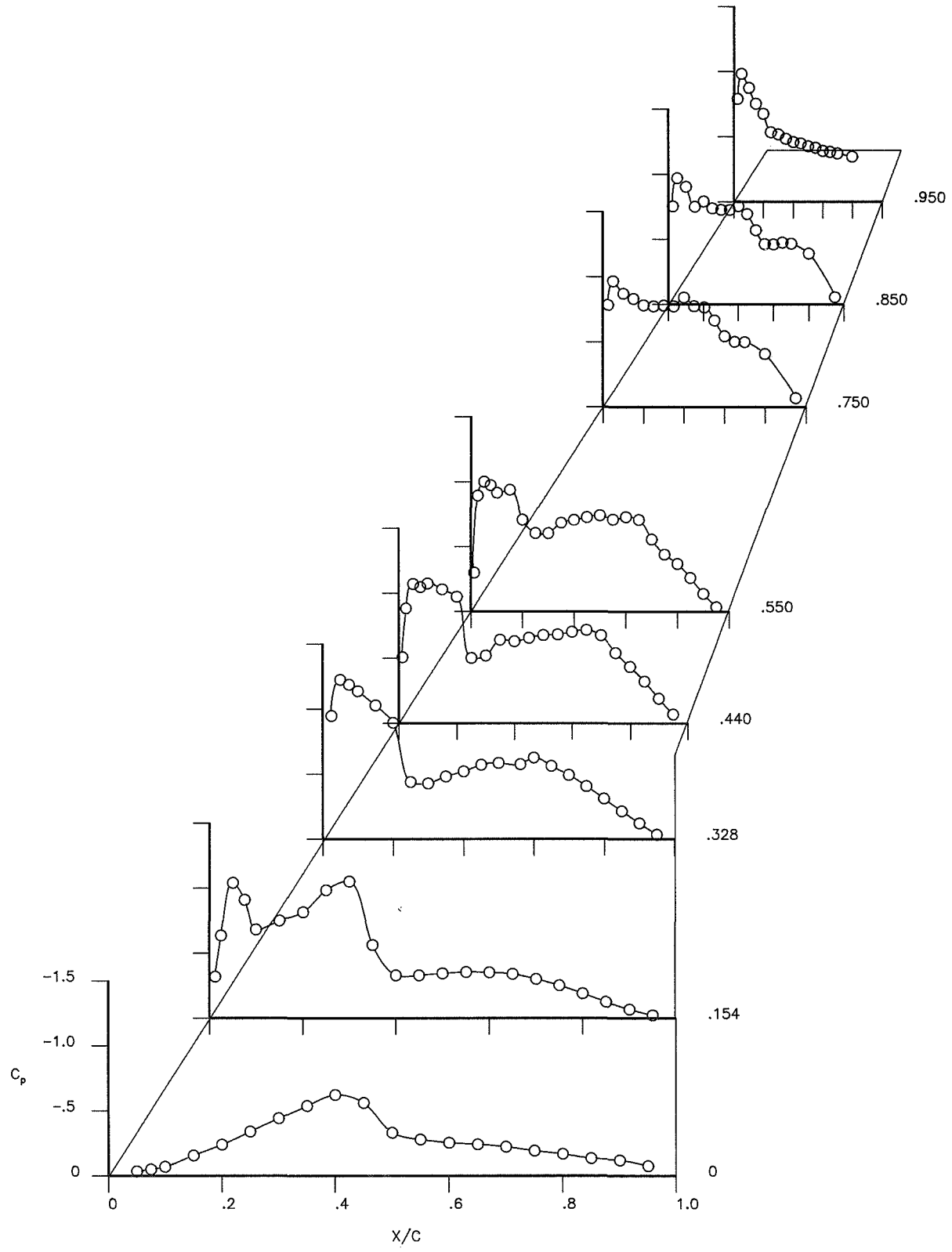


(a) Upper surface.

Figure 23.- Pressure distributions on wing for configuration with contoured nacelles and alternate pylons (OWC-B) at M = 0.80, $\alpha$ = 1.08°; $C_L$ = 0.45. Semispan stations y/(b/2) = 0 to .950 given to right of plot.

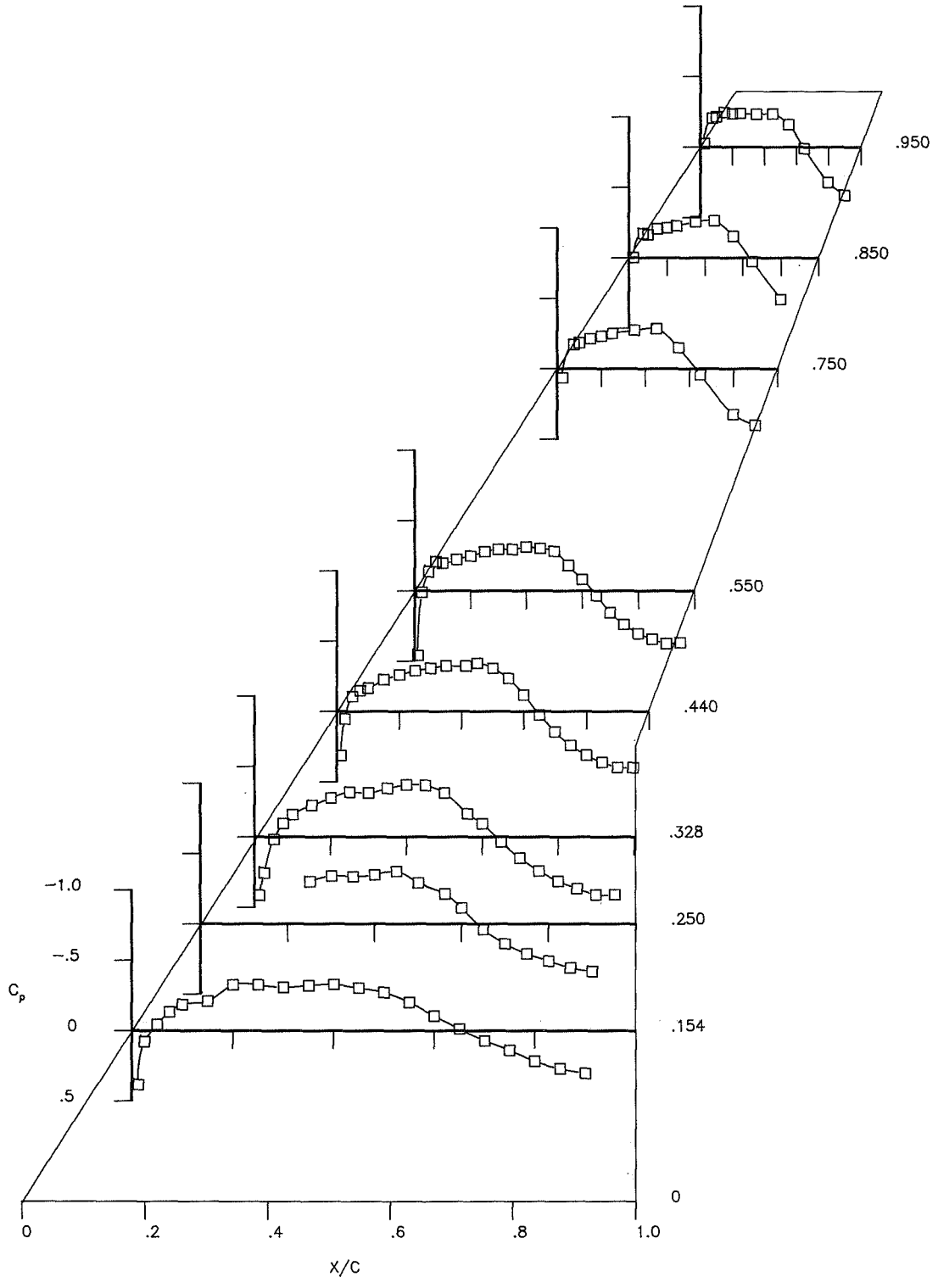


(b) Lower surface.

Figure 23.- Concluded.

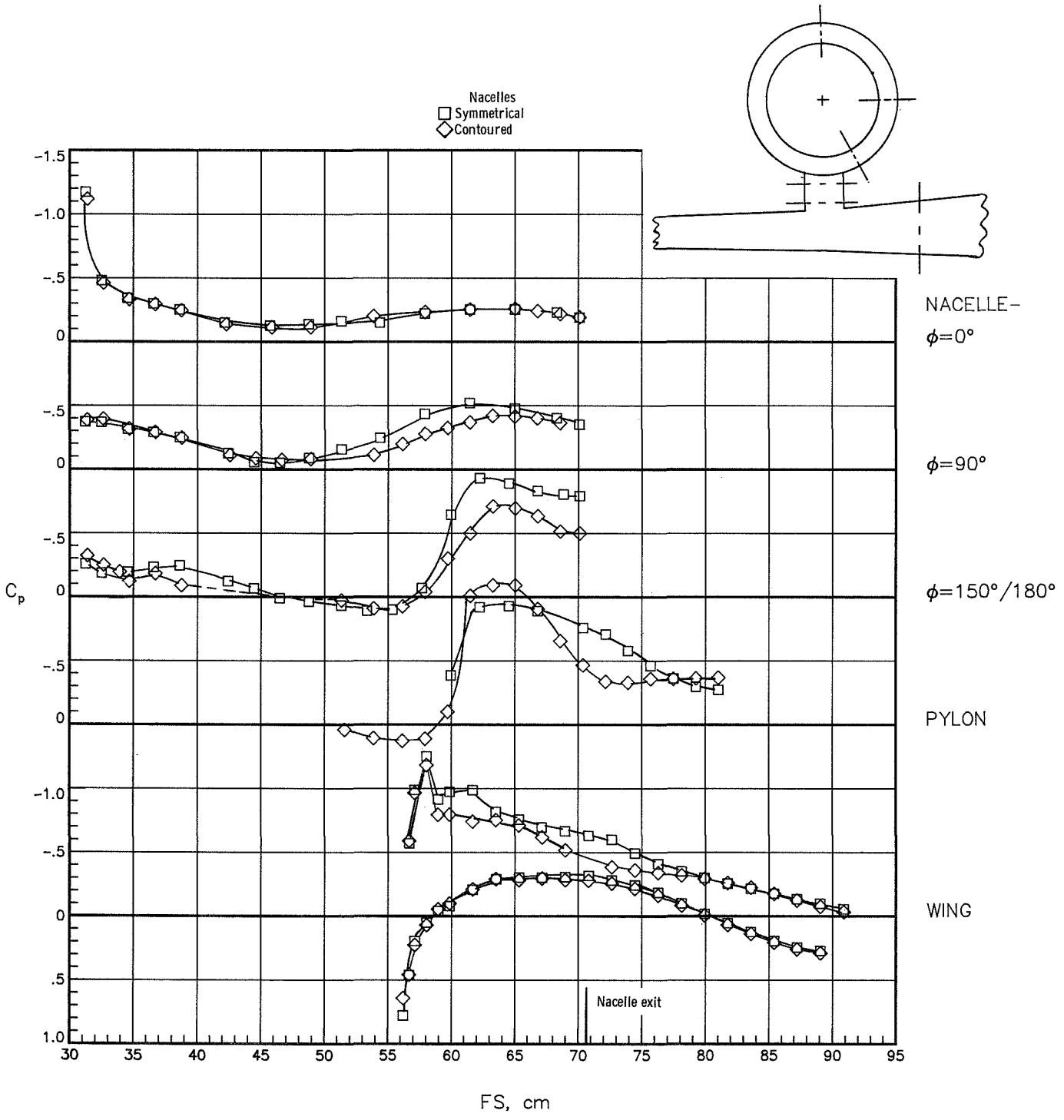


(a) Inboard side; y/(b/2) = 0.154.

Figure 24.- Effect of nacelle-pylon contouring on nacelle, pylon, and wing pressures at M = 0.70, $\alpha$ = 1.60°; $C_L$ = 0.47.

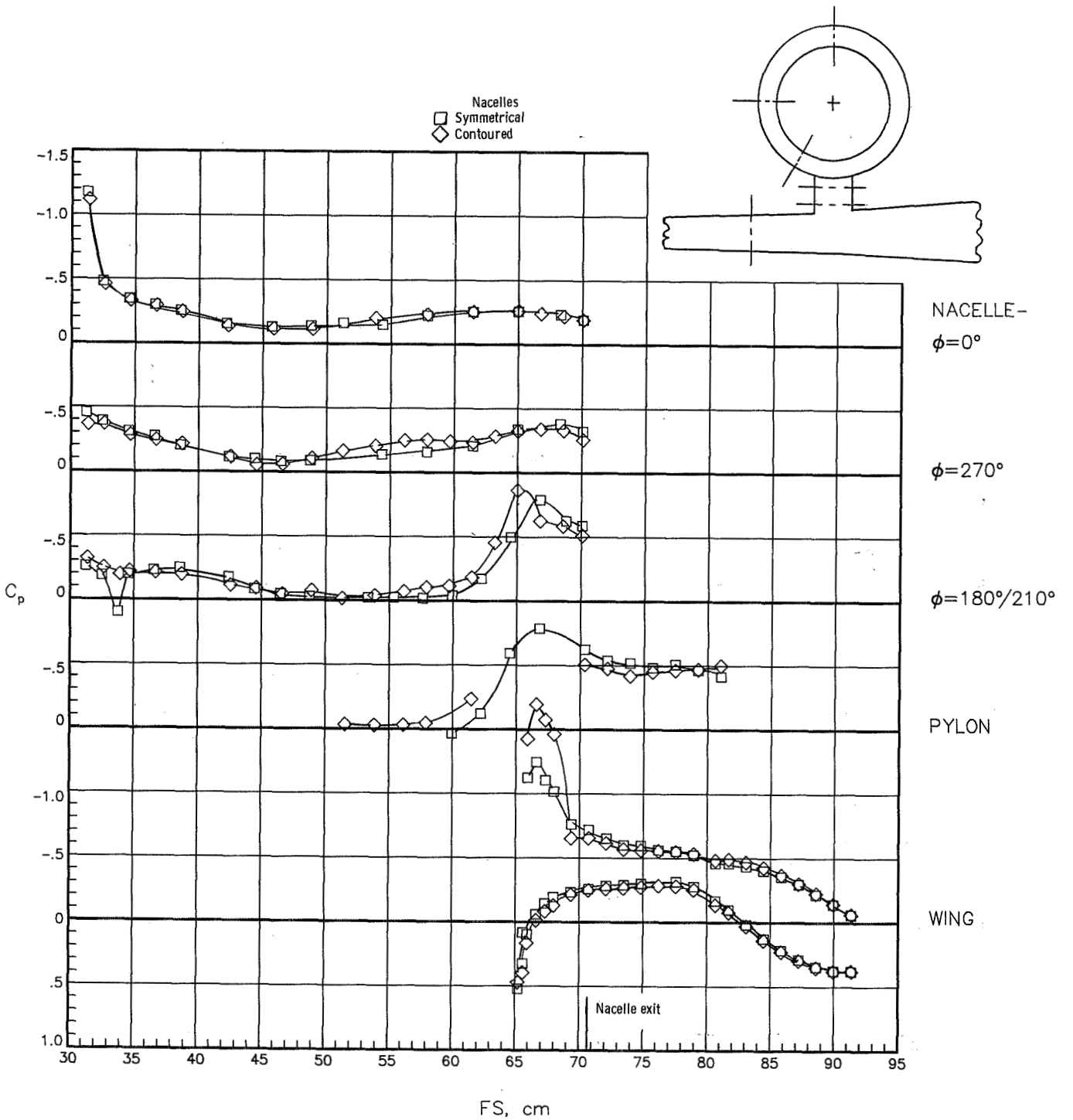


(b) Outboard side; y/(b/2) = 0.328.

Figure 24.- Concluded.

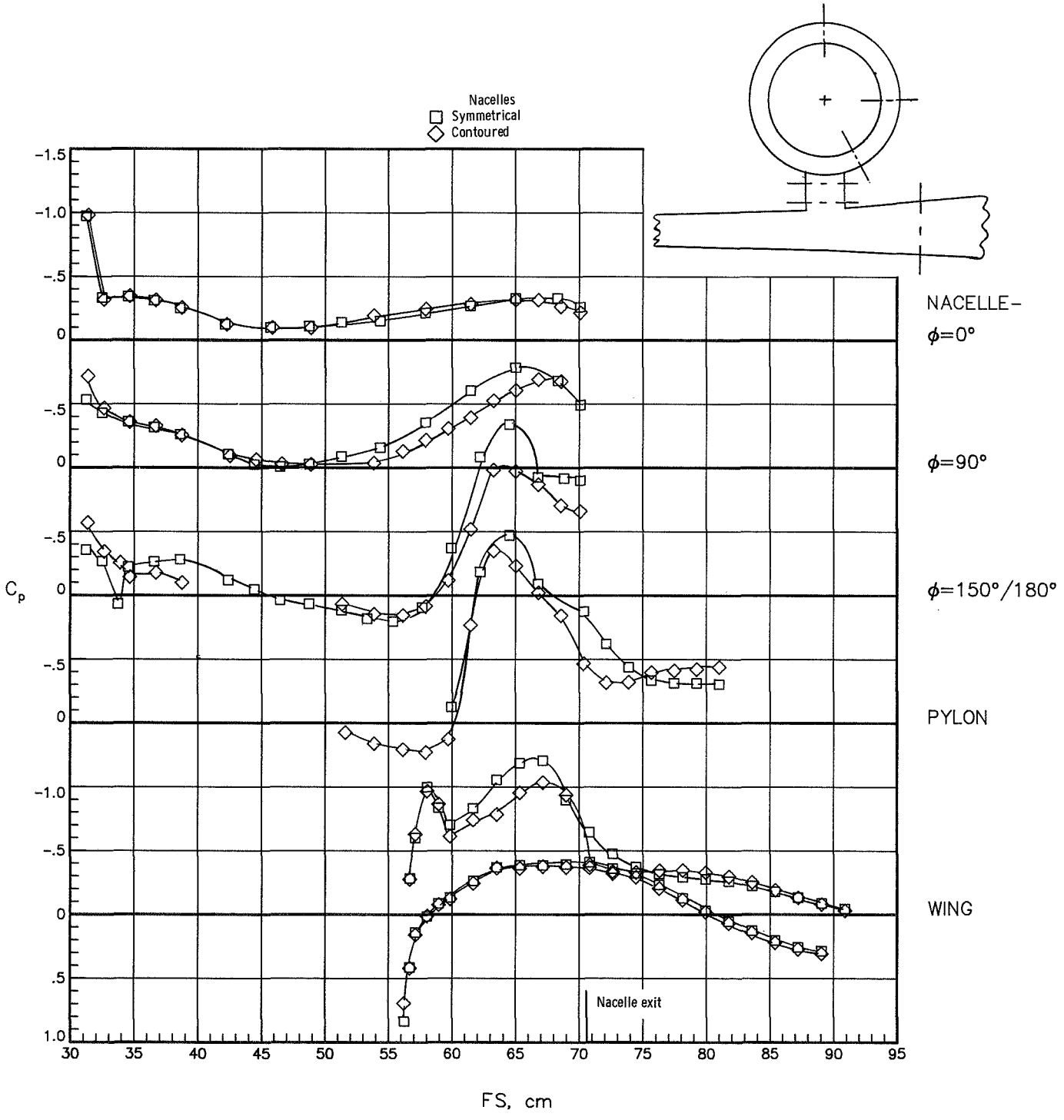


(a) Inboard side; y/(b/2) = 0.154.

Figure 25.- Effect of nacelle-pylon contouring on nacelle, pylon, and wing pressure at M = 0.80, $\alpha$ = 1.13°; $C_L$ = 0.45.

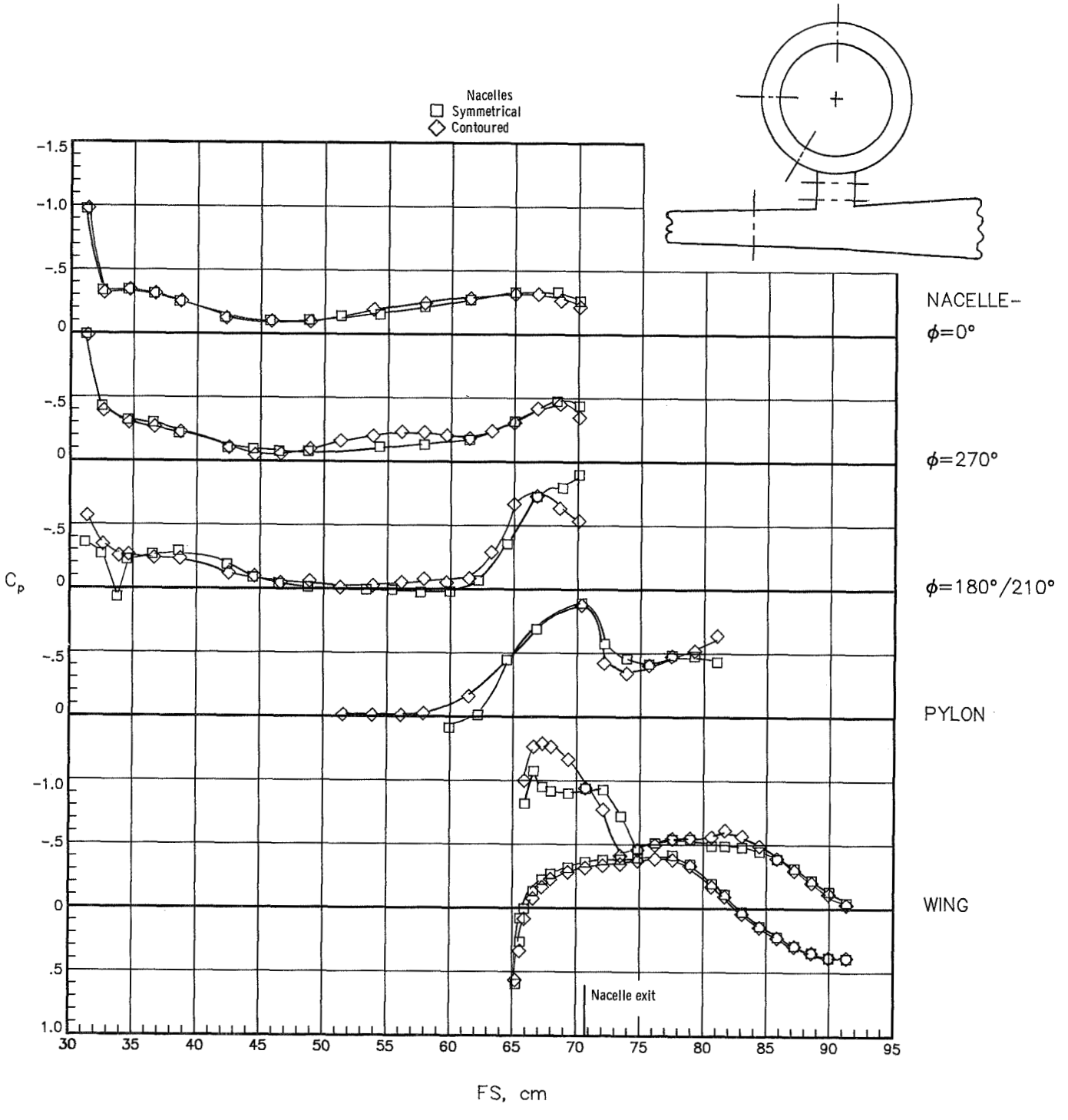


(b) Outboard side; y/(b/2) = 0.328.

Figure 25.- Concluded.

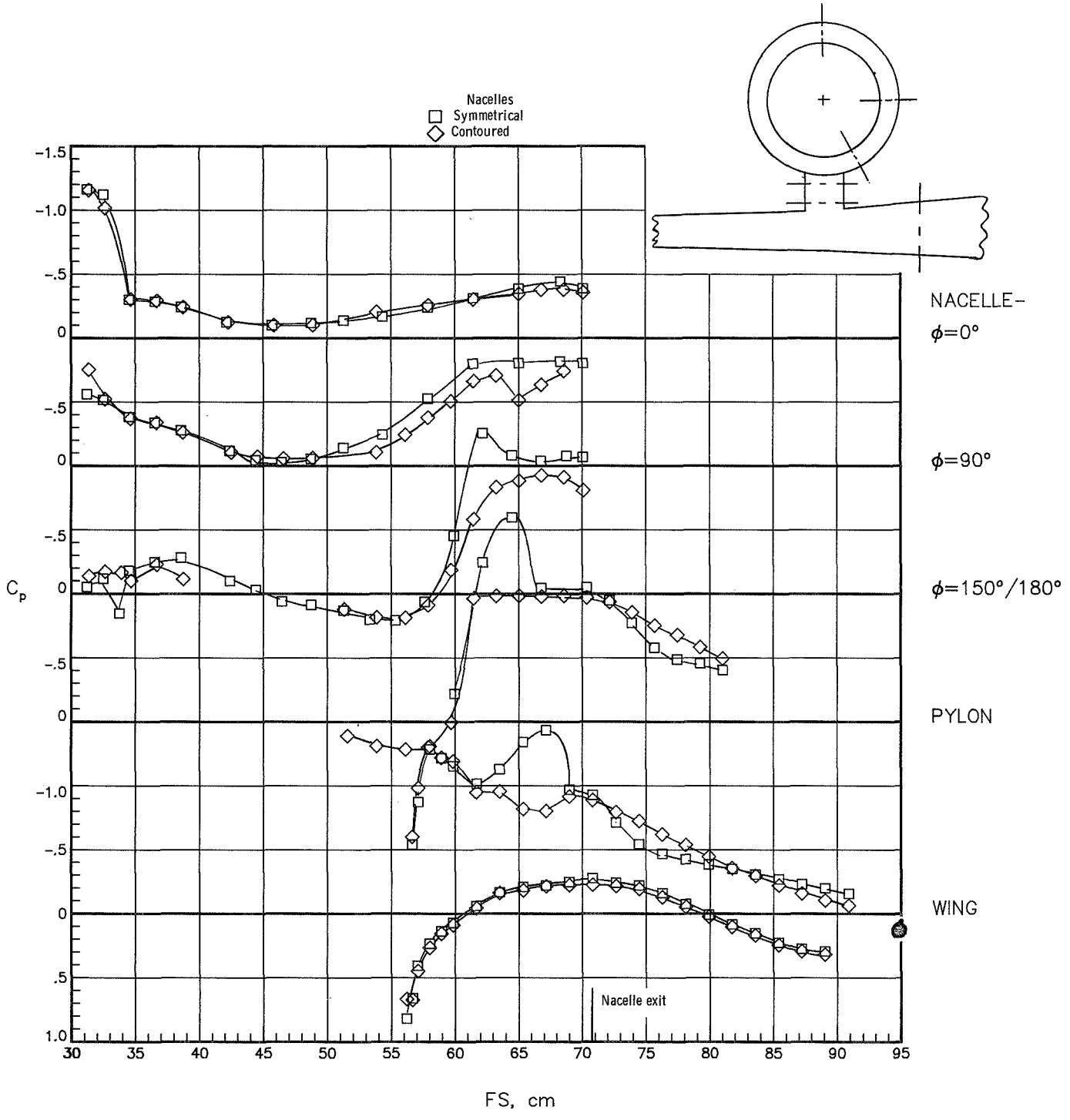


(a) Inboard side; y/(b/2) = 0.154.

Figure 26.- Effect of nacelle-pylon contouring on nacelle, pylon, and wing pressure at M = 0.80, $\alpha$ = 4.11°; $C_L$ = 0.82.

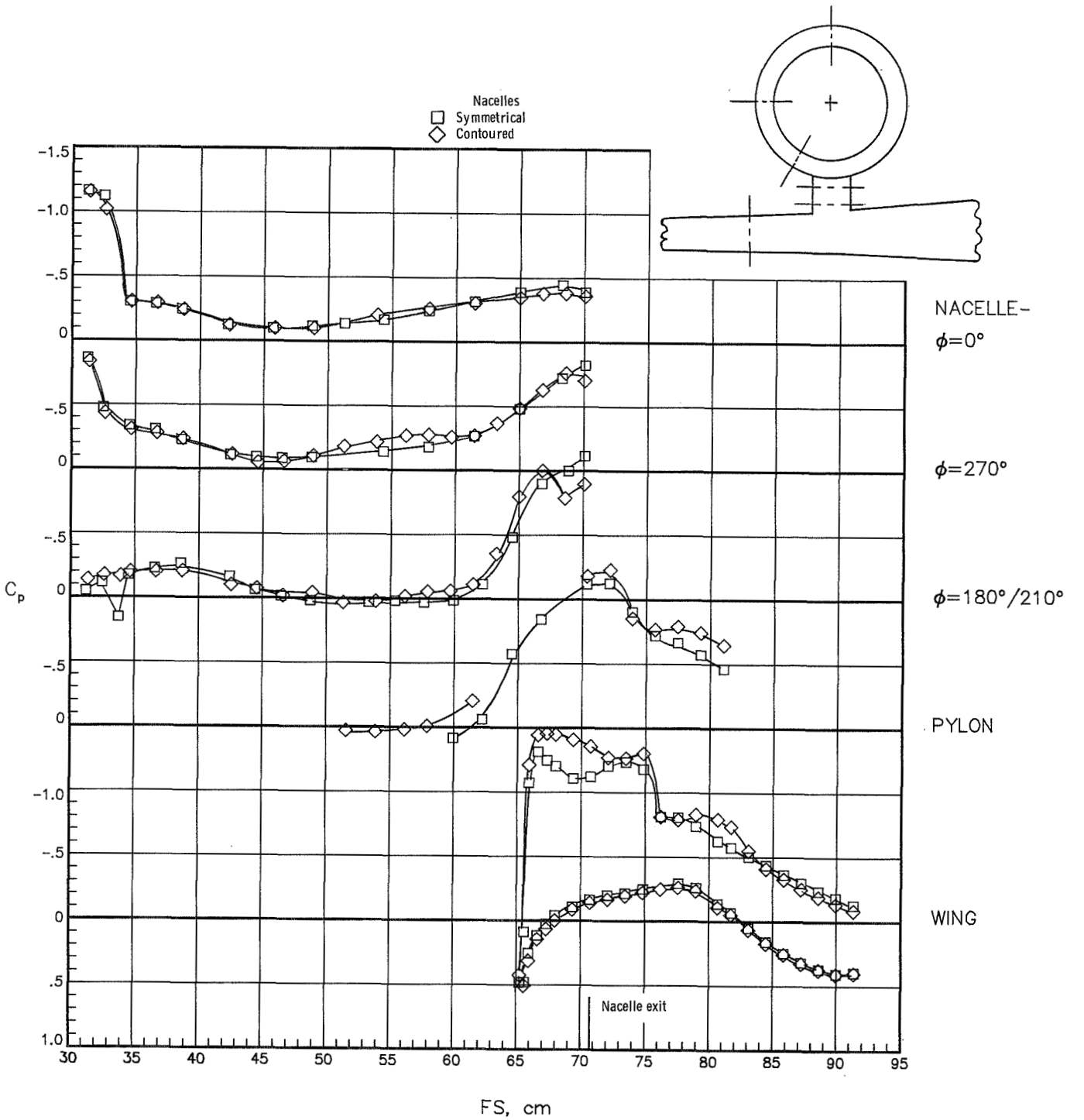


(b) Outboard side; y/(b/2) = 0.328.

Figure 26.- Concluded.

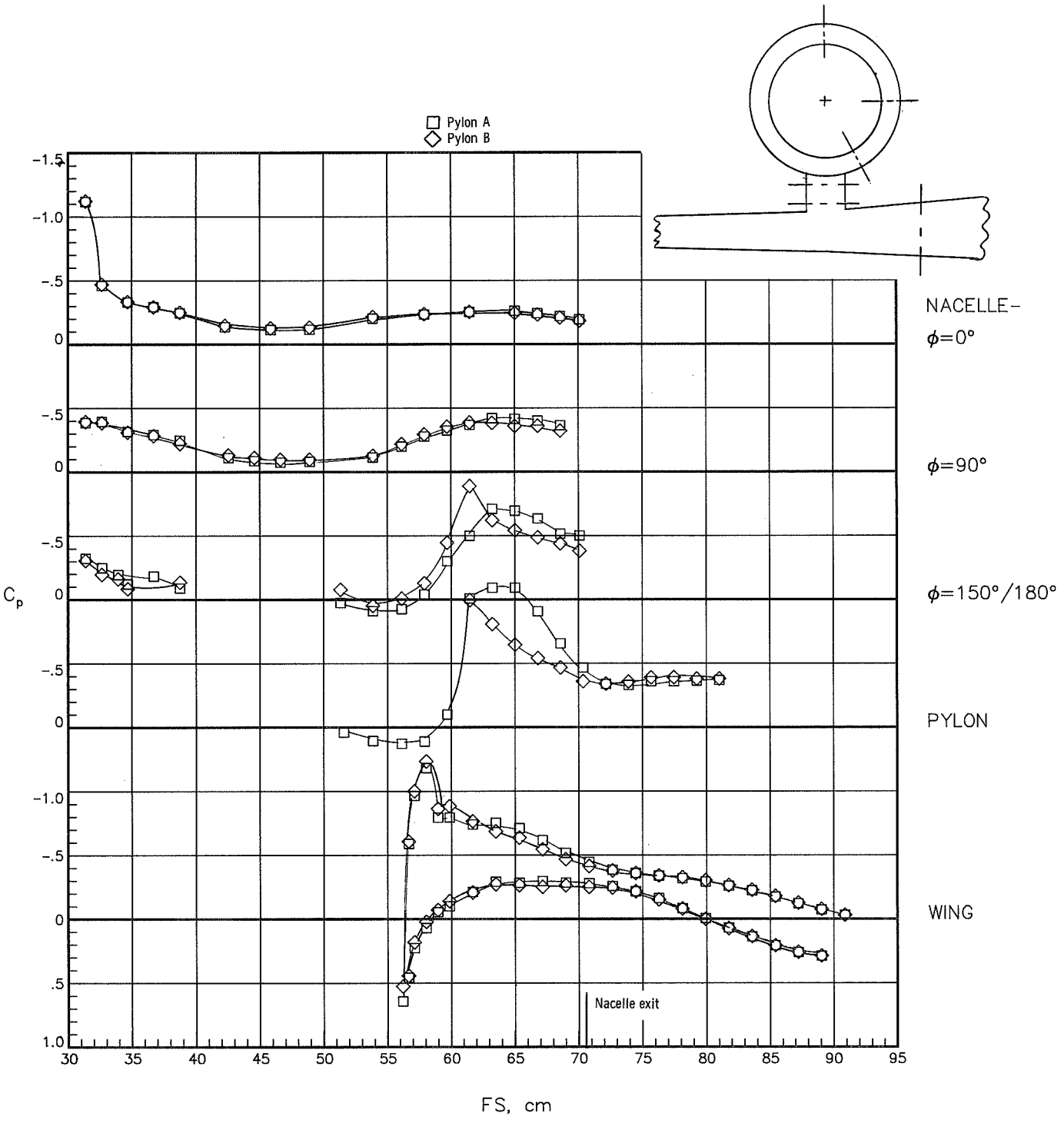


(a) Inboard side; y/(b/2) = 0.154.

Figure 27.- Effect of pylon size on nacelle, pylon, and wing pressures at M = 0.70, $\alpha$ = 1.60°; $C_L$ = 0.46.

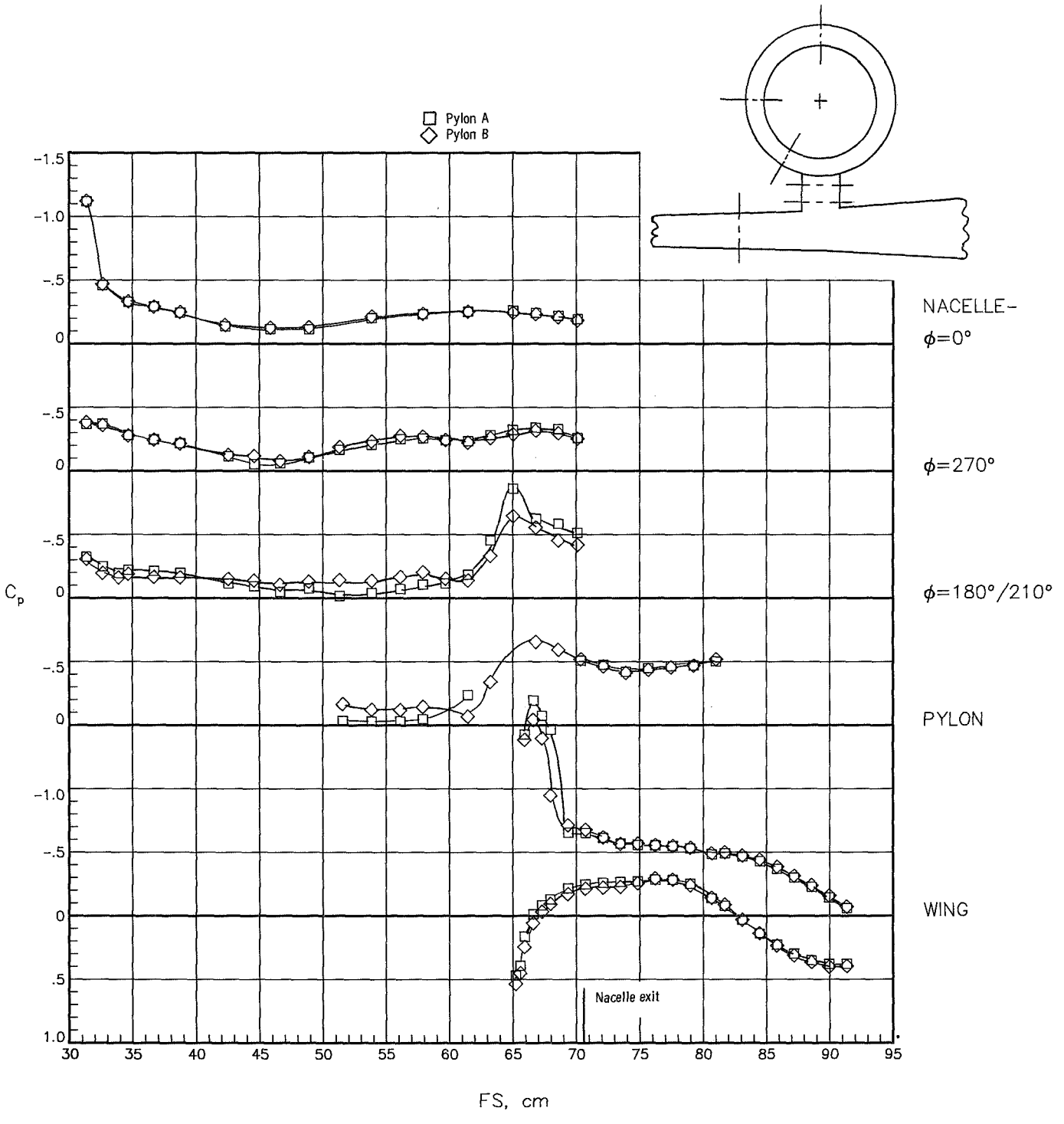


(b) Outboard side; y/(b/2) = 0.328.

Figure 27.- Concluded.

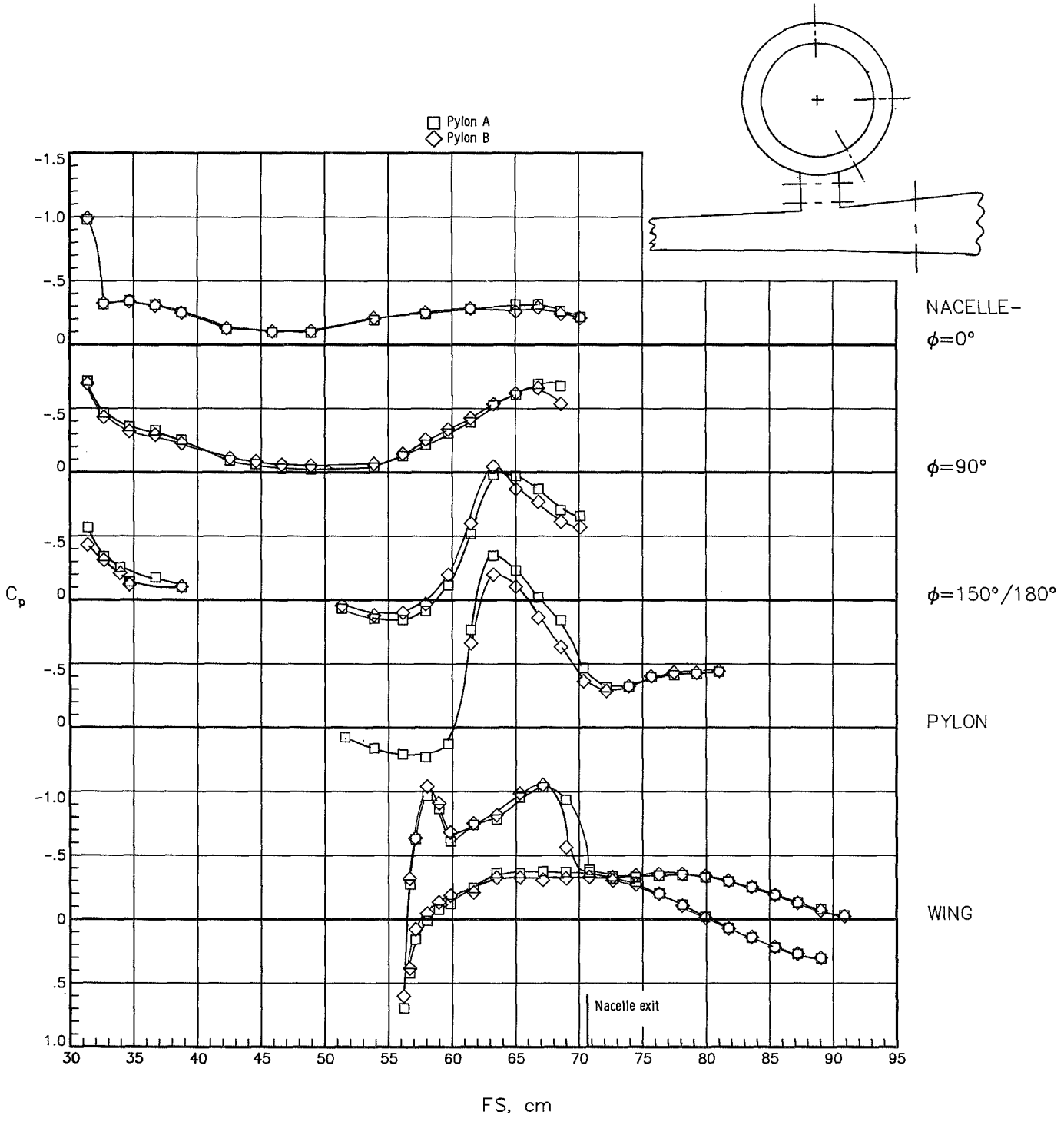


(a) Inboard side; y/(b/2) = 0.154.

Figure 28.- Effect of pylon size on nacelle, pylon, and wing pressures at M = 0.80, $\alpha$ = 1.10°; $C_L$ = 0.45.

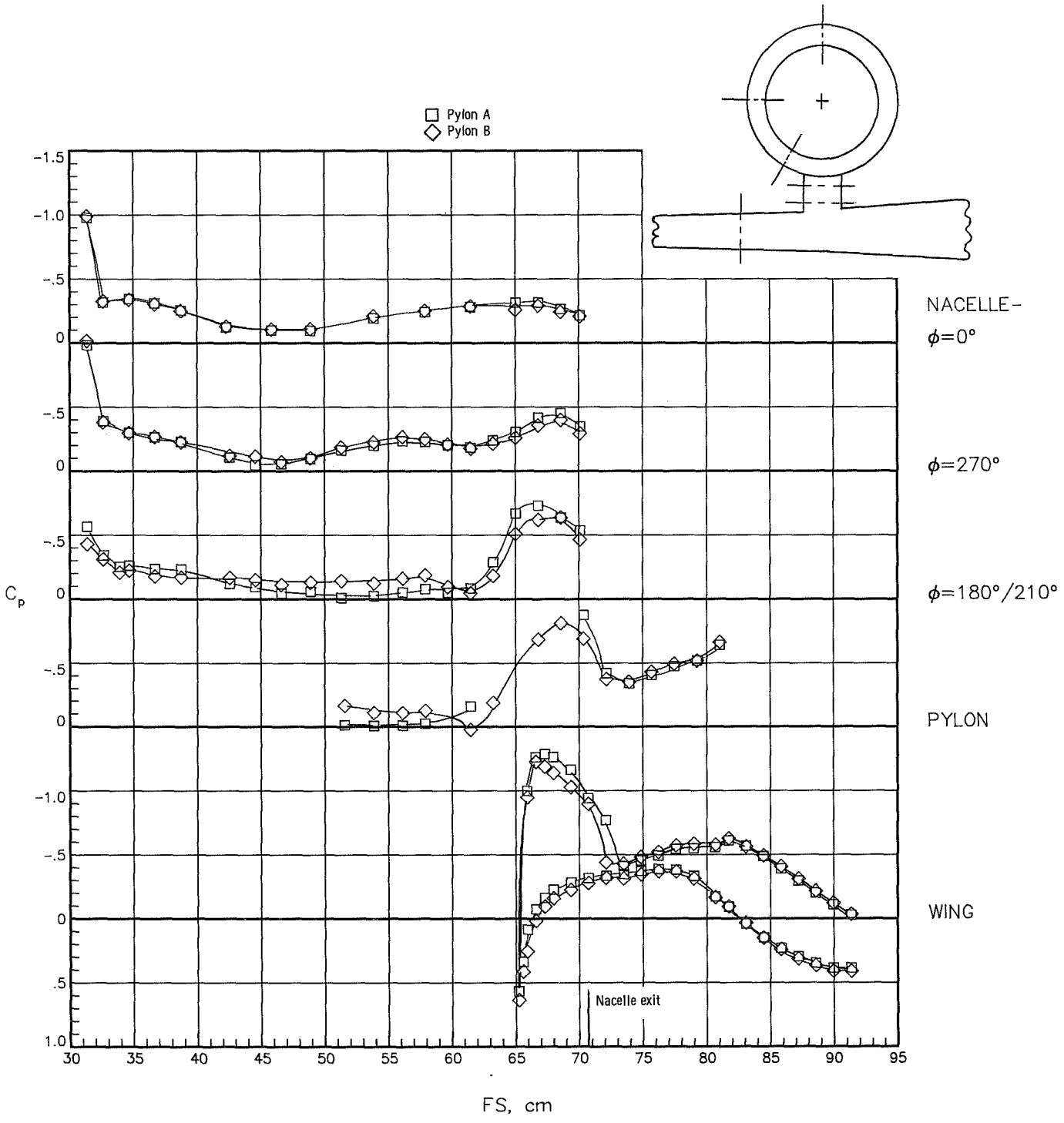


(b) Outboard side; y/(b/2) = 0.328.

Figure 28.- Concluded.

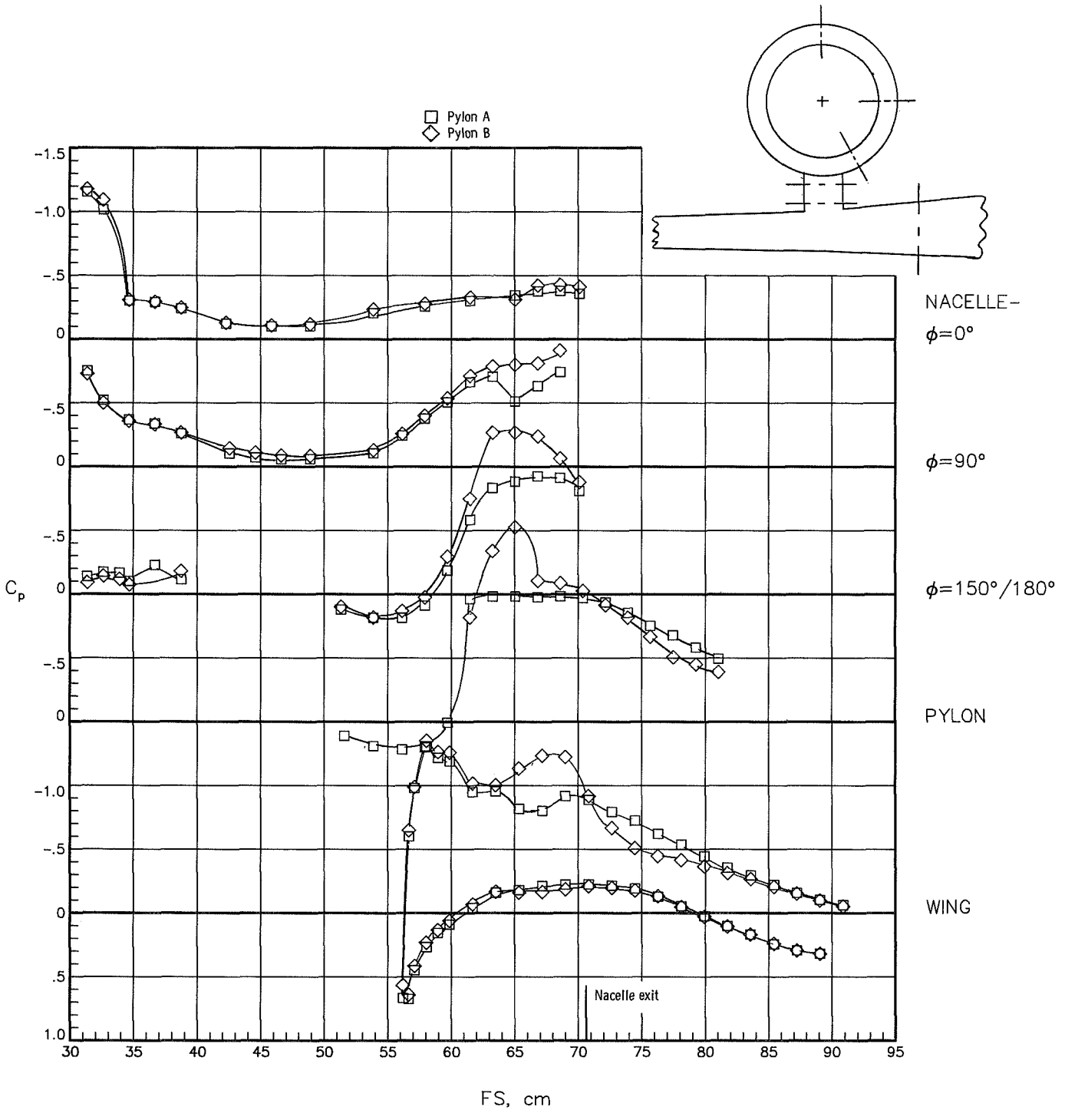


(a) Inboard side; y/(b/2) = 0.154.

Figure 29.- Effect of pylon size on nacelle, pylon, and wing pressures at M = 0.80, $\alpha$ = 4.14°; $C_L$ = 0.83.

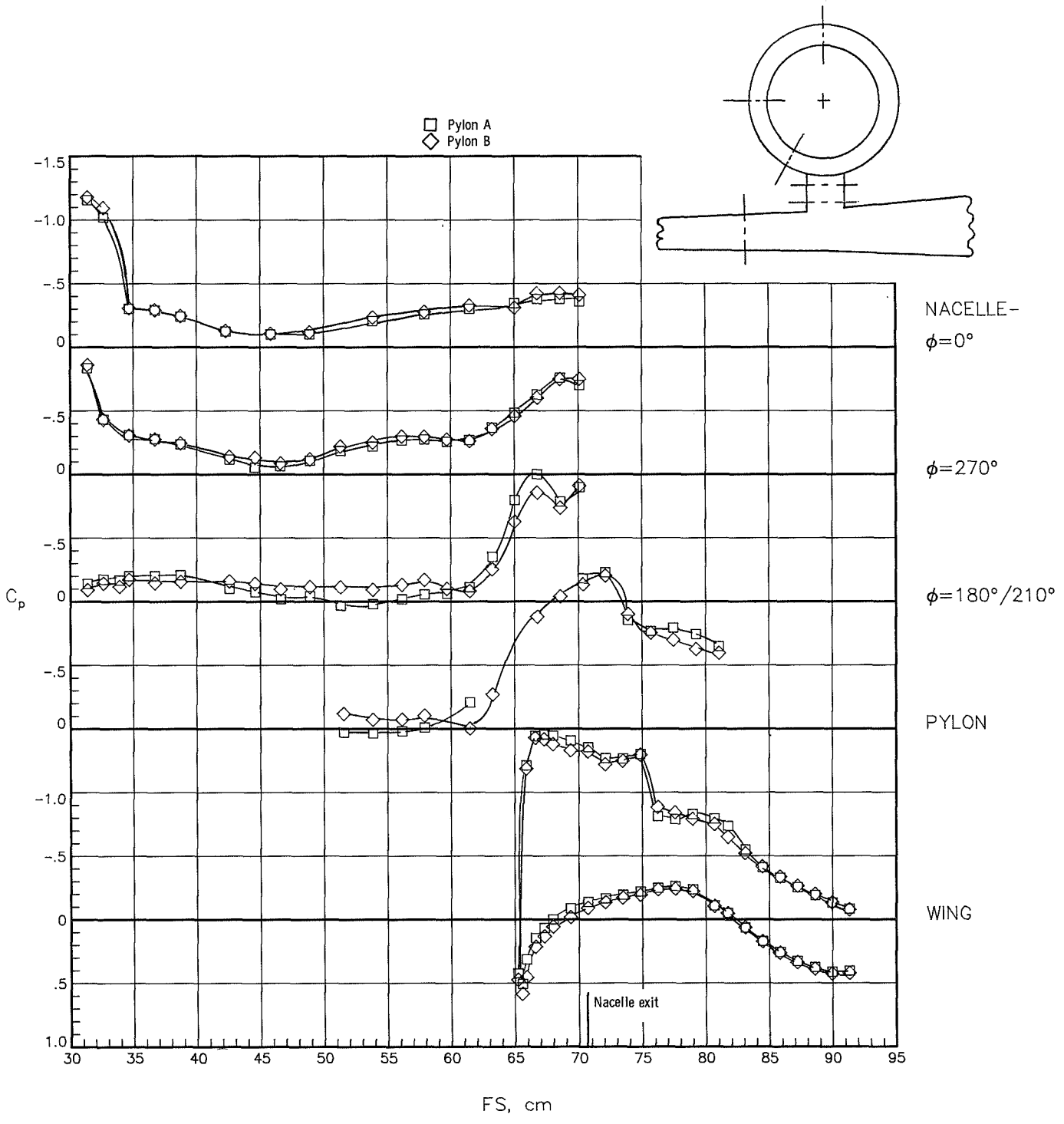


(b) Outboard side; y/(b/2) = 0.328.

Figure 29.- Concluded.

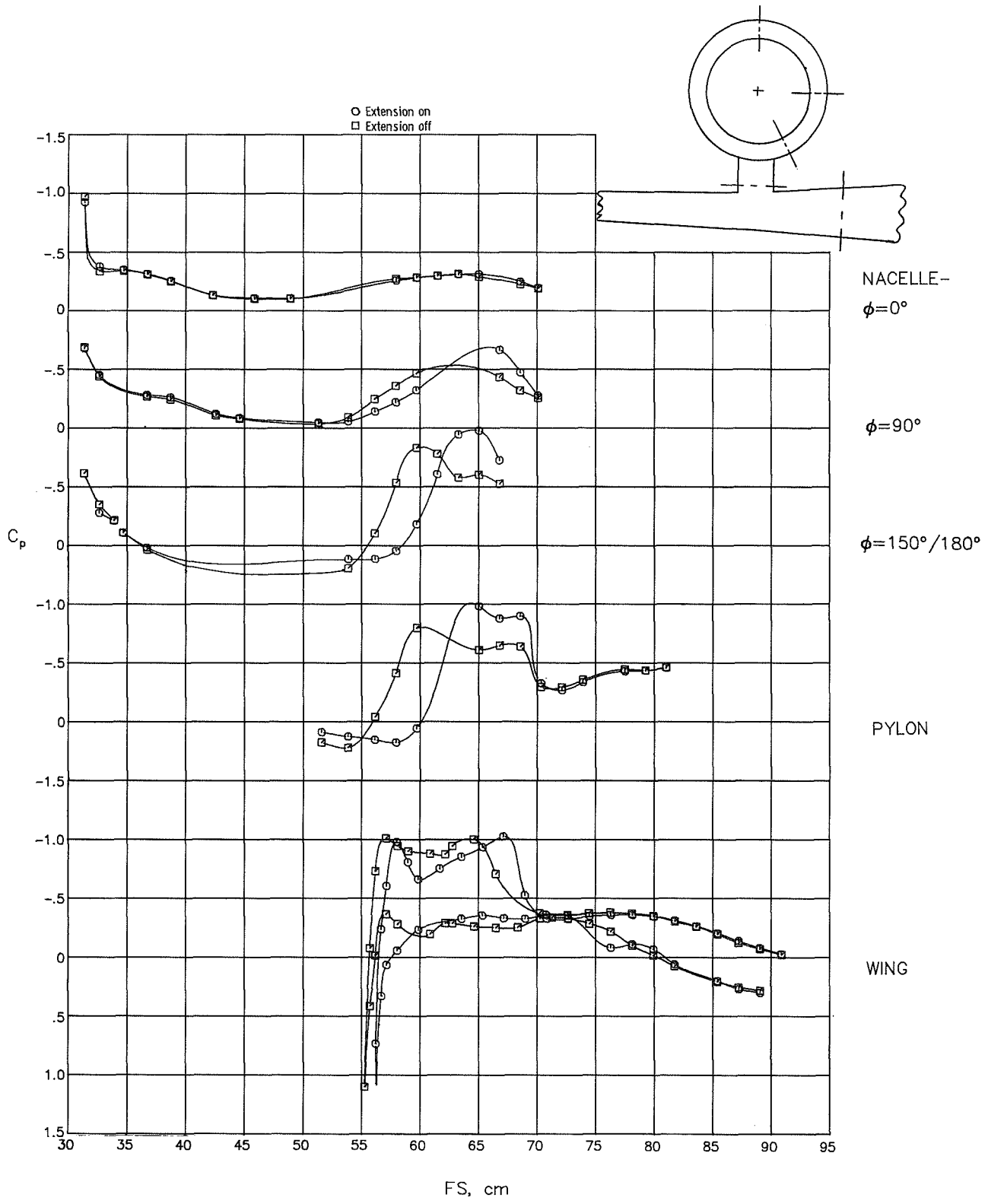


(a) Inboard side; y/(b/2) = 0.154.

Figure 30.- Effect of wing leading-edge extension on nacelle, pylon, and wing pressure distributions at M = 0.80, $\alpha$ = 0.90°; $C_L$ = 0.44.

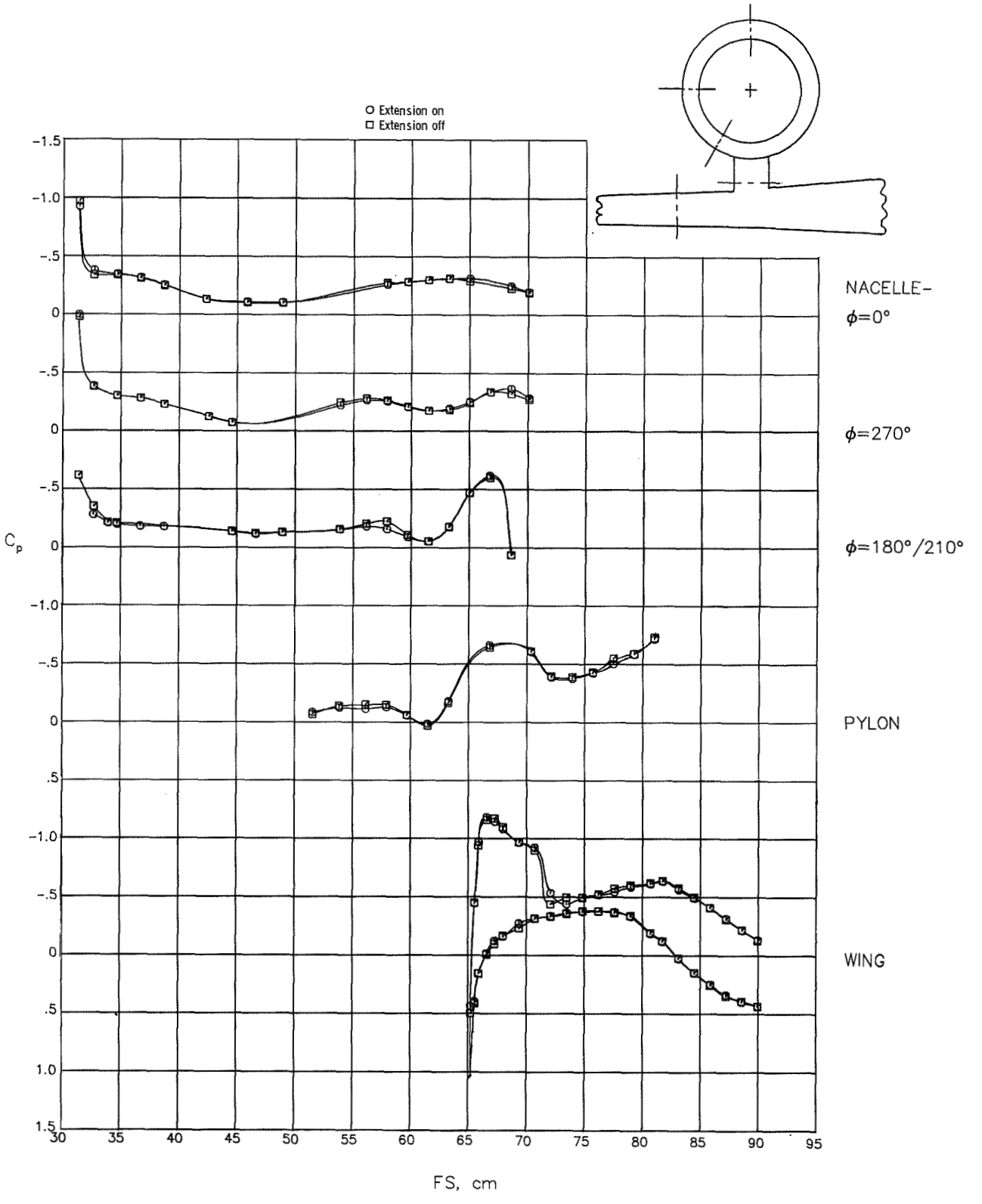


(b) Outboard side; y/(b/2) = 0.328.

Figure 30.- Concluded.

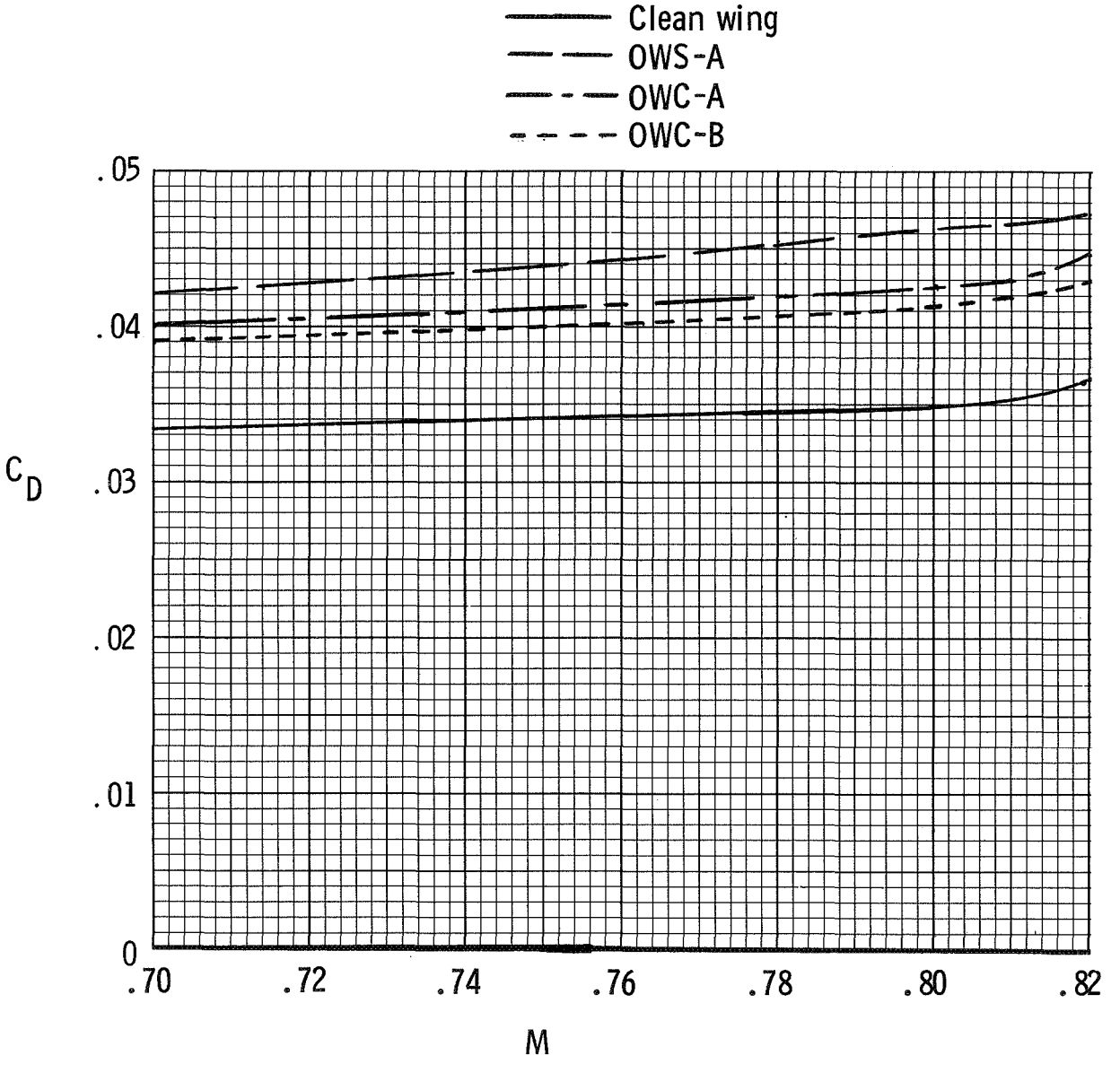


Figure 31.- Drag coefficient variation with Mach number. $C_L = 0.45$.

| 1. Report No. | 2. Government Accession No. | 3. Recipient's Catalog No. |
|---|---|---|
| NASA TP-2497 | | |

| 4. Title and Subtitle | 5. Report Date |
|---|---|
| Aerodynamic Characteristics of a High-Wing Transport Configuration With an Over-the-Wing Nacelle-Pylon Arrangement | December 1985 |
| | 6. Performing Organization Code: 505-40-90-01 |
| 7. Author(s): William P. Henderson and William K. Abeyounis | 8. Performing Organization Report No.: L-15959 |
| 9. Performing Organization Name and Address: NASA Langley Research Center, Hampton, VA 23665-5225 | 10. Work Unit No. |
| | 11. Contract or Grant No. |
| 12. Sponsoring Agency Name and Address: National Aeronautics and Space Administration, Washington, DC 20546-0001 | 13. Type of Report and Period Covered: Technical Paper |
| | 14. Sponsoring Agency Code |

15. Supplementary Notes

16. Abstract

An investigation has been conducted in the Langley 16-Foot Transonic Tunnel to determine the effects on the aerodynamic characteristics of a high-wing transport configuration of installing an over-the-wing nacelle-pylon arrangement. The tests were conducted at Mach numbers from 0.70 to 0.82 and at angles of attack from $-2^{\circ}$ to $4^{\circ}$. The configurational variables under study included symmetrical and contoured nacelles and pylons, pylon size, and wing leading-edge extensions. The symmetrical nacelles and pylons reduced the lift coefficient, increased the drag coefficient, and caused a nose-up pitching-moment coefficient. The contoured nacelles significantly reduced the interference drag, though it was still excessive. Increasing the pylon size reduced the drag, whereas adding wing leading-edge extensions did not affect the aerodynamic characteristics significantly.

17. Key Words (Suggested by Authors(s)): Airframe—propulsion-system integration; Nacelle-pylon integration; Aerodynamics; Transport aircraft

18. Distribution Statement: Unclassified - Unlimited

Subject Category 02

| 19. Security Classif.(of this report) | 20. Security Classif.(of this page) | 21. No. of Pages | 22. Price |
|---|---|---|---|
| Unclassified | Unclassified | 91 | A05 |

For sale by the National Technical Information Service, Springfield, Virginia 22161

NASA-Langley, 1985

National Aeronautics and
Space Administration
Code NIT-4

Washington, D.C.
20546-0001

Official Business
Penalty for Private Use, $300

BULK RATE
POSTAGE & FEES PAID
NASA Washington, DC
Permit No. G-27

POSTMASTER: If Undeliverable (Section 158 Postal Manual) Do Not Return